

A STUDY OF THE PULSATING GROWTH OF CUMULUS CLOUDS

by

Charles Edward Anderson

B.S., Lincoln University, Jefferson City, Mo. (1941)

M.S., Polytechnic Institute of Brooklyn (1948)

*[Handwritten notes and stamps, including "RECEIVED" and "LIBRARY"]*

SUBMITTED IN PARTIAL FULFILLMENT OF THE  
REQUIREMENTS FOR THE DEGREE OF  
DOCTOR OF PHILOSOPHY

at the

MASSACHUSETTS INSTITUTE OF TECHNOLOGY

May 1960

Signature of Author. . . . .  
Department of Meteorology, 14 May 1960

Certified by . . . . .  
Thesis Supervisor

. . . . .  
Thesis Supervisor

Accepted by. . . . .  
Chairman, Departmental Committee  
on Graduate Students

A STUDY OF THE PULSATING GROWTH OF CUMULUS CLOUDS

by

Charles Edward Anderson

Submitted to the Department of Meteorology on 14 May 1960 in partial fulfillment of the requirements for the degree of  
Doctor of Philosophy

ABSTRACT

The growth of five cumulus congestus clouds over the Santa Catalina Mountains near Tucson, Arizona was subjected to detailed examination by means of photogrammetric and statistical analysis. It was found that these clouds exhibited a pulsating form of cellular convection as they grew upward. Once maximum height was achieved, the circulation became a linearly increasing function of time.

The pulsations were found to be related to the buoyancy restoring force of the statically stable air with frequencies near ten minutes. Higher frequencies were found near one to two minutes which could not be definitely accounted for by conventional turbulence theory. An over-all acceleration of the motion was shown to be caused by an underlying flow which responded to the mean state of the cloud column.

A physical model is proposed for the circulation of a growing cumulus in which two cells are acting concurrently, yet independently, along the same vertical axis. The correct time behavior is shown to result from applying Bjerknes' circulation theorem, modified to include entrainment and mixing.

Thesis Supervisor: Henry G. Houghton

Title: Professor of Meteorology and  
Head, Department of Meteorology

and

Thesis Supervisor: Victor P. Starr

Title: Professor of Meteorology

## TABLE OF CONTENTS

	<u>Page</u>
ABSTRACT	ii
LIST OF FIGURES	iv
LIST OF TABLES	vii
I. INTRODUCTION AND REVIEW	1
II. THE DATA	32
III. ANALYSIS OF DATA	103
IV. THEORETICAL BASIS	129
V. SUMMARY AND CONCLUSIONS	147
VI. SUGGESTIONS FOR FUTURE RESEARCH	149
ACKNOWLEDGEMENTS	150
BIBLIOGRAPHY	151
BIOGRAPHICAL NOTE	157

LIST OF FIGURES

<u>Figure</u>	<u>Title</u>	<u>Page</u>
1.1	REVOLVING OSCILLATING CLOUD OBSERVED BY ABE	23
1.2	APPARENT AREA OF CLOUD WITH TIME	24
1.3	THUNDERSTORM AFTER LETZMANN	25
2.1	MAP OF TUCSON AND THE SANTA CATALINA MOUNTAINS	32
2.2	CLOUD CONTOURS	35
2.3	TUCSON RAOB, JULY 23, 24, 1956	37
2.4	CLOUD SEQUENCE PHOTOGRAPHS, JULY 23, 1956	39
2.5	CLOUD SEQUENCE PHOTOGRAPHS, JULY 23, 1956 (Cont.)	40
2.6	CLOUD SEQUENCE PHOTOGRAPHS, JULY 24, 1956	41
2.7	CLOUD SEQUENCE PHOTOGRAPHS, JULY 24, 1956 (Cont.)	42
2.8	A MULTIPLE EXPOSURE PHOTOGRAPH OF A GROWING CUMULUS CONGESTUS CLOUD	44
2.9	CLOUD TRAJECTORIES FOR A STATIONARY SOURCE MODE OF GROWTH	46
2.10	TRAJECTORIES FOR A GROWING CUMULUS TOWER	47
2.11	THE STREAMLINES FOR A SIMPLE POINT SOURCE IN A UNIFORM STREAM	48
2.12	THE RELATIVE POINTS OF THE TRAJECTORIES FOR A GROWING CUMULUS TOWER	50
2.13	CLOUD MOVEMENTS, 23 JULY 1956	56
2.14	HEIGHT VERSUS TIME, CLOUD NO. 1, 23 JULY 1956	57
2.15	VERTICAL VELOCITY VERSUS TIME, CLOUD NO. 1, 23 JULY 1956	60
2.16	VOLUME VERSUS TIME, CLOUD NO. 1, 23 JULY 1956	61
2.17	FLUX VERSUS TIME, CLOUD NO. 1, 23 JULY 1956	62



<u>Figure</u>	<u>Title</u>	<u>Page</u>
2.18	TRAJECTORIES OF CLOUD ELEMENTS FOR CLOUD NO. 3, 23 JULY 1956	64
2.19	HEIGHT VERSUS TIME, CLOUD NO. 3, 23 JULY 1956	68
2.20	VERTICAL VELOCITY VERSUS TIME, CLOUD NO. 3, 23 JULY 1956	69
2.21	VOLUME-TIME FOR CLOUD NO. 3, 23 JULY 1956	70
2.22	FLUX-TIME CURVE FOR CLOUD NO. 3, 23 JULY 1956	71
2.23	HORIZONTAL POSITIONS OF CLOUDS, 24 JULY 1956	72
2.24	TRAJECTORIES OF CLOUD ELEMENTS, CLOUD NO. 1, 24 JULY 1956	74
2.25	HEIGHT-TIME FOR CLOUD NO. 1, 24 JULY 1956	75
2.26	VELOCITY-TIME FOR CLOUD NO. 1, 24 JULY 1956	78
2.27	VOLUME-TIME FOR CLOUD NO. 1, 24 JULY 1956	79
2.28	FLUX-TIME FOR CLOUD NO. 1, 24 JULY 1956	79
2.29	TRAJECTORIES FOR CLOUD NO. 2, 24 JULY 1956	82
2.30	HEIGHT-TIME FOR CLOUD NO. 2, 24 JULY 1956	83
2.31	VELOCITY-TIME FOR CLOUD NO. 2, 24 JULY 1956	84
2.32	VOLUME-TIME FOR CLOUD NO. 2, 24 JULY 1956	87
2.33	FLUX-TIME FOR CLOUD NO. 2, 24 JULY 1956	87
2.34	VELOCITY-TIME FOR TURRET NO. 1, CLOUD NO. 2, 24 JULY 1956	88
2.35	VOLUME-TIME, TURRET NO. 1, CLOUD NO. 2, 24 JULY 1956	89
2.36	FLUX-TIME, TURRET NO. 1, CLOUD NO. 2, 24 JULY 1956	91
2.37	VELOCITY-TIME, TURRET NO. 2, CLOUD NO. 2, 24 JULY 1956	94
2.38	VOLUME-TIME, TURRET NO. 2, CLOUD NO. 2, 24 JULY 1956	95

<u>Figure</u>	<u>Title</u>	<u>Page</u>
2.39	FLUX-TIME, TURRET NO. 2, CLOUD NO. 2, 24 JULY 1956	96
2.40	HEIGHT-TIME, CLOUD NO. 3, 24 JULY 1956	99
2.41	VERTICAL VELOCITY-TIME, CLOUD NO. 3, 24 JULY 1956	100
2.42	VOLUME-TIME, CLOUD NO. 3, 24 JULY 1956	101
2.43	FLUX-TIME, CLOUD NO. 3, 24 JULY 1956	102
3.1	HARMONIC ANALYSIS, CLOUD NO. 1, 24 JULY 1956	106
3.2	POWER SPECTRUM, CLOUD NO. 1, 23 JULY 1956	113
3.3	POWER SPECTRA, CLOUD NO. 1, 24 JULY 1956	114
3.4	POWER SPECTRUM, CLOUD NO. 2, TURRET NO. 1, 24 JULY 1956	115
3.5	POWER SPECTRA, CLOUD NO. 2, TURRET NO. 2, 24 JULY 1956	116
3.6	POWER SPECTRA, CLOUD NO. 3, 23 JULY 1956	117
3.7	POWER SPECTRA, CLOUD NO. 2, 24 JULY 1956	118
3.8	POWER SPECTRUM, CLOUD NO. 3, 24 JULY 1956	119
3.9	AUTOCORRELOGRAM, CLOUD NO. 1, 23 JULY 1956	121
3.10	AUTOCORRELOGRAM, CLOUD NO. 1, 24 JULY 1956	122
3.11	AUTOCORRELOGRAM, CLOUD NO. 2, TURRET NO. 1, 24 JULY 1956	123
3.12	AUTOCORRELOGRAM, CLOUD NO. 2, TURRET NO. 2, 24 JULY 1956	124
3.13	AUTOCORRELOGRAM, CLOUD NO. 3, 23 JULY 1956	125
3.14	AUTOCORRELOGRAM, CLOUD NO. 2, 24 JULY 1956	126
3.15	AUTOCORRELOGRAM, CLOUD NO. 3, 24 JULY 1956	127
4.1	HALF CELL ILLUSTRATING THE SLICE METHOD	136
4.2	IDEALIZED CIRCULATION FOR CUMULUS CELL	137
4.3	CONDITIONAL INSTABILITY	140

LIST OF TABLES

<u>Table</u>	<u>Title</u>	<u>Page</u>
2.1	WINDS ALOFT AT TUCSON, 23 JULY 1956	38
2.2	WINDS ALOFT AT TUCSON, 24 JULY 1956	38
2.3	BASIC MEASUREMENTS, CLOUD NO. 1, 23 JULY 1956	58
2.4	BASIC MEASUREMENTS, CLOUD NO. 3, 23 JULY 1956	65
2.5	BASIC MEASUREMENTS, CLOUD NO. 1, 24 JULY 1956	76
2.6	BASIC MEASUREMENTS, CLOUD NO. 2, 24 JULY 1956	85
2.7	BASIC MEASUREMENTS, CLOUD NO. 2, TURRET NO. 1, 24 JULY 1956	90
2.8	BASIC MEASUREMENTS, CLOUD NO. 2, TURRET NO. 2, 24 JULY 1956	92
2.9	BASIC MEASUREMENTS, CLOUD NO. 3, 24 JULY 1956	97
3.1	HARMONIC ANALYSIS OF VERTICAL VELOCITY, CLOUD NO. 1, 24 JULY 1956	105
3.2	COMPUTATION OF VERTICAL ACCELERATION	109
3.3	CONFIDENCE LIMITS OF SPECTRAL ESTIMATES	120
4.1	CRITICAL VALUES OF THE RATIO $A_+/A_-$	142
4.2	THE PERIOD AS A FUNCTION OF $A_+/A_-$	145

## I. INTRODUCTION AND REVIEW

### 1. Generalized Picture of Cumulus

The growth of a cumulus cloud is an example of a hydrodynamical motion known as free convection. Free convection is characterized by the fact that the rising streams of fluid are warmer than the surrounding medium and are being forced upward because of their buoyancy. The heating may take place at one of the bounding surfaces or it may occur at points within the interior of the fluid. In either instance, fluid matter and heat are transported by the resulting convection. Cumulus clouds involve both kinds of heat sources in their development.

The sequence of events for the evolution of a cumulus cloud on a typical summer day may be described briefly. Solar rays, upon striking the ground are absorbed; the heated soil, in turn, heats the adjacent layers of air by radiation and sensible heat transfer. The local temperature lapse steepens and when the adiabatic rate is reached or is exceeded slightly, columnar convection sets in. The heated masses of air are convected aloft in chimneys of rising air and are cooled at somewhat the adiabatic rate. Provided the ascending air has sufficient water vapor, the cooling eventually leads to water vapor condensation in the form of millions of tiny water droplets. This mass of droplets appears as a cloud. While the vapor is condensing, latent heat is released which contributes further to the buoyancy and the cloud mass is able to grow vertically above the cloud base. Finally, the growth ceases when the cloudy air is no longer buoyant. This may come about by interactions with the surrounding air

either through direct mixing or by a more subtle dynamic action. Once the condensation rate becomes small, turbulence and diffusion soon destroy the cloud mass and it disappears into the surrounding air. The entire lifetime of an average cumulus is on the order of twenty minutes.

### 1.1 Aim of Present Work

Although this over-all behavior pattern is familiar to all, meteorological research has been unable to provide much detail to this description. The research reported herein is primarily an attempt to improve our observational knowledge about cumulus convection. A secondary aim is to call attention to the physical significance of certain of these findings in the hope that they may be useful in framing a more precise and quantitative analogue of this phenomenon.

### 1.2 Introduction to the General Governing Equations

Since cumulus convection involves the fields of motion, of temperature, and of moisture, the proper formulation of the problem requires a set of hydrodynamical, thermodynamical, and moisture equations. We need in some form:

- 1) An equation for conservation of momentum
- 2) An equation for conservation of mass for the fluid
- 3) An equation for conservation of moisture
- 4) An equation for conservation of energy
- 5) Equations relating the variables of state

Suitably chosen forms of the above equations, together with initial conditions and boundary conditions, will form a closed set which should yield solutions pertinent to cumulus convection. Two avenues of approach are open to the study of this system of equations.

A completely general solution might be sought which could be specialized for any specific set of conditions, or the starting equations may be highly restricted to conform to a particular case to give the special solution.

The general approach has not been rewarding in the past mainly due to the intractability of the general equations to analytical solutions. One fundamental barrier is the interaction terms which give rise to a system of non-linear partial differential equations which must be solved. Faced with this obstacle, previous investigators who wished to retain some generality in their solutions were forced to seek analytical solutions from a set of linearized derivations. In most instances, first order perturbation arguments were employed to reduce the original set of non-linear equations to more tractable linear equations much in the same manner as used by Lord Rayleigh (1916) in his classic paper on convection. The perturbation or other linear approaches have merit in that criteria may be found which control the nature of the solution to yield either stable or unstable behavior. However, nothing can be learned about the amplitudes of unstable disturbance after they have grown larger than the starting perturbations, otherwise the perturbation assumption is violated.

It is clear that the lifetime of disturbances which grow large compared to the mean state cannot be encompassed by the linearized theory. Such is the case for cumulus clouds. From the qualitative description of the evolution of a cumulus cloud, intuition would suggest the use of non-linear theory which permits the growth of an

initial disturbance at the condensation level (caused by sub-cloud columnar convection, for example) in an unstable manner, but somehow limited to amplitudes. The latter may be achieved by additional non-linear negative influences which grow to finally overwhelm the convection. Although no theoretical treatment of this sort is available for the cumulus problem, Malkus and Veronis (1958) have successfully included the non-linear terms in the Rayleigh problem by expanding the non-linear equations in a sequence of inhomogeneous linear equations dependent upon the solutions of the linear stability problem. They find the amplitude of the convection is determined by the distortion of the mean temperature field due to convection for large Prandl numbers and when the Prandl number is small, self distortion is predominant in amplitude determination. This technique is claimed by the authors to be applicable to any convection with a soluble stability problem. However, it is not clear if this method would apply to unstable solutions which grow with time.

The general equations, non-linear and non-steady, are soluble by machine methods, as has been done recently by Berkofsky (1957) and by Aubert (1957) for the hurricane circulation and the hemispheric circulation, respectively. In each instance, the latent heat energy of condensation was included in the numerical model along with the normal relevant equations. A similar numerical experiment was carried out by Malkus and Witt (1959) for the convective development of a dry, heated bubble of air. In these numerical integration methods, a fair knowledge of the physics of the process is needed as a check on the accuracy of the computations and in the choosing of proper

boundary and initial conditions. More restrictive is the fact that the machine solutions are always specialized to the set of initial and boundary conditions employed. Thus, although the general equations are used, general solutions are not obtained. Despite these shortcomings, it appears that numerical integration by high speed computers offers the best chance to thoroughly explore the whole cumulus convection problem.

### 1.3 Review of Current Models for Cumulus Convection

The bulk of the literature on the theory of cumulus convection chooses the alternate approach wherein the governing equations are suitably specialized to conform to an envisioned physical process or a mathematical analogue thereof. For the purpose of orderly examination of this not so small body of literature, the material may be divided roughly into three broad groups which offer three distinctly differing modes for cumulus convection. Type I views cumulus convection as a form of cellular convection, Type II as discrete parcel or bubble-like in character, and Type III as columnar or plume-like convection.

#### 1.3.1 Cellular Convection

The cellular mode arises when the boundary conditions limit the response of the environment to a finite volume adjacent to the disturbance. This is achieved by setting the horizontal velocities associated with the disturbance to zero at the axis of the disturbance and at some finite distance away from the axis. By virtue of the nature of the physical boundaries at the surface and at the top of the convective layer, the vertical velocities must vanish at these two levels. These two sets of conditions on the horizontal



and vertical velocities when taken with the necessity for preserving continuity of mass within the so bounded volume have to result in a cellular form of convection within this region.

If one considers an isolated cumulus cloud as the focus of an axially symmetric cellular circulation, it is obvious that fixed horizontal and vertical boundaries will restrict the available energy to this volume. Furthermore, if the principal source of the energy is in the form of latent heat of condensation, where the condensation is removed as precipitation, the circulation must cease just as soon as the overturning of the conditionally unstable stratification is completed. Hence, for a perturbation in a conditionally unstable air mass with fixed material boundaries, one would expect the circulation to increase exponentially with time as the disturbance grew and then decay as the latent energy became exhausted. The time behavior of the velocity components might be given by a form of the error function. This concept has a certain appeal because of the known short life of a typical cumulus cloud but it remains to be proved that such an impermeable vertical boundary exists during cumulus growth.

S.M.A. Hague (1952) investigated the solutions to the linear perturbation equations for an axially symmetric unstable mass of air which had fixed horizontal boundaries and was surrounded by stable air. At the vertical boundary, Hague required the radial velocity and the pressure to be continuous across the boundary. By requiring an exponential growth for the pertinent variable, in order for the initial perturbation to increase, solutions were found for the spatial distributions of velocity, pressure, and entropy. Hague found

an increase relationship between the size of the disturbance and the growth rate. The slower the growth rate the larger will be the size of the disturbance. The disturbance took on the form of a convective cell with ascending air in the unstable region and descending air in the stable region. A discontinuity in vertical velocity occurred at the vertical boundary which also was the point of maximum radial velocity regardless of sign. The vertical velocity decreased asymptotically to a zero value in the stable region. Hague extended his model to the case of unstable air surrounded and surmounted by stable air. In the latter, the same solutions were found as before in the unstable and stable regimes with an additional exponential decay with height of all variables in the overlying stable region.

In a one dimensional analysis of the effect of saturated, unstable air ascending in a dry, descending, stable environment, J. Bjerknes (1938) pointed out the net result was warming of the environment air. Petterssen (1956) and Beers (1945) incorporated this aspect into the so-called "slice method" of forecasting convection. By using either form of V. Bjerknes' circulation theorems, it is possible to derive an expression for the rate of circulation change with time, or circulation acceleration, in terms of the ratio of area of ascending unstable air to the area of stable descending air. Both Beers and Petterssen demonstrated exponential growth of the circulation when this ratio is small (less than about 0.5). This result agrees with Hague's finding that the growth rate is larger the smaller the disturbance. However, the slice method analysis predicts oscillatory solutions when the ratio is one or greater; whereas, Hague found smaller but still

exponential rates when the size of the disturbance was large.

Although it is questionable that cumulus growth ever has a steady state stage, except perhaps in the case of mature thunderstorms, several steady state cellular circulation models have been proposed. H. Christians (1935) incorporated several modern features in his model of a thunderstorm, including the concept of dynamic entrainment and the resistance of the air above the cloud top to lifting as the cloud grew upward. Christians was concerned with deriving the diameter, height, and velocity distribution for thunderstorms from the tephigram. He found the diameter of a cumulus should be proportional to the increase of velocity with altitude within the cloud. Although some of Christians' arguments are questionable, it is interesting that his relation between cloud diameter and vertical velocity is similar to conclusions reached by the parcel or bubble theory some years later.

Recently, Gutman (1957) proposed a model of a cumulus cloud based on the steady state assumption. By defining a special stream function, he was able to solve the perturbation equations for the distributions of temperature, vertical velocity, liquid water content, and pressure. Gutman's model resulted in a cloud which is characterized by rising air throughout and with no noticeable downward motion either in the cloud or outside it. He also computed that five times more air was being passed through the cloud than could be accounted for by upward flow through the cloud base and concluded that the cloud was being fed principally by moist air entering through the sides of the cloud.

A steady state cellular circulation does not seem to be appropriate for cumulus convection. For one thing, it implies a fixed cell size, horizontally and vertically. Cumulus growth, on the other hand, is notable for the vertical and horizontal extension of the circulation with time. If one wishes to represent cumulus convection as a type of cellular circulation, the cell must be capable of changing its size, particularly in the vertical. Although the cellular model suggested by Hague provides for a variable horizontal dimension, no one yet has proposed a cellular model which grows along its vertical axis.

### 1.3.2 Parcel or Bubble Convection

The parcel or bubble mode of cumulus convection applies very well to this latter feature of cumulus convection. The observation that bubble-like swellings on the upper surface of cumulus clouds seemed to rise, balloon-like, to form narrow turrets inspired the bubble theory. According to this theory, cumulus clouds are formed by discrete parcels of buoyant air. The established analysis of atmospheric thermodynamic diagrams to determine the various stability criteria employs the "parcel method" in which it is assumed that a parcel of air can be displaced vertically for a small distance without disturbing the environment or without mixing with it. Atmospheric soundings are classified stable, unstable, or conditionally unstable on the basis of the expected behavior of a parcel so displaced. It was a natural tendency to regard cumulus clouds as larger parcels of buoyant air, and this concept became fixed in the meteorological literature.

In recent years, the older parcel idea has been undergoing modifications to incorporate arguments favoring some mixing action between the rising parcel and the environment. Scorer and Ludlam (1953) proposed the "bubble theory of penetrative convection" in which buoyant bubbles are regarded as the protons from which convection is built. Equations of motion are derived for the bubble which allows for a drag in the form of a mixing term proportional to the velocity. Scorer and Ludlam suggested larger bubbles may form as aggregates of smaller bubbles and in this way larger cumulus elements are produced. Furthermore, the convection gradually builds over a greater depth by a process in which new bubbles are able to rise more quickly and are longer lived by ascending in the wake of earlier bubbles. Scorer and Ludlam (1953), Ludlam and Scorer (1953), and Malkus and Scorer (1955) claim observational support of the bubble theory. Priestley (1953) extended the bubble argument to allow for continuous mixing of heat and momentum between the buoyant element and its environment. On analyzing the equations governing the motion of such a parcel, Priestley found three different possible behavior modes: (A) ascent followed by damped oscillations, (B) asymptotic ascent to an equilibrium level, and (C) absolute buoyancy in which the ascent rate increases indefinitely. For an atmosphere with a sub-adiabatic lapse rate, the motion is of type A for sufficiently large elements but may become B for smaller elements. In superadiabatic lapse rate, C is the mode for large elements, and B for the smaller ones. Priestley presented some observed cloud top oscillation frequencies which compared favorably with those computed on the basis of his theory.

More recently, Levine (1959) attempted to define more rigorously the mixing process between bubbles and environment air. Levine chose to approximate the motions within the bubble by Hill's "Spherical Vortex" for which solutions are known, and allowed entrainment to proceed through a refined application of Stommel's (1947, 1951) method. Levine claims observed vertical distributions of vertical velocity and potential temperature in tropical cumulus agree closely with values computed from his model.

Despite the widespread popularity of the bubble theory, there are a number of weaknesses in this view of cumulus convection. Outstanding is the question of the origin of the bubbles. In the opinion of many, the bubbles are believed to break away from a superadiabatically heated layer near the ground. Yates (1953), in describing the impressions of gliding pilots, pointed out that bubbles or thermals are released from a particular site every five to fifteen minutes. The sites are about one mile squared and the thermal frequency is found to depend on the type of soil, wind strength, and solar insolation. Priestley (1959), on the basis of meteorological measurements made simultaneously at several different heights on a tower, found evidence of strong interaction between remote parts of the flow. Priestley interpreted these results as supporting a columnar or plume mode of convection and rejected the possibility of bubbles. If measurements in the boundary layer do not reveal the presence of bubbles, it is difficult to argue that the bubbles originate in this region. Combining these two sets of observations gives the picture of sub-cloud convection as a periodic upward flow which is connected over a fairly deep layer.

This conclusion, if extended into cumulus convection, would be extremely damaging to the bubble theory. It would challenge directly the view that the convection is occurring in the form of a series of unrelated, independent, buoyant units. The only set of simultaneous measurements of the vertical velocity at various levels in clouds are those made under the Thunderstorm Project (Byers and Braham, 1949). For these large cumulus clouds, the measurements suggested deep updrafts throughout most of the cloud height. Byers and Braham describe the flow as columnar convection with entrainment through the sides of the cloud.

Another problem is the one of compensating motion in the environment. The bubble theory does not require any large scale downcurrents in the surrounding air and generally ignores this aspect. Ludlam and Scorer (1953) take the position that compensation is achieved over so large an area that it is to be regarded as part of the synoptic scale motions. However, Yates (1953) in his description of thermals, pointed out that very often a downcurrent rings the upcurrent, the boundary between being a region of great turbulence. More commonly, sinks are found next to thermals but are not as strong nor as widespread.

### 1.3.3 Columnar Convection

The third proposed mode of convection does not answer all the objections raised to Types I and II and, in fact, poses some problems of its own. In contradistinction to cellular convection in which the whole of the fluid participates, the term "penetrative" convection denotes a motion occurring within a much larger mass of fluid. For example, the smoke curling upward from a lighted cigarette is

penetrative and illustrates what is known as columnar or plume-like convection. In an extensive review of the current state of theoretical development for buoyant plumes, Priestley (1959) pointed out that this mode of convection is best suited of all to allow a simple mechanistic interpretation of entrainment. As the result of many direct measurements of cloud parameters such as temperature, liquid water amount, and humidity structure, it has been concluded that the air inside the cloud is a mixture of air which has risen through the cloud base and air which somehow is entrained from the environment. Some recent measurements reported by R.M. Cunningham (1959) and M. Draginis (1958) raise doubts about the necessity for mixing in all cumulus clouds, but these latter data have not yet made an impact on the accepted viewpoint.

Many authors, starting with the early work of Stommel (1947, 1951) and Austin (1948), have offered various theories of cumulus convection built around a steady state entraining updraft. In the earlier models, the rate of entrainment was taken as an arbitrary percentage increase with height of the mass (for example, Byers and Braham, 1949) but more refinements were introduced with time. Austin (1948) and later, Houghton and Cramer (1951) based the entrainment rate on the requirement for continuity of mass and momentum in the updraft. Malkus (1954, 1955) checked the entrainment theories by comparing computed values of temperature, moisture, and vertical velocity with those observed in trade wind cumulus clouds. Perhaps the most complete columnar convection mode for cumulus is the one proposed by G. Haltiner (1959). In his model, Haltiner solves for the vertical distributions of vertical velocity, cloud temperature, liquid water content, and fractional mass increase from a



one dimensional system of steady state equations in the pertinent variables. These equations were solved on an electronic computer by successive iterations for small height intervals starting from a set of initial conditions at the cloud base and in the environment. Haltiner included the transfer of heat and momentum proportional to the vertical velocity in addition to a systematic entrainment of environment air based on the continuity of mass and momentum. The values obtained compare favorably with those measured by aircraft.

The columnar cumulus models employed by cloud physicists differ from the buoyant plume models described by Priestley (1959) in one important respect. The cumulus models assume a constant cross section area with height; i.e., a cylindrical cloud; whereas, the more classic buoyant plumes allow for spreading with height, generally at a constant rate. The latter results as a solution from the two dimensional system of equations. Hence, the buoyant plume has a vertical velocity which decreases monotonically from the source. When the release of latent heat of condensation is included for the case of a buoyant plume in a moist atmosphere, B. Morton (1957) found the vertical velocity still decreases with height even in the cloud but the vertical extent of the cloud no longer depends on the parameters characterizing the plume in the lower unsaturated air. However, when the cross section area is taken as constant, the vertical velocity was found by Haltiner to increase with height because of the continuous release of latent energy along the cloud column until, at last, the cumulative effect of continuous entrainment caused an abrupt decrease of the vertical velocity to zero or actual negative values if the cloud

top had overshoot its equilibrium level.

Thus, for columnar convection, dynamic entrainment requires an increasing vertical velocity with height to the top of the column; whereas, for the buoyant plume, dynamic entrainment is accompanied by a decreasing vertical velocity profile.

It is questionable how representative of actual cumulus convection is the columnar mode. A strong objection may be made to the use of the steady state assumption in modeling a phenomenon as transient as a cumulus cloud. The argument may be advanced that this approximation is valid for deep cumulus congestus or cumulonimbus clouds, but even for these the Thunderstorm Project (Byers and Braham, 1949) found the cells had relatively short lives. As in the parcel mode, compensating motions in the environment are assumed to be small enough to be ignored. With respect to the environment air, when the horizontal boundary conditions requires the horizontal flow to vanish as the radius becomes large, compensating down flow is obtained for plumes (F.H. Schmidt, 1957, a,b). Thus, the entrained air will enter with negative velocities instead of zero, as assumed, and this will cause a much larger loss in momentum in the rising air than that being considered in the case of a still environment.

An entirely different entrainment process has been offered by Squires (1958) to explain the presence of environment air inside the cloud. Parcels of dry air are postulated to enter the tops of growing clouds and by virtue of the evaporative cooling taking place within these drier parcels, they are able to sink considerable distances into the cloud before mixing completely. A mathematical

model based on Priestley's parcel theory was evaluated by Squires to show that considerable penetration is possible.

Three possible modes for cumulus convection have been reviewed. Each of these finds some justification in either experimental observation or theoretical logic. Each may be facets of the actual mode and thus all three may be capable of being unified under some higher scheme. Likewise, some or all of these may be rejected in favor of a new interpretation. The state of our ignorance does not favor immediately one possibility over another. As in the case of all scientific theories, truth is associated with the one which most consistently explains observations and whose predictions are borne out more often by new observations. Therefore, observational evidence will have to bear the major role in the ultimate decision as to the nature of cumulus convection. Real progress will necessitate quantitative, pertinent, observational data on cumulus convection of which there is little at the present.

#### 1.4 Observational Conclusions on the Nature of Cumulus Convection

Our knowledge of the properties of cumulus clouds has been obtained through four principal methods: aircraft (powered and sail plane), radar, photographic, and aerological sondes. To the end of drawing a composite picture of cumulus convection from the observational facts gathered by these different techniques to date, it may be desirable to examine their contributions to the fundamentals of the problem; i.e., to our understanding of the fields of motion, temperature, and moisture involved in cumulus convection.

The importance of the circulations and smaller motions inside and around cumulus clouds in determining the internal amount and distribution of cloud liquid water, precipitation, temperature, and other micro features is being recognized increasingly by workers in cloud physics. Most of the recent investigations into precipitation rates, cloud electrification, raindrop spectra, and the like, suffer from a lack of more complete descriptions of the motion fields in cumulus. Ideally, what is required is the measurement of the total velocity at a large number of points in a three dimensional grid encompassing the whole of the convective region. The grid points should be spaced every ten meters or so to keep within the time scale of the motion and the velocity should be observed at each point about every ten seconds. The structure would extend from the surface to the stratosphere and be at least ten miles in diameter. It is clear that physical limitations will restrict us to actual data which will be considerably less than the ideal.

#### 1.4.1 A Summary of Aircraft Results on the Motion Field

The most comprehensive attack on this problem was undertaken during the Thunderstorm Project, 1945-1948. Simultaneous penetrations by five airplanes, equipped to measure up and downdrafts and separated by 5,000 ft (m.s.l.) to 25,000 ft (m.s.l.). Each aircraft made as many traverses as possible at the assigned level. In addition to the vertical motions so obtained, a number of carefully tracked balloons released simultaneously within and around thunderstorms provided data on the horizontal winds. The project divided the life cycle of a thunderstorm into three phases: a growing or cumulus stage, a mature

stage, and a dissipating stage. During the cumulus stage, the cloud was found to have updrafts throughout its vertical extent with the strongest updraft in the uppermost portion. The mature stage was characterized by both updrafts and downdrafts and precipitation particles throughout the cloud with rain reaching the ground. The strongest updrafts were still found at the highest level of penetration. In the dissipating stage, the vertical motions were small and generally downward, being accompanied by falling precipitation. The majority of cumulus clouds did not develop into thunderstorms and flights inside these showed only weak upward and downward motions of less than 1 m/sec with no obvious pattern of distribution of vertical velocities. The smaller scale motion or turbulence was found to be directly produced by the draft: the strongest gusts were associated with the strongest drafts.

Subsequent to the Thunderstorm Project there have been many explorations of the interiors of cumulus clouds by single research aircraft. The Woods Hole Oceanographic Institution made several expeditions to the Caribbean area to study tropical cumuli with a specially equipped PB4 aircraft. Earlier, Bunker (1952) conducted flights in the Cape Cod, Massachusetts area with the same aircraft to investigate the sub-cloud layer. Bunker found a very high correlation between simultaneous values of air temperature and air turbulence when a convective current was penetrated and further found that the nature of the current shifted from a series of small discrete parcels near the surface to something resembling a broad draft near the cloud base. This latter result is consistent with gliding experience (Yates, 1953) where

the diameter of thermals was found to decrease below 1,000 ft. Yates reported the strength of the updraft increased generally inside the cloud and the upcurrent very often was surrounded by a ring of downcurrent less strong and not very widespread.

Malkus (1954, 1955), of the Woods Hole group, described the vertical velocity structure of trade cumuli and found that these relatively small clouds could be modeled fairly satisfactorily using the steady state, entraining, circular updraft with the vertical velocity increasing along the vertical. Malkus found the updrafts inside the clouds could have simultaneous downdrafts adjacent to the cloud tower, the stronger ones near the top of the tower. Malkus explained the downshear downdrafts as being a mixture of new cloud air with old cloud air, but no explanation was offered for the downdrafts observed on the upshear side.

Indirect support for the simultaneous downdraft surrounding growing cumulus towers is provided by sensitive measurements of the air temperature obtained during horizontal traverses through such towers. Vulfson (1957) in the U.S.S.R. and Cunningham (1956, 1959) have many examples of temperature profiles in which the air immediately exterior to the cloud is warmer than that of the ambient surroundings. Vulfson did not find a sharp boundary between the compensating currents and the cloudless air which he interpreted to mean the descending flow gradually slackens along the horizontal. Near cumulus, the descending currents were always observed near the upper portion of the clouds, and occasionally, Vulfson found evidence of descending air below the cloud base and between clouds. According to his measurements, he concluded

that the horizontal dimensions of the compensation currents were comparable in area to those of the clouds.

Cunningham (1956), using highly sensitive and rapidly responding temperature and humidity probes, carried out a series of penetrations through relatively small cumulus clouds during the Summer of 1955. Many of the clouds had in-cloud temperatures colder than ambient while several highly buoyant towers exhibited warming immediately near the cloud as well as warming in the interior of the cloud. From Cunningham's published results, the average width of the warmed annulus to the width of the cloud was about 0.5. Assuming no separation between cloud and annulus (Cunningham's data indicate this to be less than 50 ft.), this value compares favorably with the computed ratio of 0.4 for equal areas of cloud and descending ring of air. Like Vulfson, Cunningham observed the most pronounced effects near the upper parts of the growing towers and agreed with the former's conclusion that the air descended only for a short distance (less than 1,000 ft.) before coming to rest. In a later study, Cunningham (1959) found evidence from the observed temperature and humidity that corroborates Vulfson's claim that air sinks between clouds and spreads out below the cloud base to form stable layers.

The direct observation of vertical motions around cumulus clouds by aircraft leads one to the following picture of the motion field. For small to medium cumulus clouds, individual rising columns or towers have a vertical velocity which increases with height from somewhere beneath the cloud base but not necessarily extending to the ground. The column is roughly circular and is surrounded by a ring of

descending air which is most pronounced near the upper portions of the tower. Crude estimates give about equal areas to the updraft and the downward moving air. The larger cumulus clouds, including giant cumuli, have updrafts throughout their interiors while the smaller clouds may find the updraft occupying only a fraction of their horizontal dimension. No real evidence is provided to contribute to a conclusion regarding the time dependence of the motion field. Presumably, the above description applies to actively growing clouds. Decaying clouds would have no outstanding draft structure, either up or down, although this is not true for thunderstorms.

#### 1.4.2 Results of Photographic Studies on the Motion Field

Photographic studies of cumulus growth have the advantage of being able to maintain a watch over the cloud cycle and thereby provide data on the time behavior of the growth. Malkus and Scorer (1955) and Scorer and Ludlam (1953) made measurements on the rate of ascension of protuberances or "bubbles" at the tops of cumulus clouds from 16 mm time lapse film and reported relatively constant upward velocities. Malkus and Scorer also measured the so-called "erosion" of the bubbles to establish the numerical value of the mixing process. Since the vertical velocity would not be constant during the initial growing period and during the final stages, the claim of constant vertical velocity applies to the time between. Scorer and Ludlam used an equation which allowed the vertical velocity to damp out asymptotically to account for the terminal behavior. Priestley (1953), as mentioned earlier, proposed a more general equation which includes oscillatory solutions as well as asymptotic, the former arising if the cloud top



penetrated into a stable layer. This problem of stable oscillations by a buoyant parcel in a stable environment was mentioned by Brunt (1927) and independently by Väisälä (1925) earlier, and pertains to the oscillations a non-interacting parcel will describe about an equilibrium level due to density changes following adiabatic expansion and contraction. Priestley published observations of cloud top oscillations which range in period from about eight minutes to thirty minutes, depending, as in the Brunt-Väisälä case, on the static stability of the atmosphere.

Workman and Reynolds (1949), in photographic studies of the life cycle of thunderstorm cells, were struck by the nearly equal rise and fall times of cumulus towers. An average period of about sixteen minutes is given for a sample of 47 such towers. In another study using weather radar, the rise and fall time of the precipitation echo for twelve storms was about twenty minutes, according to these same authors. For the group of 47 clouds, 39 had radar echoes and 8 did not, but it was noteworthy that there was little difference in period between the two classes.

Abe (1928) observed an interesting oscillation in the projected area of a small convective cloud mass over Mt. Fuji, Japan. In addition, Abe was able to describe the apparent trajectories of elements of this cloud. Figure 1.1 is taken from Abe's article. According to Abe's account, those cloud elements which formed at the left portion of the cloud base moved upward and to the left and thence in an arc-like path to the right. The right side of the cloud had a constantly changing shape and seemed to move horizontally to the right and those parts which spread to the right seemed to disappear at a

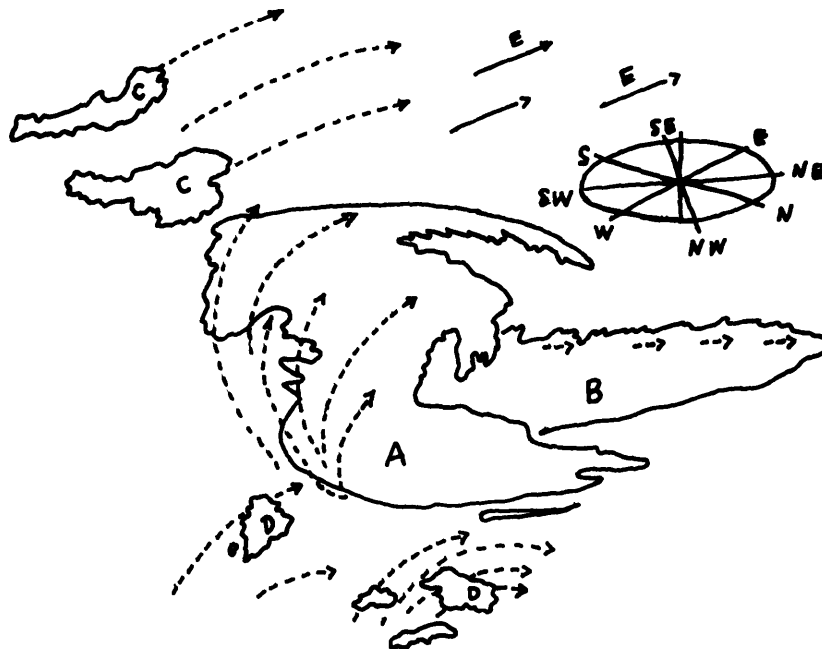


Fig. 1.1 Revolving oscillating cloud observed by Abe.  
 Taken from article by Abe (1928).

certain spot. Cloud B was a shelf-like mass which seemed to spread horizontally to the right and to disappear also at a particular spot. Cloud A seemed to have a fixed point of generation and from time to time a small cloud mass formed a little lower than the main mass. As the small mass increased in size, it rose and united with the main mass at its lower boundary. As this cycle was repeated, the point of union remained the same and corresponded to the point of cloud formation. All the arc-like trajectories seemed to emanate from near this point.

When Abe plotted the time variation of the apparent area of Cloud A, a period of about ten minutes emerged for the formation of the large mass of cloud. His result is shown in Fig. 1.2.

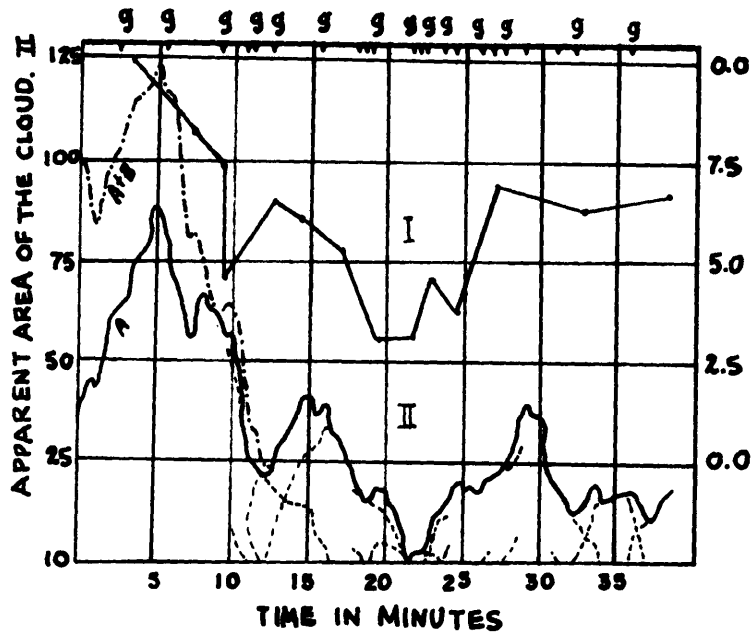


Fig. 1.2 Apparent area of cloud with time.  
Taken from Abe (1928).

A shorter period of 2.5 minutes was found for the intermittent formation of Cloud A; the time for this is indicated by the letter g at the top of the graph. Although Abe ascribed the cloud formation to a spiral path around a vertical axis caused by a vertical vortex, it is more likely that the phenomenon was due to a combination of orographic and convective effects.

Another account of pulsating cloud formation was given by Letzmann (1930) who also observed the trajectories of some of the cloud elements. Letzmann, using unusually careful visual observation of a slowly moving thunderstorm, noted the period of tower formation was about once every twenty minutes. Six such cycles were observed

during which a phase of rapid ascent to the anvil was followed by dissolution, and so on. In the thunderstorm, the base of the new tower seemed to shift to the left so that this was not a case of pulsations in the same cloud but rather the formation of new cells. The same type of progressive development of thunderstorms has been well documented in the literature; e.g., Byers and Braham (1947). Letzmann noted a rising and swelling motion at the top of the tower that had a clearly discernible diverging flow. The sides of the tower had no apparent motion and seemed to be enveloped by passive cloud. Around the base of the towering cumulus was a convective area of smaller cumulus and the whole moved as one. The cloud is shown in Fig. 1.3.

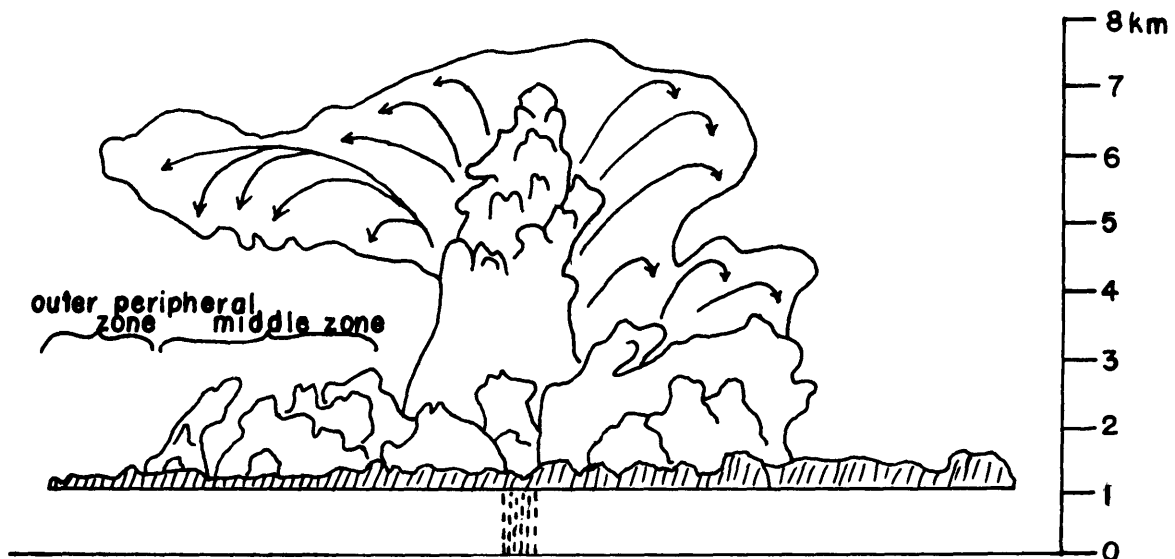


Fig. 1.3 Thunderstorm after Letzmann (1930).

In summary, the study of cloud development by time lapse photography introduces a new element into the previously drawn picture of the motion field. Although asymptotic decay of the vertical

motion is to be expected, periodic behavior as observed was not associated with the aircraft measurements with the exception of the cycle observed in mature thunderstorms. Here the cause has been attributed to precipitation initiated downdrafts.

#### 1.4.3 The Motion Field From Weather Radar

Weather radar studies of precipitation echoes associated with thunderstorms provide an additional, but cruder method of studying the motion field. Battan (1959), in an excellent monograph on weather radar, reviews the pertinent contributions that this technique has made to cloud and precipitation physics. He finds the growth of thunderstorm cells has the following characteristics:

1. Cumulonimbus clouds grow in "steps," with several steps needed before the cloud reaches the stratosphere.
2. About 10.3 minutes are required for a cell to reach maximum diameter.
3. About eleven minutes are required for a cell to reach maximum height.
4. The horizontal diameter is of the same order as the vertical extent, or the cell is nearly symmetrical.
5. The echo grows faster than the visible cloud top and catches up to the top and may simultaneously be descending.
6. The average lifetime of a cell is about thirty minutes.

If one accepts the view that the thunderstorm cumulus is similar, but greatly exaggerated, to the average cumulus, the radar results reinforce the photographic evidence of pulsating growth behavior. These

results also sustain the aircraft finding that the vertical velocity may be larger within the cloud than at the cloud top.

#### 1.4.4 Summary of Observational Evidence on the Motion Field Around Cumuli

Combining the results from all three sources, the motion field is seen to be more organized into cellular patterns than into discrete parcels, with compensating downward motions in the clear air accompanied by some kind of oscillatory behavior with time. The latter seems to be present regardless of whether the cell is growing upward or if it is oscillating about some equilibrium height. It is not clear if the same cell is able to undergo more than one such cycle. The evidence of periodic growth may be fitted to the "bubble theory" very nicely, as has been done by many authors who require a progressive moistening of the air by successive bubble penetrations in order for the cloud to grow upwards. However, the definite presence of compensating downdrafts was not contemplated by either the columnar or the parcel modes of convection. A columnar convection accompanied by compensating downflow becomes identical to the cellular mode in most respects, as pointed out by F.H. Schmidt (1957). Hence the choice lies between discrete parcel and organized cellular convection as best representing cumulus motion.

If long range forces could be demonstrated to exist between different levels along the cumulus updraft similar to those found in the early stages of the thunderstorm, the choice would narrow to the cellular mode. None of the evidence cited bears on this problem since one needs simultaneous measurements of the vertical velocity at two or

more levels in the cloud. Recently, Vonnegut, Moore, and Botka (1959, Fig. 3), in a field study of the relationship between thunderstorm electrification and precipitation, showed a high correlation between the vertical velocity at the top of growing cumulus and the tension on a captive balloon line reaching about midway up into the cloud. If this high correlation between distant parts of the flow can be interpreted much in the same manner as Priestley (1959, Chap. 4,5) does for his evidence of strong interaction between different levels in the sub-cloud layer, then the concept of discrete, independent bubbles comprising the flow in cumulus has to be discarded.

#### 1.5 Summary of Observations of the Temperature and Moisture Fields Around Cumuli

The fields of temperature and moisture in and around cumulus clouds cannot be observed except by direct probing. The only suitable tool is the aircraft equipped with highly sensitive, quick response instruments. Vulfson (loc. cit.), Cunningham (loc. cit.), the University of Chicago group (see Draginis, 1958; Ackerman, 1959), Woods Hole (Malkus, loc. cit.) and the Australian Cloud Physics Groups (see Warner, 1955; Squires, 1958b) have made many traverses through a variety of cumulus with sometimes conflicting results. In regard to the temperature, the following is a reasonable summary of the different investigations.

1. On entering a cumulus from the clear air, very often the temperature will drop about 0.5 degree right at the cloud-air boundary. This is due presumably to the evaporative cooling brought on by mixing cloud air with clear air.

2. The fine structure of the temperature profile will exhibit

rapid fluctuation across the cloud diameter. If the cloud is a well defined turret, a rise of about 0.5 degree over ambient is found in the updraft. If the cloud is older and consists of the remnants of previous turrets, the structure is chaotic and may be uniformly colder than the surrounding air.

3. The temperature rise normally is less than that which a moist adiabatic ascent of cloud air from the base would show. This feature is used to support entrainment theories.

4. In freshly ascending large towers, the updraft temperature approximates very closely the moist adiabatic (Cunningham, 1959).

5. Rapidly growing cumuli are found to have a ring of warmer descending air adjacent to the updraft in the clear air, most pronounced near the upper part of the updraft.

A similar summary may be made for the liquid water content of cumuli, relying on the recent works of Cunningham, Draginis, and Squires.

1. In small cumulus clouds, the liquid water content is always less than the computed moist adiabatic amount and shows rapid fluctuation along a horizontal path.

2. "Holes" or regions of low liquid water content are found well inside the clouds and regions of high liquid water content are found near the cloud edge frequently. This suggests the mixing and entrainment process is real.

3. The departure of the observed liquid water from the computed increases upwards from the cloud base.

4. For clouds which have or which produce radar precipitation echoes, the adiabatic value is exceeded in a narrow core region. This



is taken to indicate some type of storage process operating in these larger clouds.

#### 1.6 Over-all Conclusions on the Nature of Cumulus Convection as Provided by Observational Evidence

The final picture of a cumulus is provided by the synthesis of the pertinent features of the micro structure into the assumed motion field. The stage of development of the cloud has an important bearing on the observed temperature and moisture fields. Freshly building clouds will approximate more closely the moist adiabatic than older, decaying clouds. Mixing or entrainment appear to be real. However, this effect might be of lesser importance for the very large clouds, particularly in the updraft cores. The question is raised as to what extent these smaller scale motions affect the over-all circulation, particularly the observation that cumulus growth proceeds in steps.

For the interactions of the fields of temperature, moisture, and motion, many interesting possibilities are foreseen, but we are interested in how nature handles this problem in the case of cumulus convection. The classical, non-steady, cellular solution requires an exponential growth but observation of individual clouds and storms indicates asymptotic and oscillatory behavior. This difficulty is avoided if the parcel or bubble mode is adopted; but other problems, such as the evidence of compensating downcurrents, are raised. The mixing processes are most important to the bubble mode, while the cellular mode responds perhaps to the average properties of the temperature and moisture fields.

This study was undertaken to shed more light on these problems. My approach has been to accept the conclusion of Draginis that the mixing

processes leading to the fine scale distribution of temperature and moisture are similar for all clouds in similar stages of development regardless of weather situation and geographical location. The important task is to study the resultant over-all behavior of the clouds in the hope that some clues will be found which bear on their development as finite entities. It appears that this aim is achieved best at the present time by time lapse photographic studies. In the Southwest U.S. conditions are ideal for this work; in a clear atmosphere, relatively isolated, slow moving orographic clouds whose entire life cycles may be studied, appear day after day during the summer months.

## II. THE DATA

### 2.1 Description of Data Acquisition

The cloud photographs which form the basic data for this study were made available through the cooperation of the Institute of Atmospheric Physics, University of Arizona, at Tucson. Tucson is situated in the south-central part of Arizona and is almost surrounded on three sides by local mountains, Fig. 2.1. Extending in an arc from NE to E of Tucson are the Santa Catalina Mountains whose foothills are some ten miles distant. These are joined by the Rincon Mountains which

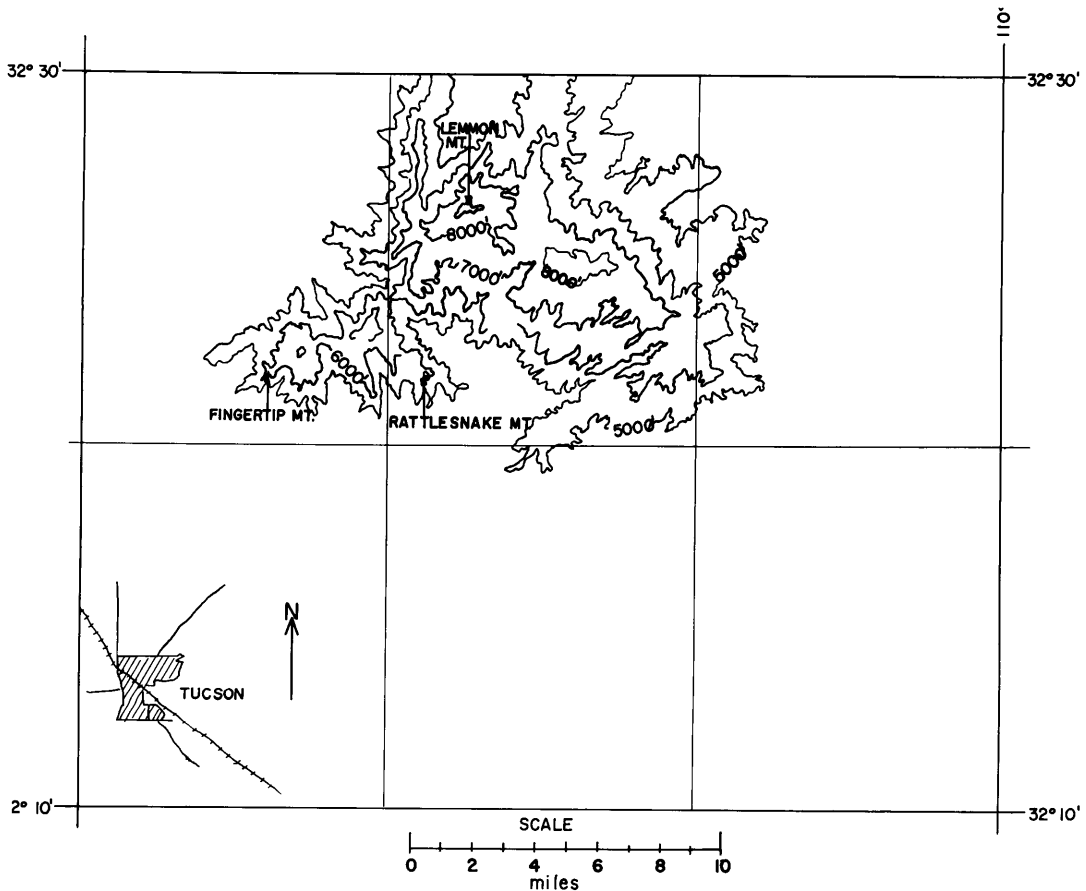


Fig. 2.1 Map of Tucson showing the Santa Catalina Mountains.

continue in a southerly direction. The highest peak is Mt. Lemmon, in the Catalinas, with an elevation of 9,150 ft. m.s.l. Numerous minor peaks, ridges, and canyons characterize the topography in the mountains. The clouds studied grew over a ridge extension from Mt. Lemmon. A position-time chart is included with the case histories in Section 2.4.

The months of July and August in the Southwestern U.S.A. are marked by a monsoon-like flow of moist, tropical air into the New Mexico-Arizona region from the Gulf of Mexico. Strong surface heating and chain after chain of mountains across New Mexico and eastern Arizona combine to set up intense local convection. This region has the second highest thunderstorm frequency in the U.S.A., and it peaks with the summer monsoon.

At Tucson, convective clouds build over the mountains nearly every day during July and August and frequently develop into thunderstorms. Normally, when the air is moist at the lower levels, the extent of cloudiness is so great that observation of isolated cumulus over the mountains is obscured.

On two days, July 23 and 24, 1956, conditions were ideally suited for photographing the entire sequence of a cumulus growth cycle. The moisture content was low enough to discourage cumulus development everywhere except near the highest peak, Mt. Lemmon. The synoptic map for the two days showed no distinguishing features for the Southwestern U.S.A. The region was covered by its typical "heat low" that appears on surface weather maps during summer.

The University of Arizona set up and operated two K-17 aerial cameras on a 1.3 mile base line, Kassander and Sims (1957). About 25

stereo pairs of photographs were taken on each day at two minute intervals. This gave almost one hour of observation at the height of the cumulus activity between 1330 and 1430 local time. In addition to the 9 x 9 inch photographs, a 16 mm time lapse camera took pictures at ten second intervals throughout the day. Unfortunately, the K-17 cameras had been swung some  $20^{\circ} 13'$  from their original perpendicular base line to the optical axis of the camera. This changed their orientation from the normal case; e.g., Zeller (1952), to a case of averted axis which rendered the analysis more difficult. An additional complication was caused by the tilting of the cameras some  $30^{\circ}$  upwards from the horizontal. In order to restore the photographs to the normal case so that their analysis would be greatly simplified, the photographs were rectified through a resultant tilt angle of  $35^{\circ} 38'$ . Perspective contours of the clouds were drawn using a stereocomparagraph, but it was found that an error persisted throughout each analysis. On subsequent conversation with the University of Arizona, it was learned that the red filter on the left hand camera had been crudely polished to remove the anti-vignetting film. This left the filter far from being optically flat and introduced considerable distortion in the images.

Arrangements were made with the U.S. Air Force Aeronautical Chart and Information Center, St. Louis, Missouri, to produce cloud contours and horizontal cross sections through the clouds at the 12,000 foot level on the Zeiss C-8 stereo plotter, American Society of Photogrammetry (1952). This instrument was capable of removing the errors due to tilt and lens distortion so that the orthographic contour positions bore the true spatial relationships. Twenty-five such cloud contour

charts were produced for each of the two days. An example of the contour chart is shown in Fig. 2.2. These contour charts served as the primary standard for scaling.

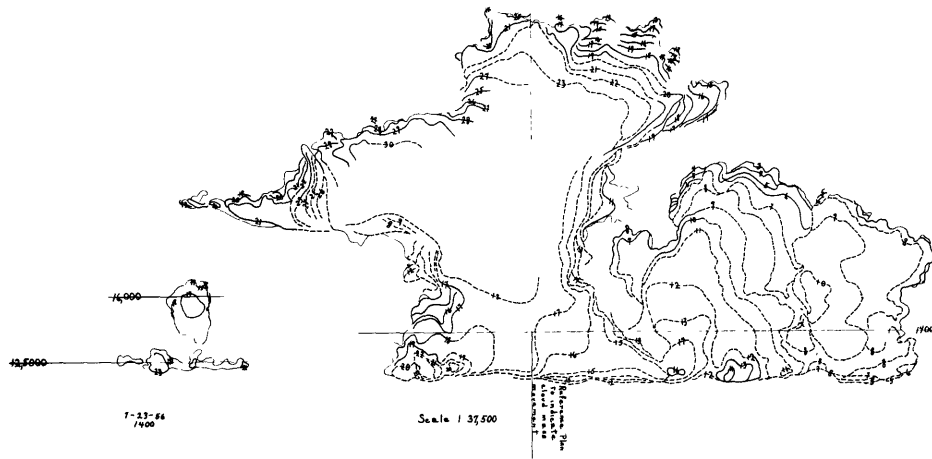


**Fig. 2.2 Cloud Contours**

The contour lines shown are at 1000 ft. intervals from an arbitrary reference plane behind the cloud. The numbers increase as the cloud extends toward the observer.

Since the very accurate contour charts were at two minute intervals only, the 16 mm motion picture film was used to fill in measurements at shorter times. The proper scale to use with the 16 mm projections was obtained from the contour charts. Three kinds of measurements were made from the raw data. The height of the cloud was measured and plotted as a function of time. The 16 mm time-height curve was fitted to the two minute curve to form a consistent body of data for every thirty seconds. The highest point on the cloud was the height used. The projected area of the cloud was measured at each time and converted into volume on the assumption that the clouds were

axially symmetric. Differences in volume were computed from the measurements and these were used for the volume flux. The third measurement was the plotting of the trajectories of noticeable cloud knobs or protuberances which seemed to move without much apparent change in shape. These protuberances deviated from the axis of the cloud as the cloud top moved upward and acted as tracers for the associated air flow.

From these three basic measurements, several quantities were derived. The velocity at the cloud top was computed from the time-height measurements. This velocity was plotted against time. Likewise, the volume was plotted against time as well as the change in volume against time and this latter quantity indicated the volume flux, or the strength of the flow versus time.

Any special features noticed during a cloud's development were documented by an appropriate qualitative description. Such features as the growth of anvil-like sheets from the cloud tops, unusual cloud shapes, and asymmetrical growth or evaporation occasionally occurred. In Section 2.4 the case history for each cloud is detailed.

## 2.2 Cloud Data

The sample is composed of two clouds on 23 July and three clouds on 24 July 1956. In Fig. 2.3 the Tucson RAOB is shown for 0800 local time, 23 and 24 July 1956. The lifting condensation level (LCL) was at 7,000 ft. m.s.l. and the level of free convection (LFC) at 13,000 ft. m.s.l. on the 0800 local sounding of the 23rd. The cloud base formed near 12,000 ft. which indicated that the air had been lifted to this height by the orographic heating effect of the mountains. On the 24th, the 0800 local sounding gave the LCL at 5,000 ft. m.s.l. and the LFC at

10,000 ft. The cloud base was near 10,000 ft. The winds aloft were light and from the northeast on both days which meant that any cloud drift would be towards the camera sites. The strongest winds were above 30,000 ft. and reached about 30 mph between 30,000 and 40,000 ft.

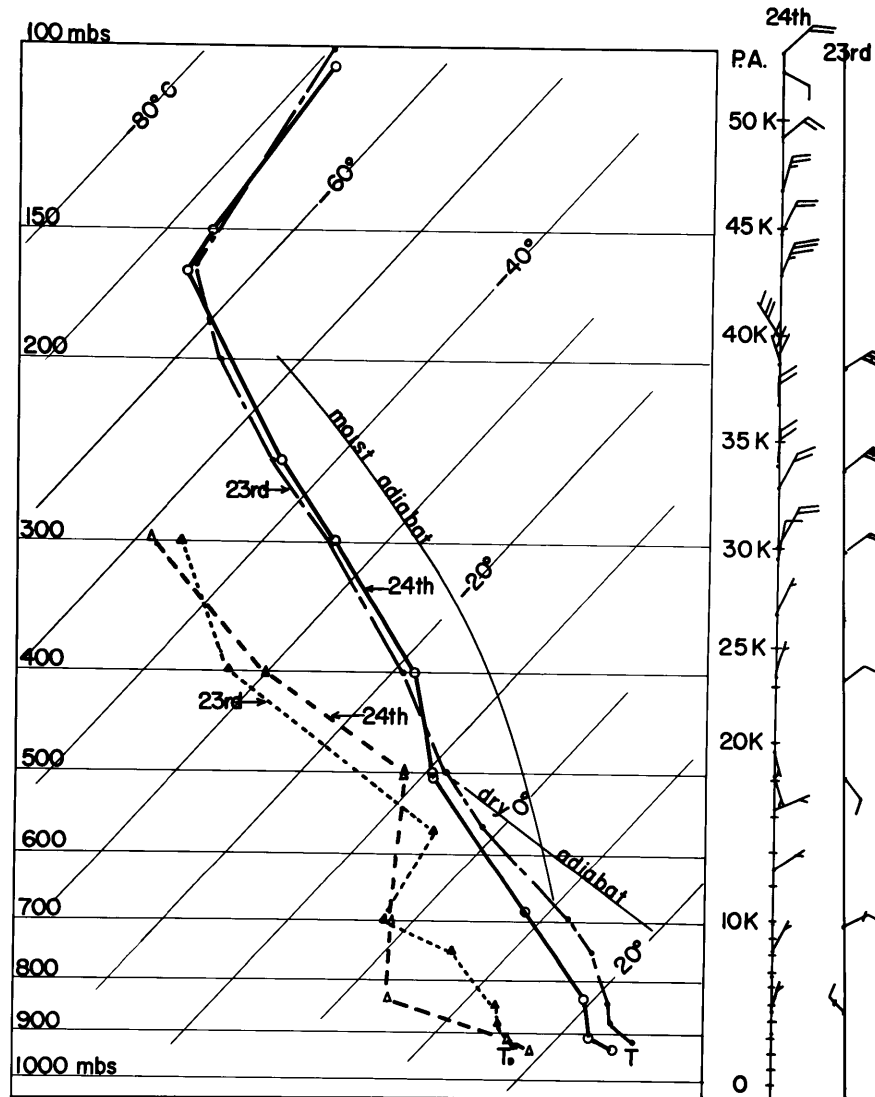


Fig. 2.3 Tucson RA0B, 1500Z (0800 local time)  
 The temperature soundings for the two days are indicated by the solid and broken lines and the corresponding dew point soundings by the dashed lines, each marked for the day by appropriate arrows.



The sounding on the 23rd was conditionally unstable, but the positive area was thin. No inversions were present until the tropopause was reached at 44,000 ft. The same general conditions continued on the 24th.

The winds aloft were light northeasterlies, as shown in Tables 2.1 and 2.2 for 1400 local time on the two days.

TABLE 2.1

Winds Aloft at Tucson, 23 July 1956

<u>Height (meters)</u>	<u>Direction (degrees)</u>	<u>Speed (m.p.s.)</u>
1,000	288	7
2,000	318	11
3,000	335	5
4,000	60	3
5,000	168	4
6,000	163	4
7,000	90	1
8,000	80	5
9,000	27	4
10,000	51	8
11,000	53	9
12,000	47	12
13,000	40	16

TABLE 2.2

Winds Aloft at Tucson, 24 July 1956

<u>Height (meters)</u>	<u>Direction (degrees)</u>	<u>Speed (m.p.s.)</u>
1,000	288	7
2,000	318	11
2,500	315	12
3,000	335	5
4,000	60	3
5,000	168	1
6,000	163	4
7,000	90	1
8,000	80	5
9,000	27	4
10,000	51	8
11,000	53	9
12,000	47	12
13,000	40	16
14,000	55	14

As a guide to the over-all cloud numbering system, Figs. 2.4 through 2.7 are sequences of photographs which illustrate the cloud groupings where the subject ones are identified by number.



Fig. 2.4 Cloud Sequence Photographs, 23 July 1956.  
The pictures are at two-minute intervals taken looking toward Mt. Lemmon from Tucson. The time shown on each plate is local time.



Fig. 2.5 Cloud Sequence Photographs, 23 July 1956, continued.

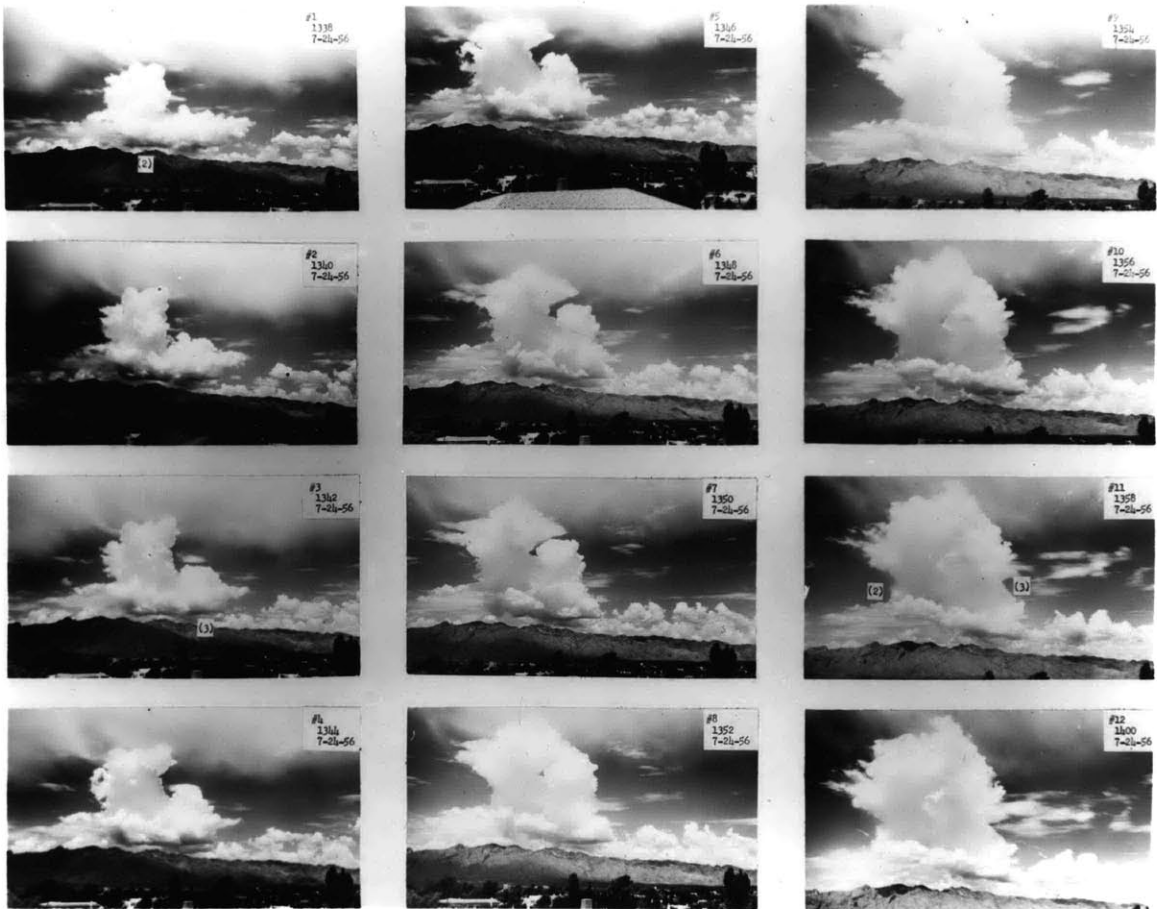


Fig. 2.6 Cloud Sequence Photographs, 24 July 1956.  
 The pictures are at two-minute intervals taken looking towards  
 Mt. Lemmon from Tucson. The time shown is local time.

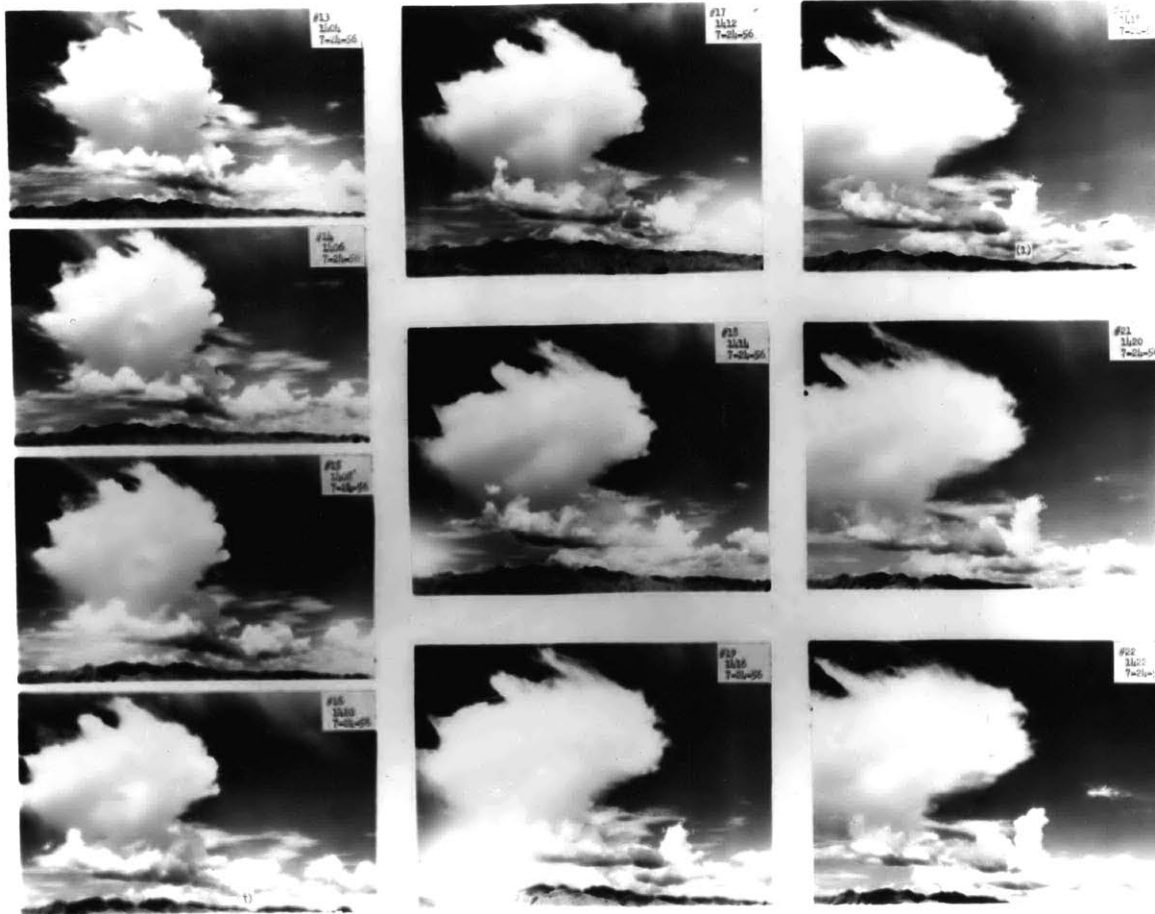


Fig. 2.7 Cloud Sequence Photographs, 24 July 1956, continued.

### 2.3 Discussion of the Observational Methods

The starting point for drawing inferences from observational data is a thorough realization as to just what are the data. Since the bulk of the observational material consisted of cloud photographs, it might be instructive to study for a moment the implication of this fact.

A photograph is a record of angular relationships among the objects in space which have made a light impression on the film. If the photograph is a metric photograph; i.e., one taken with a camera whose internal geometry is calibrated, one may make reliable measurements of these angles from the photograph. In this way, the true spatial relationships among the objects photographed may be recovered.

In the case of clouds, one captures on the film an image of the cloud boundary at a particular instant. On a succession of photographs, as in time-lapse photography, one captures the position of this boundary at different times. From the location of this interface, we can learn something about the size, the height, the inclination, and other macroscopic features of the cloud. By taking time derivatives of the position, various rates may be computed from the movement of the boundary. A cloud represents a region in space in which the condensed phase of water exists as an aerosol. The cloud-air boundary is the transition zone between saturated air and ambient air. If the boundary is advancing with time, it may be caused by: (1) the transport of cloudy air into previously cloud free air, which means a simultaneous retreat of the ambient air; (2) the extension of cloud forming forces into the ambient air which may bring about saturation conditions. Fortunately for growing cumuli, the upper boundary has a bumpy appearance. The

more prominent of these protuberances seem to retain some degree of identity over several minutes during which time their trajectories may be followed. The displacement appears to be accomplished through the bodily movement of cloudy air which previously lay inside the cloud in such a way that the bump remains attached to the cloud and forms part of its bounding surface. This point is illustrated by Fig. 2.8, a multiple exposure of a growing cloud, where considerable movement of easily identifiable elements is evident.



Fig. 2.8 A multiple exposure photograph of a growing cumulus congestus cloud. Courtesy of B. Vonnegut, A.D. Little Co.

We would like to use this property of growing cumulus clouds to learn something about the flow accompanying the growth. A path line

or trajectory may be constructed which is a record of the spatial position of the object at different times. A stream line is a line everywhere tangent to the instantaneous velocity vectors and is the line sought. A streak line, on the other hand, is the line joining the end points of trajectories at a particular instant which all passed through a common point in space at some earlier time. When the motion is steady; i.e., no time changes in the local velocity field, all three lines will be identical. When the motion is unsteady, all three lines will be different; e.g., Prandtl and Tietjens (1934). If the unsteady motion can be referred to a moving set of coordinates such that the local change in velocity is removed, the motion is steady to an observer moving with the coordinates.

When the trajectories of protuberances such as those shown in Fig. 2.8 are made for a growing cumulus cloud, two types of patterns are possible. The trajectories either will seem to originate from some common point within the cloud and the boundary moves as a radial displacement outwards from this center, or the trajectories seem to originate from a common line extending vertically. The line may have tilt, depending on the magnitude of the wind shear along the vertical.

The first category is called the stationary source. Here, the cloud seems to grow by swelling equally along radials from some common center. When a horizontal wind is present, some asymmetry will be introduced in the actual amount of radial displacement on the upwind and downwind sides. The downwind side will receive much greater displacement than the upwind side. The movement of the boundary will be similar to a tracer material in a pre-existent velocity field like that of



the upper hemisphere of a point source. The flow in this analogy may be conceived as air entering into the base of the cloud from below and diverging immediately into a hemispherical region. Since the local velocity remains fairly constant, the stationary source is an example of steady flow and the trajectories may be regarded as stream lines. In Fig. 2.9 the successive outlines of an actual growing cumulus are shown together with a few stream lines or trajectories as an example of the stationary source mode of growth. It is observed that although the position of the point source remained fixed during the time interval, the horizontal wind caused greater growth in the downwind direction.

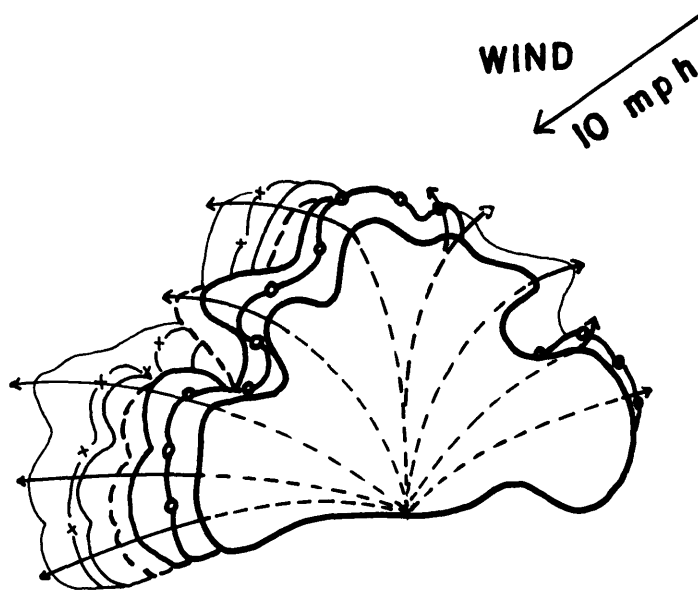


Fig. 2.9 Cloud Trajectories for a Stationary Source Mode of Growth. Outlines shown are for Cloud No. 1, 23 July 1956 between 1406 and 1409 at thirty second intervals.

The stationary source mode of growth seems to occur more with the earlier stages of cumulus development, although it is suspected that this mode is also responsible for the horizontal growth in large congestus clouds.

When one examines the trajectories for upward thrusting towers or turrets, they seem to originate from a common line along the vertical. An example of turret growth is shown in Fig. 2.10. Here, the trajectories are not simultaneous, since the lower ones occur earlier than the upper ones.

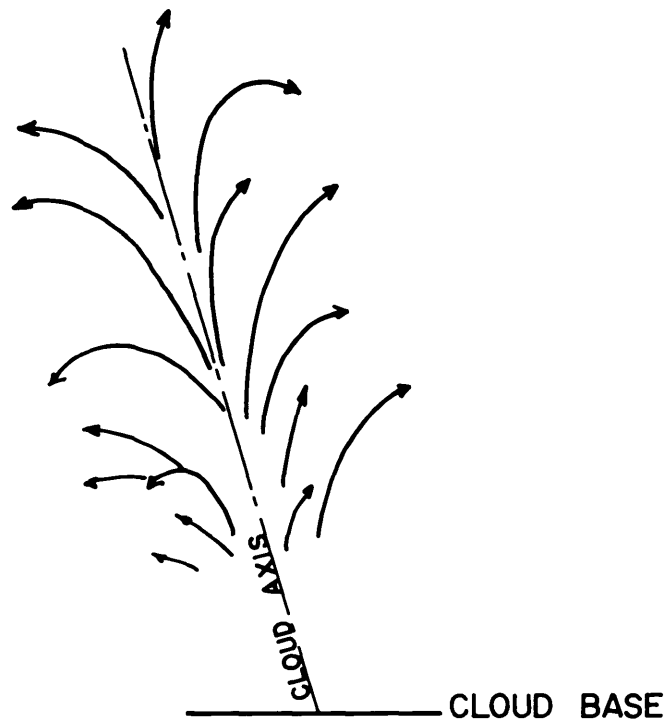


Fig. 2.10 Trajectories for a Growing Cumulus Tower.  
Data taken from Cloud No. 3, 23 July 1956  
between 1340 and 1350 hours.

The pattern of trajectories resembles the one which would be generated if a stationary source were moved vertically. For this reason, this second mode of growth is called the flow due to a moving source. In order to generate the stream lines from the trajectories of this mode of growth, a velocity field equal and opposite to the apparent velocity of vertical translation is superimposed on the moving source which then transforms the motion into the steady case. The trajectories, stream lines, and streak lines are identical for the transformed motion. The well-known hydrodynamical example of this type of flow is shown in Fig. 2.11.

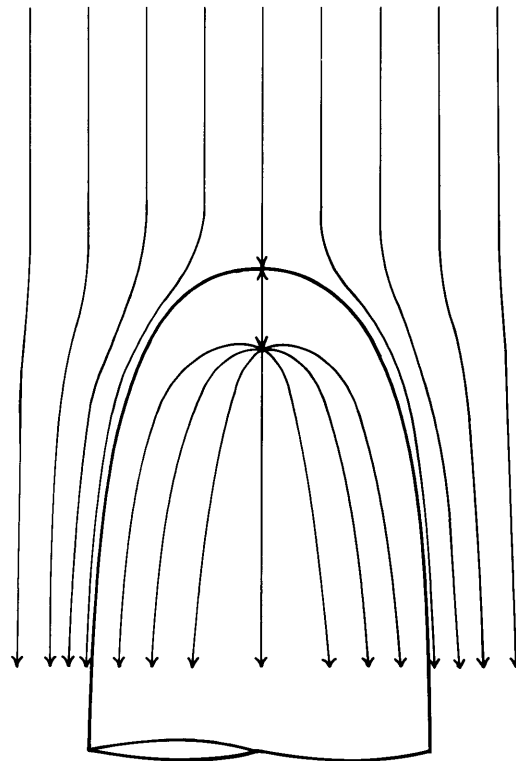


Fig. 2.11 The Stream Lines for a Simple Point Source in a Uniform Stream. The solid line marks the material boundary between source fluid and stream fluid and generally is referred to as the dividing stream line.

In Fig. 2.11, a fictitious point source of volume exists at the origin and would tend to spread radially in three dimensions. However, the source is placed in a uniform stream which alters the stream lines to yield the shapes as shown. The solid line in the figure is called the dividing stream line since it separates the fluid in the uniform stream from that emitted by the source. In this sense, it is a material boundary and there is a tangential component only of the local velocity at this boundary with no material transport across it. Hence, the dividing stream line is the same type of boundary as the cloud-air interface and is the analog of the streak line for the unsteady case. To prove this similarity, various positions which made up the trajectories shown for the growing tower similar to Fig. 2.10 were reduced to the steady case by subtracting the average vertical velocity of the tower. The result is given in Fig. 2.12. Now, all the trajectory points lie on a common line or dividing stream line, very similar in shape to that in Fig. 2.11. It is clear that to generate a cloud shape in the form of a tower or turret, some type of flow which resembles a moving source is involved.

As will be seen in Section 2.4, when the vertical velocity is computed from successive height-time measurements, a widely varying vertical velocity is obtained for the upward movement of the cloud boundary. The computed velocity is the time averaged value (thirty seconds) for the time between successive positions of the cloud tops. Since the cloud top changes its position by the movement of cloud air into previously ambient air, the velocity computed is the average over thirty seconds for the parcel of air which happens to be at the cloud top.

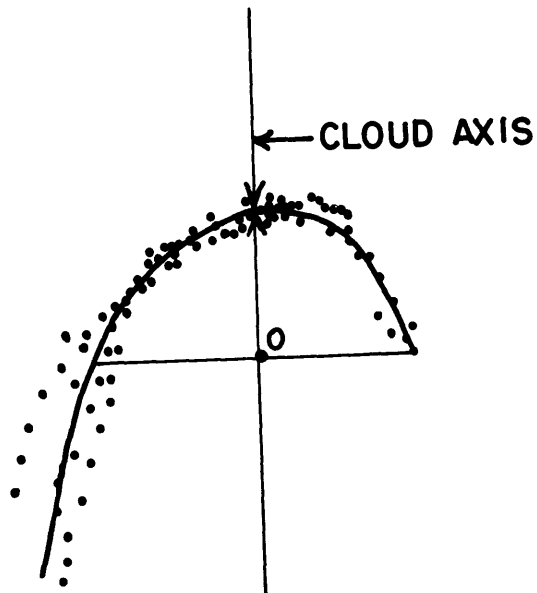


Fig. 2.12 The relative points of the trajectories for a growing cumulus tower.

For a parcel which lies very close to the vertical axis of the cloud, it will remain the highest point and can be followed for several minutes. In this case, we are measuring clearly the particle velocity of cloud air at the cloud top. This velocity will vary from minute to minute. After a few minutes, the parcel of cloud at the cloud top will begin to deviate from a strictly vertical path and will be deflected in a manner as shown in Fig. 2.11. Its position with respect to the cloud top will continue to shift down and outward until it is apparently at rest and forms a portion of the outer surface of the cloud tower. Meanwhile, another parcel occupies the cloud axis for

several minutes and its velocity is measured. By always making the measurement of vertical velocity as close to the vertical axis as possible, it is felt that such velocities are representative of the instantaneous (averaged over the time between successive measurements) vertical velocity of the cloud air at the position in space where the measurement was conducted. Let  $w(t,z)$  be the local air velocity anywhere along the vertical axis at any time. The velocity computed for the moving cloud top is a total velocity,  $W$ .

The change in the total velocity with time for a fluid at the vertical axis may be represented by the sum of the local change plus

$$\frac{dW}{dt} = \frac{\partial W}{\partial t} + w \frac{\partial W}{\partial z}$$

the advective change for each different particle being followed. To have a flow where the time behavior is independent of position, the advective contribution to the total flow has to be small enough so that

$$\frac{dw}{dt} = \frac{\partial w}{\partial t} .$$

For this condition, it does not matter where on the axis of the fluid the velocity is measured; different particles may be observed at different times, and these observations may be combined to form a continuous time series. A growing cumulus cloud will be expected to have connected flow over considerable distance so a reasonable assumption is to take the advective contribution to the observed vertical velocities as small. This condition certainly applies below and near the cloud base; no momentum transport takes place through the earth's

surface. The striking evidence of Vonnegut et al (loc. cit.) suggests that simultaneous changes also occur at different levels in a large cumulus congestus. Finally, in a linearized treatment the advective term would be dropped. For these reasons, it will be assumed in this study that the measured change in velocities at the cloud top may be interchangeably interpreted as either total or local vertical accelerations. Another way of expressing this argument is to view the fluctuations in measured vertical velocities as deviations from a longer time average (say ten minutes) vertical velocity which would represent the average translation upward of the cloud boundary. Hence, relative to the cloud boundary, the fluctuations may be regarded as local accelerations. Since the height of the cloud boundary is unspecified, this definition requires also that the advective contribution to the acceleration be negligible.

The analogy between the trajectories and external appearance of cumulus towers with hydrodynamical sources suggests this concept may be useful in describing the intensity of growth. Utilizing this concept, we may describe the intensity in terms of the production of new cloud volume per unit time, or the volume flux. For a three-dimensional source, the output or emission rate,  $M$ , is defined as:

$$M = 4 \pi m \quad (2.1)$$

where  $m$  is the intrinsic flux or strength of the source (Milne-Thomson, 1950).

One may use either the output or the strength to define the intensity of growth. The output may be measured in two ways: by the

rate of increase of apparent cloud volume obtained by direct measurement from the orthogonal projection of the cloud outlines; or calculated from the strength as defined in (2.1) wherein the strength is defined as:

$$m = \frac{w d^2}{4} \quad (2.2)$$

and

$$1.5 w d^2 = M \quad (2.3)$$

$d$  = measured diameter of the cloud cap,

$w$  = rate of outward growth of the boundary, preferably along the vertical axis.

When  $M$  is obtained from the change in cloud volume,  $V$ :

$$\frac{d V}{d t} = M, \quad (2.4)$$

it is identical with the flux of volume where the flux is the rate of transport across some fixed surface. Hereafter, volume flux and output are considered the same, which implies there are no sinks in the region under consideration.

Since the clouds grow by taking air through the base, Equation (2.1) should be modified to correspond to a hemispherical source, or some close geometrical similarity. Hence, a better approximation is:

$$M = 2 \pi m. \quad (2.5)$$

The flux has been measured by methods of Eq. (2.3) and Eq. (2.4) on the same data and found to agree within reasonable limits.



A note of caution should be observed when working with actual cloud data. The measured flux will vary from moment to moment even for well defined cloud shapes. If one wishes to test the validity of the relationships between strength and output for cumulus clouds, time averaged data may be better; that is, averaged over a five-minute or so interval. A rapidly growing cumulus tower is perhaps the most unambiguous form to use and here one can with confidence assume cylindrical symmetry in order to compute cloud volumes. These towers are marked by a rounded cap which many times allows the over-all tower to take on the outline of a semi-paraboloid. It is necessary to be able to fit the projected cloud cross section with some figure of revolution before volume computations are possible. We have used hemispheres, paraboloids, ellipses, cylinders, or portions thereof in our work. The direct flux measurement works equally well or poorly for either mode of growth but the strength method of Eq. (2.3) is more suitable to growing towers (moving sources) than to stationary sources.

Typical values of volume flux range from  $10^8$  ft<sup>3</sup>/min for small cumuli to  $10^{12}$  ft<sup>3</sup>/min for congestus. A cell in a thunderstorm very possibly would exceed  $10^{13}$  ft<sup>3</sup>/min, although we have no measurements as yet.

The volume flux is a valuable parameter since it may be used to compute the flux of other properties, provided their specific concentration is known. For example:

$$\text{Mass flux} = \text{density} \times \text{volume flux} = \frac{\text{gm}}{\text{sec}},$$

$$\text{Kinetic energy flux} = \frac{\text{k.E.}}{\text{cm}^3} \times \text{volume flux} = \frac{\text{k.E.}}{\text{sec}}, \text{ etc.}$$

It is to be noted that flux, as used here, differs from unit flux which is the flux per  $\text{cm}^2$  of surface, or,

$$M = \int_s \text{unit flux } d s \quad (2.6)$$

where  $s$  = surface area.

#### 2.4 The Case Histories of Five Cumulus Clouds Observed near Tucson, Arizona

The winds aloft at Tucson on 23 July 1956 were very light and variable up to 7 km. Above 7 km the winds were moderate from the northeast. The winds aloft are given in Table 2.1. The RAOB (Fig. 2.3) indicated the level of free convection to be near 13,000 ft m.s.l. which was near the actual cloud base.

Cloud No. 1 formed over the southern slope of Lemmon Mountain just to the west of Marshall Gulch. The cloud drifted SE for about two miles as it grew (Fig. 2.13). Some ten minutes earlier, a cloud formed, grew, and dissipated by 1400 hrs. in the same vicinity where Cloud No. 1 formed. From Fig. 2.4 and Fig. 2.5, Cloud No. 1 is seen to grow as a towering cumulus and to die with the base disappearing.

The basic measurements of height and volume together with the derived vertical velocity and flux are listed in Table 2.3. The starred quantities are interpolated values. During the early stages of its growth, the expansion resembled that due to a fixed point source and is shown in Fig. 2.9. The height, vertical velocity, volume, and flux values are plotted against time in Figs. 2.14 through 2.17. In Fig. 2.14, it may be seen how the 16 mm data were fitted to the 9 x 9 inch

data to form a consistent set of measurements at every 30 seconds until 1416:30. After the initial radial growth, the cloud grew rapidly and then decayed with an actual sinking at the end.

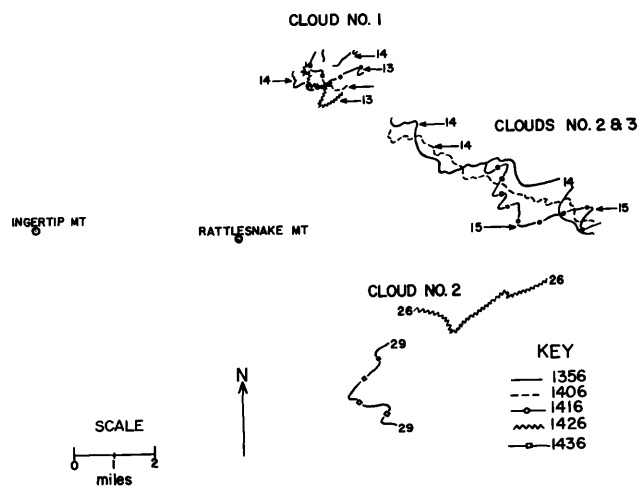


**Fig. 2.13 Cloud Movements, 23 July 1956.**  
The successive positions of the leading edges of the clouds are shown for a horizontal plane at 12,000 ft.

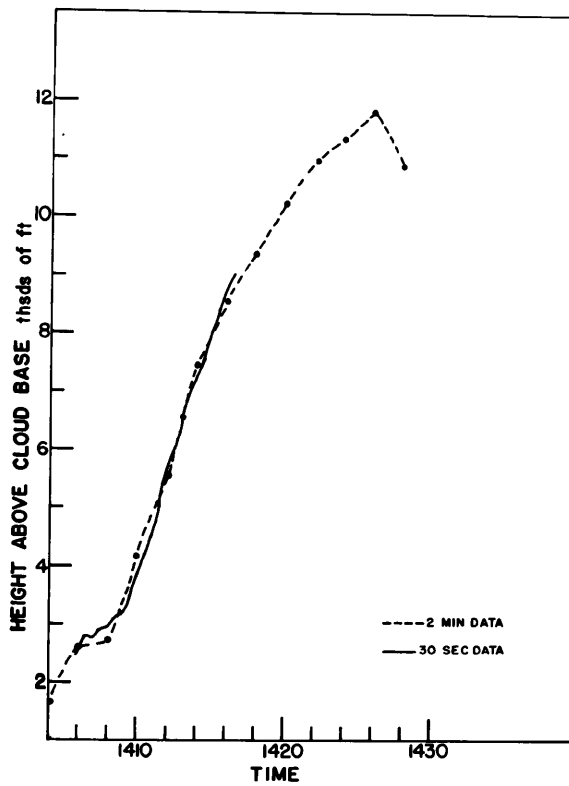


Fig. 2.14 Height Versus Time for Cloud No. 1, 23 July 1956.  
 The two-minute data were obtained from the 9 x 9  
 stereo photographs and the 30 second data  
 from the 16 mm time lapse film.

TABLE 2.3

Basic Measurements, Cloud No. 1, 23 July 1956, Tucson

<u>Time</u>	<u>Height Above Base</u> (10,135 ft)		<u>Velocity</u>		<u>Volume</u>	<u>Flux</u>
	30 sec. Data	2 min. Data	30 sec. Data	2 min. Data	ft <sup>3</sup> x 10 <sup>10</sup>	ft <sup>3</sup> x 10 <sup>10</sup> min.
1402:00					.59	
1403:00						.24
1404:00		1600			1.06	
:15						
:30						
:45						
1405:00		2092*		492		.3
:15						
:30						
:45						
1406:00	2477	2584			1.66	
:15	2636*		634			
:30	2794					
:45	2779*		-60			
1407:00	2764	2646*		61.5		1.24
:15	2845*		324			
:30	2926					
:45	2924*		-10			
1408:00	2921	2707			4.14	
:15	3015*		376			
:30	3109					
:45	3130*		82			
1409:00	3150	3445*		738		0
:15	3332*		730			
:30	3515					
:45	3701*		742			
1410:00	3886	4183			4.14	
:15	4037*		602			
:30	4187					
:45	4352*		658			
1411:00	4516	4860*		676.5		1.54
:15	4785*		1076			
:30	5054					
:45	5343*		1154			
1412:00	5631	5536			7.22	
:15	5803*		690			
:30	5976					
:45	6281*	6490*	1222			

TABLE 2.3 (Contd.)

<u>Time</u>	<u>Height Above Base</u> (10,135 ft)		<u>Velocity</u>		<u>Volume</u> ft <sup>3</sup> x 10 <sup>10</sup>	<u>Flux</u> ft <sup>3</sup> x 10 <sup>10</sup> min.
	30 sec. Data	2 min. Data	30 sec. Data	2 min. Data		
1413:00	6587			953.5		2.49
:15	6768*		726			
:30	6950					
:45	7092*		570			
1414:00	7235	7443			12.20	
:15	7390*		618			
:30	7544					
:45	7777*		932			
1415:00	8010	7997*		554		-.11
:15	8196*		744			
:30	8382					
:45	8570*		752			
1416:00	8758	8551			12.00	
:15	8890*		528			
:30	9022					
:45						
1417:00		8951*		400		19.7
1418:00		9350			51.40	
1419:00		9781*		431		22.3
1420:00		10,212			96.00	
1421:00		10,581*		369		-33.35
1422:00		10,950			29.30	
1423:00		11,135*		185		-.15
1424:00		11,319			29.0	
1425:00		11,811*		492		-17.0
1426:00		12,303			12.0	
1427:00		11,565*		-738		
1428:00		10,827				

The rapidly fluctuating nature of the vertical velocity is brought out clearly in Fig. 2.15. This highly oscillatory behavior is a characteristic of fast growing cumulus towers. In the figure, a smoothed curve has been drawn using the envelope method described by Manley (1945). The smoothed curve would correspond to a running mean which removes the higher frequencies to reveal the very interesting low frequency component. The start of the low frequency cycle is near 1406 hours, which marks the minimum of the preceding cloud cycle. Only one growth cycle was experienced by Cloud No. 1 as it seemed to consume itself by the vigor of its growth.

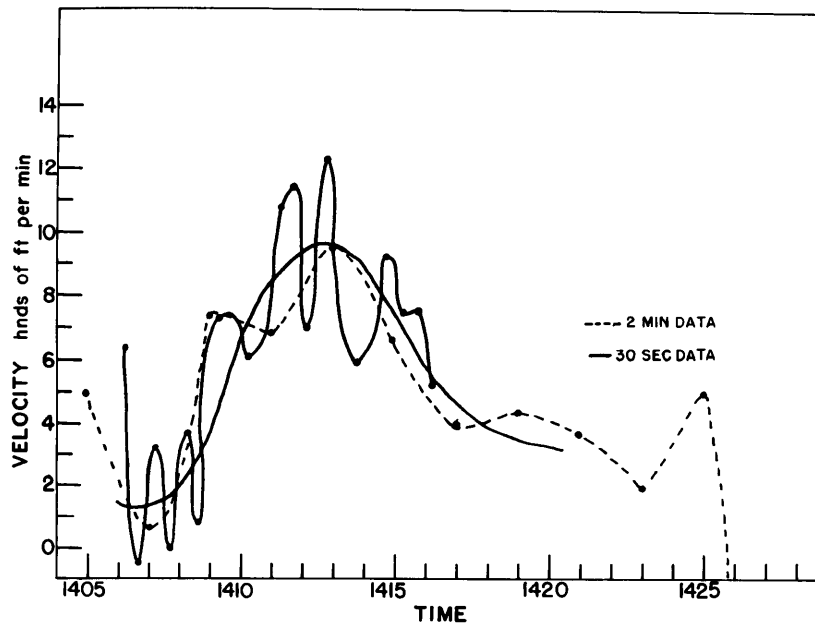


Fig. 2.15 The Vertical Velocity versus Time, Cloud No. 1, 23 July 1956.

In Figs. 2.16 and 2.17, the volume and flux curves are displayed. As shown, the volume increased very sharply around 1417 hours to a value almost an order of magnitude higher than before. This large increase was preceded by a jump in the flux near 1415 hours which peaked near 1420 hours. It is interesting that the period of maximum flux lags the time of maximum vertical velocity by 5-6 minutes. Careful watching of the 16 mm time lapse film revealed that a large mass of cloud growing to the left base of the subject cloud (Plate No. 9,

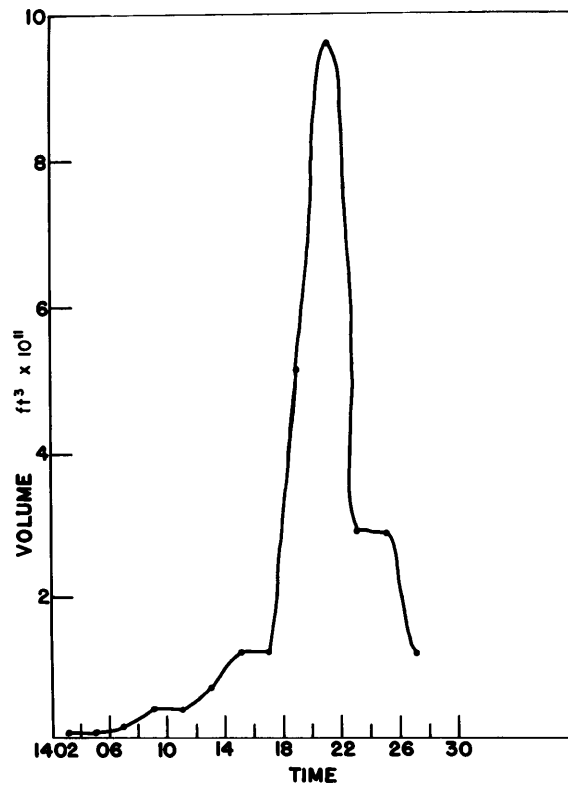


Fig. 2.16 Volume versus Time for Cloud No. 1,  
23 July 1956.



Fig. 2.4) was added wholly to Cloud No. 1 starting around 1414 hours which was about one minute after the cloud had reached its peak velocity.

As this was taking place, the entire column thickened considerably and the cloud volume and flux spurted to high values (Plates 11 and 12, Fig. 2.4). Thus, it appears that, although the velocity field may respond instantaneously and throughout the cloud as suggested in Section 2.3, mass transport requires a finite interval of time.

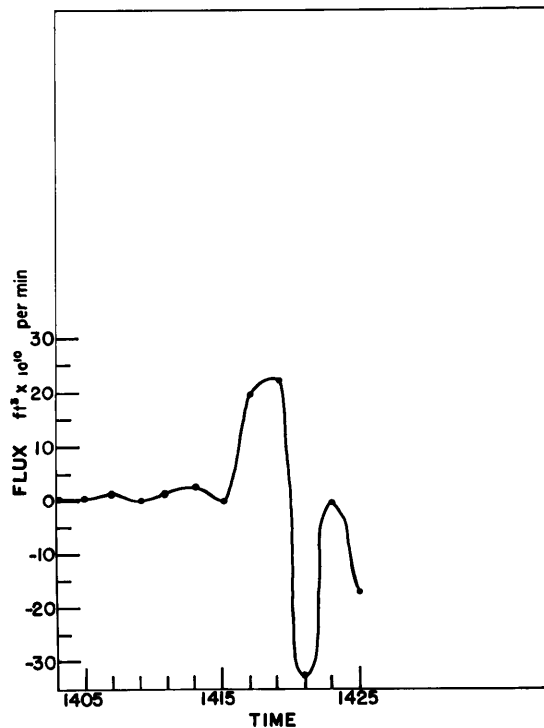


Fig. 2.17 Flux versus Time for Cloud No. 1,  
23 July 1956.

The symmetry of the rise and fall (Fig. 2.15) velocities for the smoothed curve about the maximum is similar to the symmetry reported by Workman and Reynolds (1949) for the rise and fall of cumulus towers. There was a slight indication of the start of another cycle around 1425 but the cloud decayed rapidly after that time, with the stem evaporating entirely by 1430 hours. A new cloud appeared at 1432 in the approximate position previously occupied by Cloud No. 1 but it did not develop beyond a small cumulus humilis.

#### Cloud No. 3 - 23 July 1956

Cloud No. 3 developed over the more gentle slopes to the southwest of Kellogg Peak and northwest of Sycamore Park (Fig. 2.1). Sixteen mm time-lapse cine film was the only record available on its growth from 1335 to 1356 hours when the 9 x 9 inch stereo photographs commenced (Figs. 2.4 and 2.5). The cloud became a cumulus congestus by 1356 and yielded precipitation after 1408 hours. In the late stages of its development there was considerable horizontal spread in the upper portion to form an anvil-like appearance (Plates 2 through 22, Figs. 2.4 and 2.5). After about 1400 hours, the vertical development ceased and the top subsided. However, the mass continued to spread horizontally, anvil-like in its upper portions. A nearby cumulus congestus (Plate 7, Fig. 2.4), labeled No. 2, grew and merged with the fibrous looking mass remaining of Cloud No. 3 after 1406 hours, making it impossible to separate the two. The measurements were discontinued after 1401 hours because of the indistinctness of the cloud mass.

The basic measurements are given in Table 2.4. Again the starred heights indicate interpolated values to correspond to the vertical velocity obtained every thirty seconds by the averaging procedure. The trajectories of various bumps which first appeared near the cloud axis are shown in Fig. 2.18. The effect of the horizontal wind is evident in the slanted cloud axis. The trajectories illustrate very well the concept of a moving source described in Section 2.3.

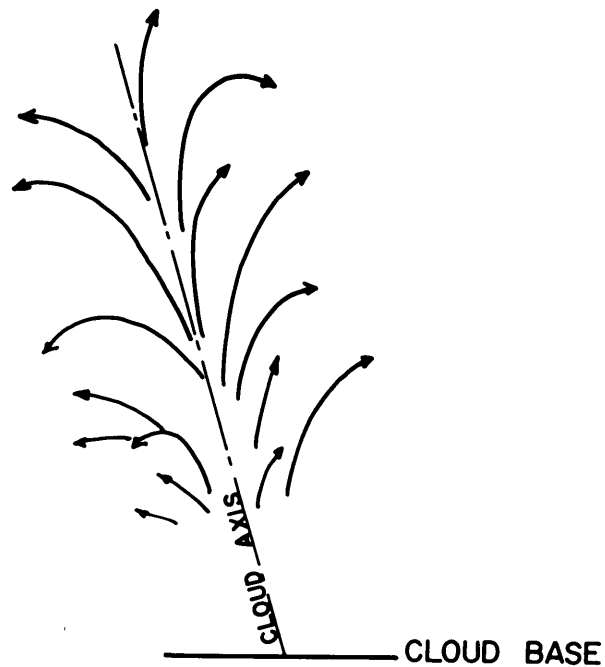


Fig. 2.18 Trajectories of Cloud Elements  
for Cloud No. 3, 23 July 1956.

TABLE 2.4

Basic Measurements, Cloud No. 3, 23 July 1956, Tucson

<u>Time</u>	<u>Height (Above Cloud Base)</u> 11,300 ft	<u>Velocity</u> ft/min.	<u>Volume</u> ft <sup>3</sup> x 10 <sup>-10</sup>	<u>Flux</u> ft <sup>3</sup> x 10 <sup>-10</sup> min.
1335:30	4,888			
:45	5,018*	520		
1336:00	5,148			
:15	5,304*	624		
:30	5,460			
:45	5,590*	520		
1337:00	5,720			
:15	5,852*	528		
:30	6,136			
:45	6,240*	416		
1338:00	6,344			
:15	6,552*	832		
:30	6,760			
:45	6,916*	624		
1339:00	7,072		.021	
:15	7,254*	728		.156
:30	7,436		.099	
:45	7,540*	416		.222
1340:00	7,644		.210	
:15	7,774*	520		.56
:30	7,904		.490	
:45	8,054*	600		.40
1341:00	8,216		.690	
:15	8,370*	312		.74
:30	8,424		1.06	
:45	8,450*	104		1.00
1342:00	8,476		1.56	
:15	8,500	936		1.88
:30	8,632		2.50	
:45	8,740	1,456		3.46
1343:00	9,204		4.23	
:15	9,438*	936		2.02
:30	9,672		5.24	
:45	9,932*	1,040		4.20
1344:00	10,192		7.10	
:15	10,504	1,248		4.80
:30	10,816		9.50	
:45	11,232*	1,664		5.20

TABLE 2.4 (Contd.)

<u>Time</u>	<u>Height (Above Cloud Base)</u> 11,300 ft	<u>Velocity</u> ft/min.	<u>Volume</u> ft <sup>3</sup> x 10 <sup>10</sup>	<u>Flux</u> ft <sup>3</sup> x 10 <sup>10</sup> min.
1345:00	11,648		12.1	
:15	11,908*	1,040		2.8
:30	12,168		13.5	
:45	12,428*	1,872		4.0
1346:00	12,688		15.5	
:15	13,182*	1,976		5.6
:30	13,676		18.3	
:45	14,118*	1,768		5.8
1347:00	14,560		21.2	
:15	15,002*	1,768		10.0
:30	15,444		26.2	
:45	15,678*	936		5.6
1348:00	15,912		29.0	
:15	15,964*	1,040		11.0
:30	16,432		34.5	
:45	16,796*	1,456		16.4
1349:00	17,160		42.7	
:15	17,368*	832		5.4
:30	17,576		45.4	
:45	17,862*	1,144		10.8
1350:00	18,148		50.8	
:15	18,304*	624		18.4
:30	18,460		60.0	
:45	18,512*	208		18.2
1351:00	18,564		79.1	
:15	18,538*	-104		12.8
:30	18,512		85.5	
:45	18,434*	-312		3.0
1352:00	18,356		86.0	
:15	18,252*	-416		4.6
:30	18,148		88.3	
:45	18,018*	-520		-4.8
1353:00	17,888		85.9	
:15	17,810*	-312		-6.4
:30	17,732		82.7	
:45	17,940*	832		17.4
1354:00	18,148		91.4	
:15	18,252*	416		9.8
:30	18,356		96.3	
:45	18,564*	832		16.8

TABLE 2.4 (Contd.)

<u>Time</u>	<u>Height (Above Cloud Base)</u> 11,300 ft	<u>Velocity</u> ft/min.	<u>Volume</u> ft <sup>3</sup> x 10 <sup>10</sup>	<u>Flux</u> ft <sup>3</sup> x 10 <sup>10</sup> min.
1355:00	18,772		104.7	
:15	18,928*	624		14.6
:30	19,084		112.0	
:45	19,266*	728		13.6
1356:00	19,448		117.8	
:15	19,552*	416		17.4
:30	19,656		126.5	
:45	19,682*	104		21.8
1357:00	19,708		137.4	
:15	19,760*	208		29.4
:30	19,812		152.1	
:45	19,812*	0		15.4
1358:00	19,812		159.8	
:15	19,864*	208		16.2
:30	19,916		167.9	
:45	19,994*	312		23.0
1359:00	20,072		179.4	
:15	20,150*	312		17.4
:30	20,228		188.1	
:45	20,306*	312		24.2
1400:00	20,384		200.2	
:15	20,488*	416		33.0
:30	20,594		216.7	
:45	20,672*	312		30.2
1401:00	20,748		231.8	
:15	20,696	-208		
:30	20,644			

The height-time curve (Fig. 2.19) shows three cycles during the active period of growth. The first two occurred while the whole cumulus was developing into a cumulus congestus, while the third (after 1350 hours) is the upward growth of a smaller turret from the main cloud mass. During this last cycle, the main mass appears to be involved in the horizontal spreading effort which produced the anvil-like shape the cloud took on after 1356 hours.

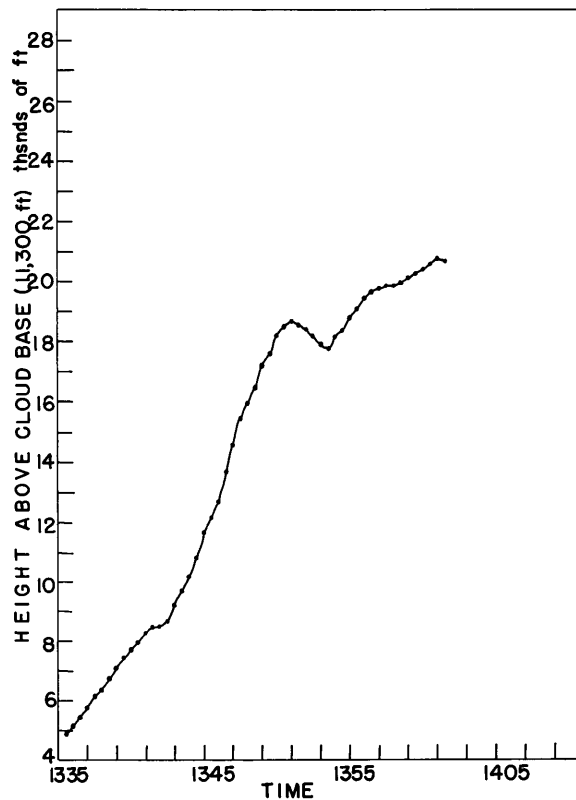


Fig. 2.19 Height of Cloud Top versus Time.  
Cloud No. 3, 23 July 1956.

The vertical velocity curve (Fig. 2.20) bears out the existence of three major cycles of growth, each lasting nearly ten minutes. Superimposed on these longer period oscillations are high frequency components evidenced by the rapidly fluctuating trace. During the first two cycles, the whole cloud appears to be involved in upward development and it is interesting to observe that the second cycle has a much larger mean value than the first. This feature is repeated in the growth of large cumulus congestus on the following day.

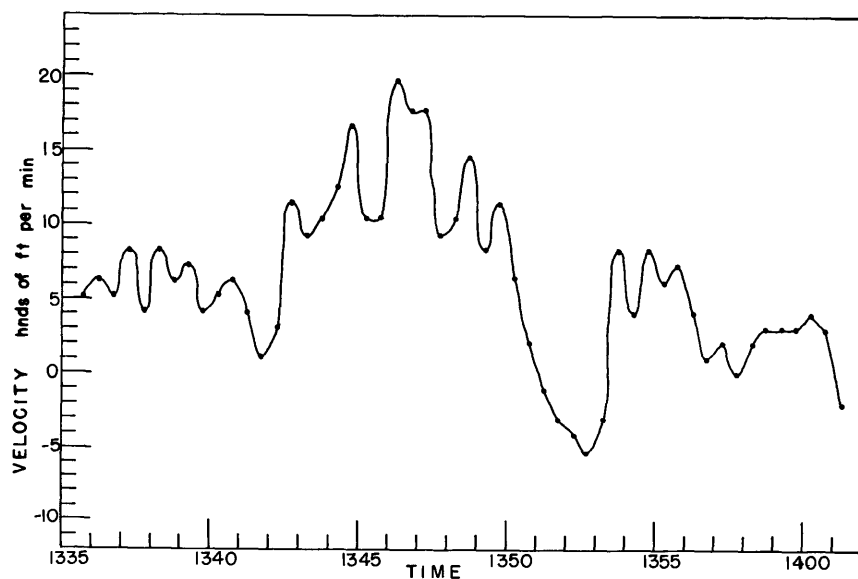


Fig. 2.20 Vertical Velocity versus Time.  
Cloud No. 3, 23 July 1956.



The third cycle is associated with the smaller turret which developed after the main cloud mass had ceased its upward growth. After rising at a high rate, the entire turret developed a negative velocity so that its oscillation was more nearly about a mean of zero; whereas, the first two cycles showed a net positive vertical motion, increasing with time. The volume-time curve exhibits a steady growth except for a pause around 1353 hours. Although the main cloud mass ceased its

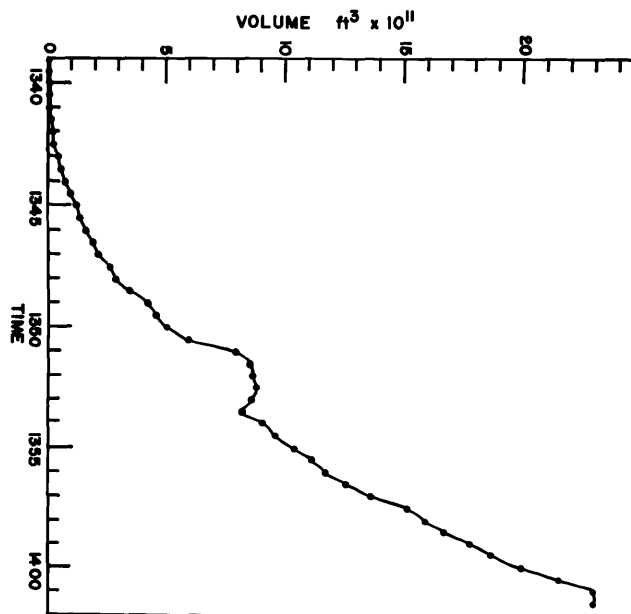


Fig. 2.21 Volume-Time Curve for Cloud No. 3,  
23 July 1956.

upward motion after 1350 hours, the volume continued to increase up to 1400 hours. This increase was due to the horizontal development of the cloud mass.

The flux-time curve (Fig. 2.22) reveals that the flux also increases with time at a fairly constant rate except for the negative dip around 1353 hours. Until the cloud merges with Cloud No. 2, the impression is gained that this large cumulus congestus was increasing its strength as it grew larger, and this increase took place in a linear fashion from the trend shown in Fig. 2.22.

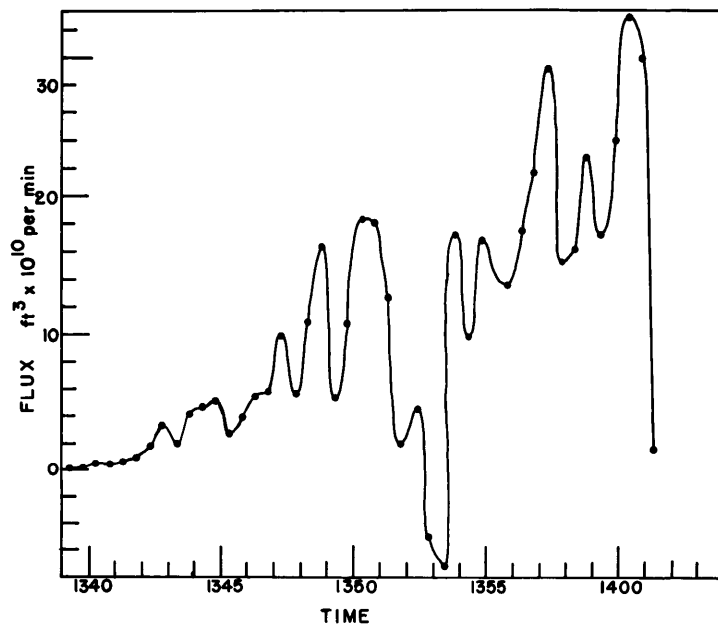


Fig. 2.22 Flux-Time for Cloud No. 3, 23 July 1956.

The RAOB for the next day, 24 July 1956, indicated the lifting condensation level to be at 10,000 ft. The actual cloud base was near 10,000 ft. The winds aloft (Table 2.2) were light and northeasterly. On this day, three good examples of cumulus growth were studied and these are labeled Clouds No. 1, No. 2, and No. 3. The location and movement of these three are given in Fig. 2.23.

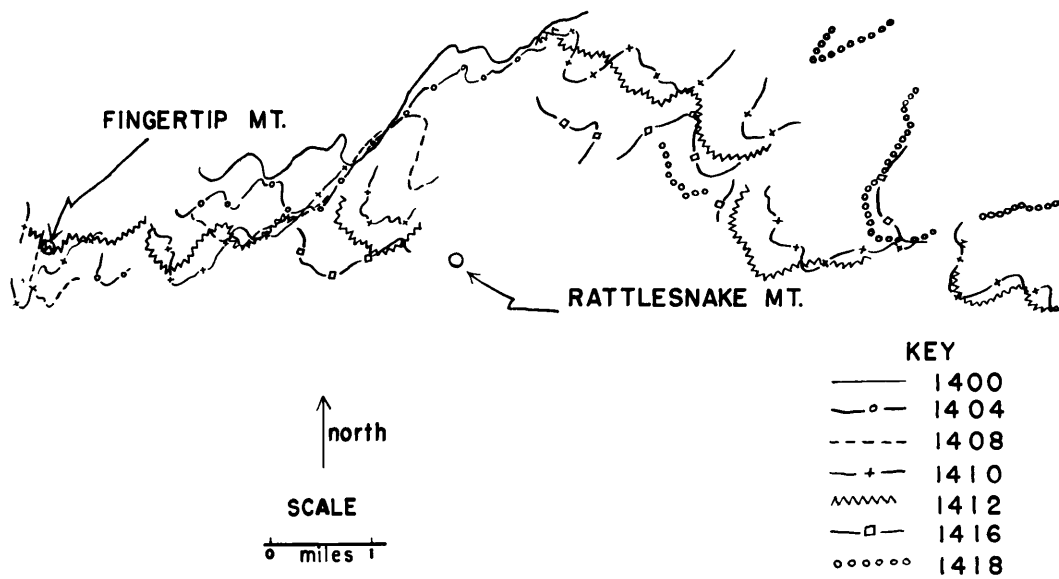


Fig. 2.23 Horizontal Positions of Clouds Observed on 24 July 1956.

Cloud No. 1 - 24 July 1956

This was the most perfect example of cumulus tower formation in the entire sample. It made its appearance from a moderate sized swelling cumulus which had put up two short towers previously, around 1400 hours, Plate No. 12 (Fig. 2.6). Some ten minutes later, a noticeable swelling appeared on the upper surface (Plate No. 16, Fig. 2.7) which became a bulging tower by 1412 (Plate No. 17, Fig. 2.7). From 1412 until 1422 hours the tower grew almost straight up and maintained about the same cross section during its growth. Although the later stages of its cycle are not shown, the cloud ceased its upward penetration by 1425 hours and dissipated afterwards. The dissipation was evident first at the lower portion of the stem and the stem decayed from bottom to top. The last vestige of the cloud was the uppermost portion which drifted unattached in the wind field.

There was no indication of any residual motion in the tower top while the stem was decaying. Occasionally, a top will spread horizontally before all motion ceases.

From the ground position (Fig. 2.23) it appeared that the parent cloud grew over a minor peak 7,073 ft high, some  $3\frac{1}{2}$  miles west of Mt. Lemmon. A little SW drift in the direction of Rattlesnake Peak accompanied the growth of the tower. At most, the cloud drifted one mile.

The trajectories of elements at the growing cloud top are given in Fig. 2.24. The presence of the horizontal wind is believed to be responsible for the extreme asymmetry of the trajectories. Very little

growth is evident on the upwind side, whereas long trajectories occurred on the downwind side of the tower. The fact that the trajectories were very short on the upwind side lends substantiation to the analogy between a moving source and growing cumulus towers. In each case the velocity decreases radially from the axis and this decrease is evident in Fig. 2.24, where the velocity of the radial component soon is balanced by the wind on the upwind side and is reinforced by the horizontal wind on the downwind side.

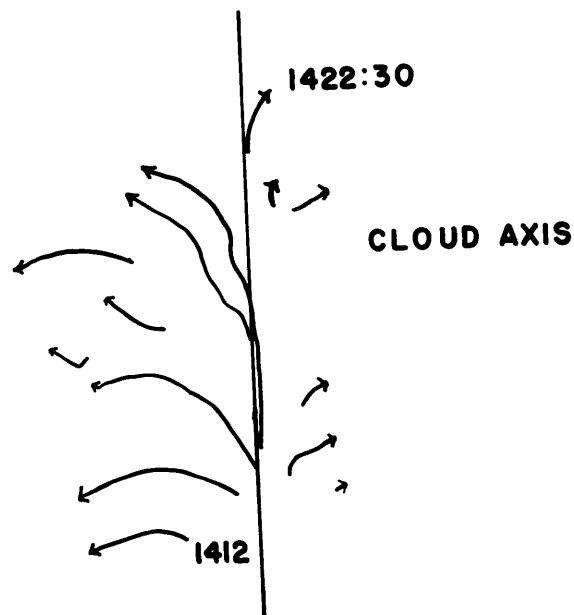


Fig. 2.24 Trajectories of Cloud Elements for Cloud No. 1, 24 July 1956.

The basic measurements for Cloud No. 1 are given in Table 2.5. The corresponding curves for the time variation of height, vertical velocity, volume, and flux are shown by Figs. 2.25, 2.26, 2.27, and 2.28, respectively. The development of this cloud was achieved as a sudden burst of vertical motion which reached its peak and decayed in an asymptotic manner. The time-height curve indicates a leveling off at the end but this is due to the over-all decay of the cloud column as an abrupt cessation of growth throughout.

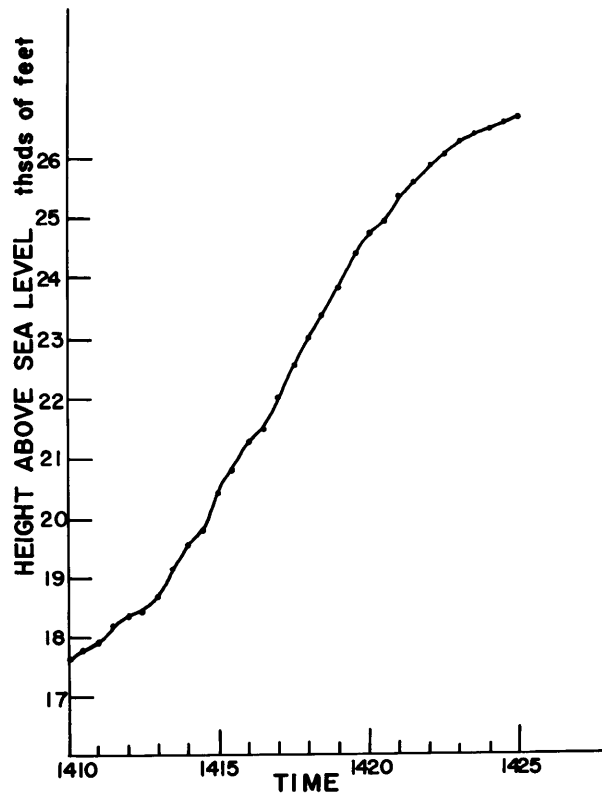


Fig. 2.25 Height-Time for Cloud No. 1, 24 July 1956.

TABLE 2.5

Basic Measurements, Cloud No. 1, 24 July 1956, Tucson

<u>Time</u>	<u>Height</u> (Ft Above msl)	<u>Velocity</u> (Ft/min)	<u>Volume</u> (Ft <sup>3</sup> x 10 <sup>10</sup> )	<u>Flux</u> (Ft <sup>3</sup> x 10 <sup>10</sup> ) min.
1410:00	17,620			
:15	17,720*	340		
:30	17,790			
:45	17,843*	214		
1411:00	17,897			
:15	18,039*	284		
:30	18,180			
:45	18,268*	352		
1412:00	18,356		1.55	
:15	18,383*	106		.60
:30	18,409		1.85	
:45	18,537*	512		1.90
1413:00	18,665		2.80	
:15	18,912*	988		2.70
:30	19,159		4.15	
:45	19,367*	830		2.70
1414:00	19,574		5.50	
:15	19,702*	512		2.60
:30	19,830		6.80	
:45	20,130*	1200		4.70
1415:00	20,430		9.15	
:15	20,620*	760		3.80
:30	20,810		11.05	
:45	21,039*	918		4.90
1416:00	21,269		13.50	
:15	21,387*	470		4.80
:30	21,504		15.90	
:45	21,766*	1048		3.80
1417:00	22,028		17.80	
:15	22,248*	882		4.40
:30	22,469		20.00	
:45	22,729*	1042		2.40
1418:00	22,990		21.20	
:15	23,188*	794		1.20
:30	23,387		21.80	
:45	23,558*	684		2.20
1419:00	23,829		22.90	
:15	24,076*	988		3.60
:30	24,323		24.70	
:45	24,543*	882		5.80

TABLE 2.5 (Contd.)

<u>Time</u>	<u>Height</u> (Ft Above msl)	<u>Velocity</u> (Ft/min)	<u>Volume</u> (Ft <sup>3</sup> x 10 <sup>10</sup> )	<u>Flux</u> (Ft <sup>3</sup> x 10 <sup>10</sup> ) min.
1420:00	24,764		27.60	
:15	24,888*	494		5.60
:30	25,011		30.40	
:45	25,209*	794		2.40
1421:00	25,408		31.60	
:15	25,510*	406		3.60
:30	25,611		33.40	
:45	25,757*	584		2.00
1422:00	25,903		34.40	
:15	26,013*	440		4.30
:30	26,123		36.55	
:45	26,212*	354		6.30
1423:00	26,300		39.70	
:15	26,375*	300		4.20
:30	26,450		41.80	
:45	26,481*	124		7.60
1424:00	26,512		45.60	
:15	26,578*	264		-6.00
:30	26,644		42.60	
:45	26,684*	160		-5.10
1425:00	26,724		40.05	



The velocity-time plot (Fig. 2.26) contains only one major cycle and this has been emphasized by drawing in the low frequency component using the envelope method (Manley, 1945). As in the previous examples, higher frequency oscillations are superimposed on the low frequency component. The volume-time curve (Fig. 2.27) shows a steady increase in volume until the time of actual decay of the stem. This is supported by the behavior of the flux (Fig. 2.28) which also increases until decay sets in.

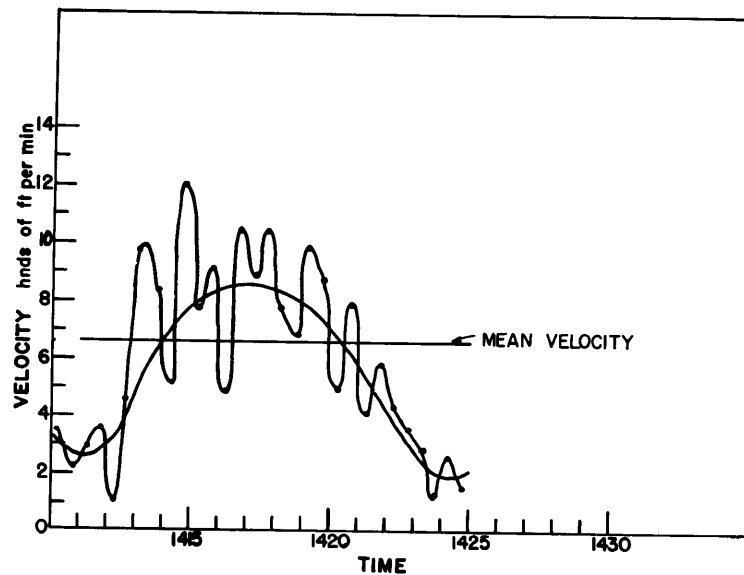


Fig. 2.26 Velocity-Time for Cloud No. 1, 24 July 1956.

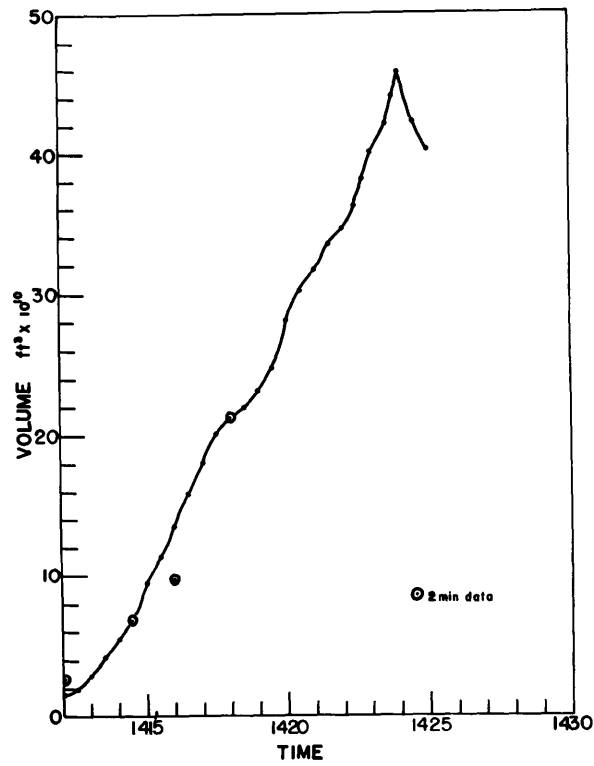


Fig. 2.27 Volume-Time for Cloud No. 1, 24 July 1956.

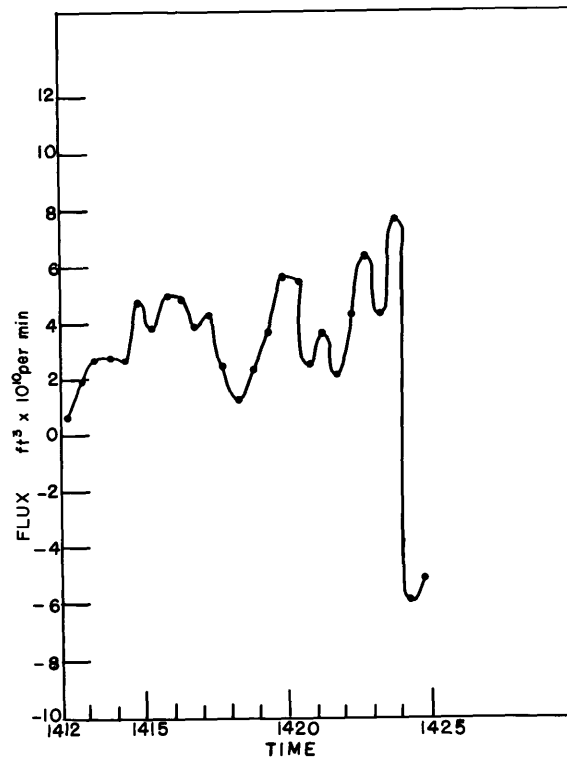


Fig. 2.28 Flux-Time for Cloud No. 1, 24 July 1956.

Cloud No. 2 - 24 July 1956

Referring to Figs. 2.6 and 2.7, one sees that this is a large, towering, cumulus cloud which developed at least two turrets during the course of its evolution. Although the 9 x 9 inch stereo photographs were not available before 1338 hours, the 16 mm film was analyzed to cover the early history of the development. The horizontal position (Fig. 2.23) covered a large area with the main cloud mass extending from Romero Canyon to Samanico Ridge behind Lemmon Mountain. As the cloud grew, it drifted into the Cathedral Rock region in the direction of Rattlesnake Peak.

The forerunners of Cloud No. 2 were detected as early as 1255 hours as small intermittently growing cumuli. Between 1255 and 1320 hours, several small towers pushed up and decayed. In the interval, 1320 to 1325:30 hours, the whole mass was a medium-sized cumulus which seemed to pause before another cycle of growth commenced at 1325:30. From 1325:30 to 1333 hours, the cloud continued to grow principally by a radial growth all over its bounding surface but exaggerated in the down wind direction. After 1339 hours, a strong upward growth was noted over the whole upper surface and resulted in a column extension of the cloud mass. While the column was pushing up, an even more vigorous upward extension was evident on the left top of the column which became a small turret growing into the wind from 1334 hours until it died down some ten minutes later.

All the while, radial-like growth continued on the lower downwind side of the main mass. About 1339 hours, a strong upsurge seemed to start near the lower portion of the cloud and took the outward form of

a large ball-like mass of cloud as if a neighboring smaller cumulus were actually ingested into the flow of the main cloud. As this second surge took place, it was evidently affecting the flow of the first turret since the latter appeared to be pushed aside as the former rushed up through the main cloud mass. This second surge burst through the cloud top at 1342 hours and grew briefly as a turret. For convenience of reference, the main cloud is called Cloud No. 2, while the two surges are labeled Turret No. 1 and Turret No. 2 in the order that they appeared.

From the above narrative of observed events, it is apparent that Cloud No. 2, 24 July, is a complex affair. From the two minute contour plots and from the trajectories (Fig. 2.29), it appears that the main cloud continued to grow independently of the turrets in a manner suggestive of a fairly stationary radial outflow in the presence of horizontal winds. The turrets, however, present trajectories which are unmistakably those generated by a growing tower; hence, an upward moving stream line field.

The turrets developed within the main cloud mass along some central axis because the second surge obviously took place along the same axis as the first and was able to push it aside. As the second turret pushed up, the entire cloud mass seemed to be in an upward diverging flow so that a horizontal shelf was extended at 24,000 feet on the upwind side, building into the wind, and another shelf built out rapidly on the downwind side near 21,000 feet. The cloud diameter seemed to contract in the height interval 21,000 to 24,000 feet while the shelf

extension was in progress. The contraction was very noticeable on the upwind side.

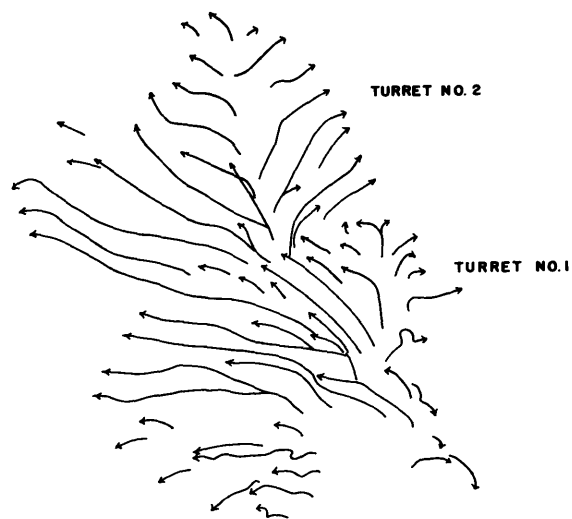


Fig. 2.29 Trajectories for Cloud No. 2,  
24 July 1956.

The basic measurements for the main cloud are given in Table 2.6. The two turrets will be treated separately. Figure 2.30 illustrates the way the turrets appeared almost independently on the original cloud which started around 1325 hours and was identifiable until 1346 hours.

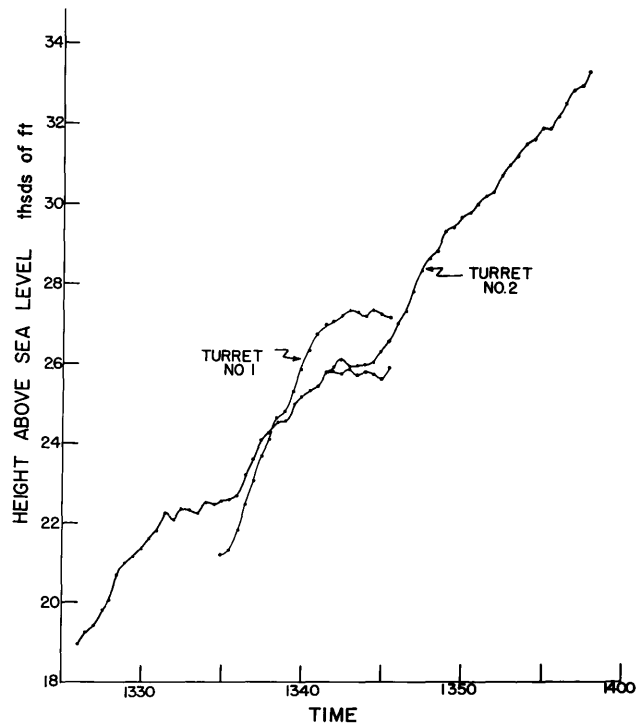


Fig. 2.30 Height-Time for Cloud No. 2, 24 July 1956.

When the velocity was computed for the cloud top, a surprisingly regular curve emerged. In Fig. 2.31, the vertical velocity measured at the cloud top for the main cloud is shown. From the location of the earliest point, it is clear that the cloud was undergoing an oscillation between 1320 and 1332 hours. Since after 1342 hours the second turret dominated the upper part of the main cloud, the curve is cut off after 1445 hours. It is noted that the minimum value was less than zero. This provides an opportunity for the high frequency oscillation to drag ambient air into the cloud top during the time the low frequency component was at a minimum.

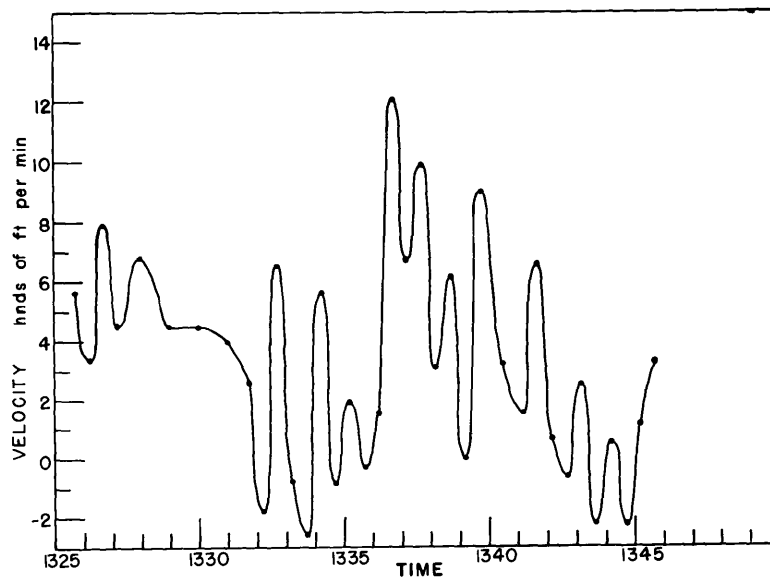


Fig. 2.31 Velocity-Time for Cloud No. 2,  
24 July 1956.

TABLE 2.6

Basic Measurements, Cloud No. 2, 24 July 1956, Tucson

<u>Time</u>	<u>Height</u> (Ft Above msl)	<u>Velocity</u> (Ft/min)	<u>Volume</u> (Ft <sup>3</sup> x 10 <sup>10</sup> )	<u>Flux</u> (Ft <sup>3</sup> x 10 <sup>10</sup> ) min.
1325:30	18,950		5.84	
:45	19,091*	564		.14
1326:00	19,232		5.91	
:15	19,317*	340		1.22
:30	19,402		6.52	
:45	19,600*	790		4.16
1327:00	19,797		8.60	
:15	19,910*	452		3.24
:30	20,023		10.22	
:45				
1328:00	20,362*	678		1.67
:15				
:30	20,701		11.89	
:45				
1329:00	20,927*	452		2.17
:15				
:30	21,153		14.06	
:45				
1330:00	21,379*	452		2.94
:15				
:30	21,695		17.00	
:45				
1331:00	21,809*	407		3.38
:15				
:30	22,012		20.38	
:45	22,077*	262		6.32
1332:00	22,143		23.54	
:15	22,098*	-180		1.80
:30	22,053		24.44	
:45	22,219*	662		3.26
1333:00	22,384		26.07	
:15	22,366*	-74		2.14
:30	22,347		27.14	
:45	22,284*	-254		3.48
1334:00	22,220		28.88	
:15	22,364*	576		3.24
:30	22,508		30.50	
:45	22,488*	-78		2.86
1335:00	22,469		31.93	
:15	22,519*	198		2.98
:30	22,538		33.42	
:45	22,560*	-30		1.86



TABLE 2.6 (Contd.)

<u>Time</u>	<u>Height</u> (Ft Above msl)	<u>Velocity</u> (Ft/min)	<u>Volume</u> (Ft <sup>3</sup> x 10 <sup>10</sup> )	<u>Flux</u> (Ft <sup>3</sup> x 10 <sup>10</sup> ) min.
1336:00	22,553		34.35	
:15	22,593*	160		3.96
:30	22,633		36.33	
:45	22,935*	1210		5.92
1337:00	23,238		39.29	
:15	23,406*	672		5.54
:30	23,594		42.06	
:45	23,820*	994		4.20
1338:00	24,066		46.26	
:15	24,145*	314		1.48
:30	24,223		47.0	
:45	24,378*	618		10.78
1339:00	24,532		52.39	
:15	24,532*	0		1.96
:30	24,531		53.37	
:45	24,758*	902		7.63
1340:00	24,982		57.19	
:15				
:30	25,153*	342		2.78
:45				
1341:00	25,324		59.97	
:15	25,364*	158		6.66
:30	25,403		63.30	
:45	25,570*	666		5.40
1342:00	25,736		66.00	
:15	25,754*	72		6.90
:30	25,772		69.45	
:45	25,759*	-52		-.62
1343:00	25,746		69.14	
:15	25,811*	260		-.88
:30	25,876		68.7	
:45	25,821*	-220		
1344:00	25,766			
:15	25,782*	64		
:30	25,798			
:45	25,743*	-220		
1345:00	25,688			
:15	25,718*	120		
:30	25,748			
:45	25,831*	332		
1346:00	25,914			

The volume-time curve (Fig. 2.32) and flux-time curve (Fig. 2.33) give the general trends noted earlier for Cloud No. 3, 23 July 1956, which also was a large cumulus congestus. The flux increased during the active growth as in the previous examples, making this trait a regular feature of developing clouds.

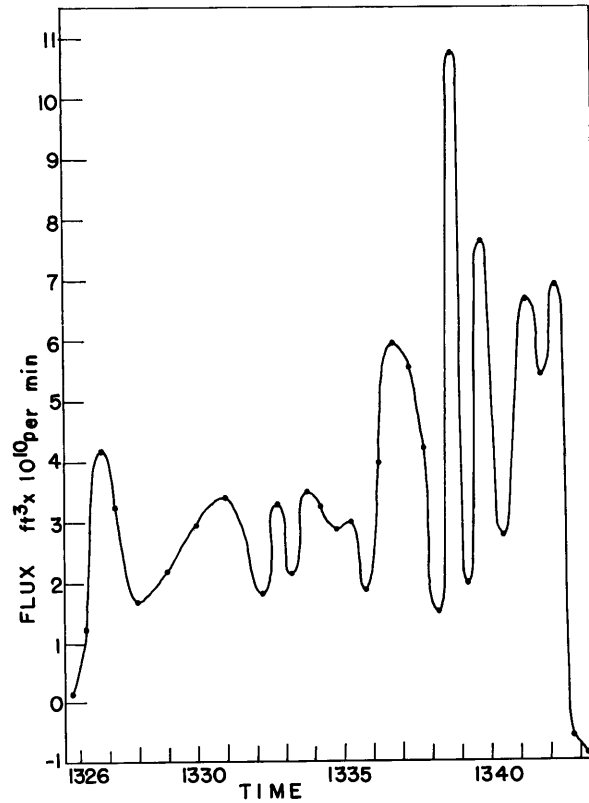
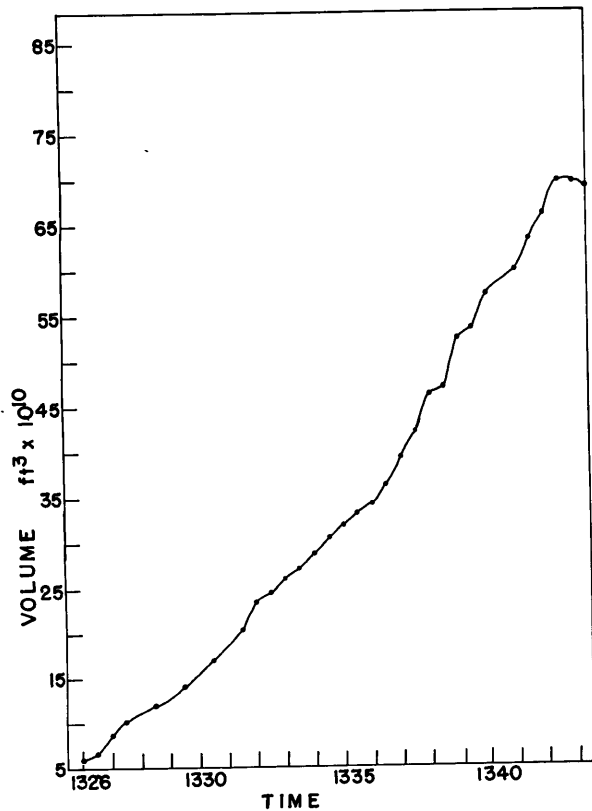


Fig. 2.32 Volume-Time for Cloud No. 2,  
24 July 1956.

Fig. 2.33 Flux-Time for Cloud No. 2,  
24 July 1956.

Cloud No. 2, Turret No. 1, 24 July 1956

While the parent cloud was undergoing a more radial-like expansion, Turret No. 1 developed as an independent entity. When the velocity-time curve (Fig. 2.34) for this turret is inspected, it is apparent that the turret has its origin at a much earlier time than it appeared at the top of Cloud No. 2. If it is permissible to extrapolate the curve back in time to the possible beginning of its cycle, assuming a fourteen-minute period, we get the result that Turret No. 1 arose somewhere near the base of the main cloud.

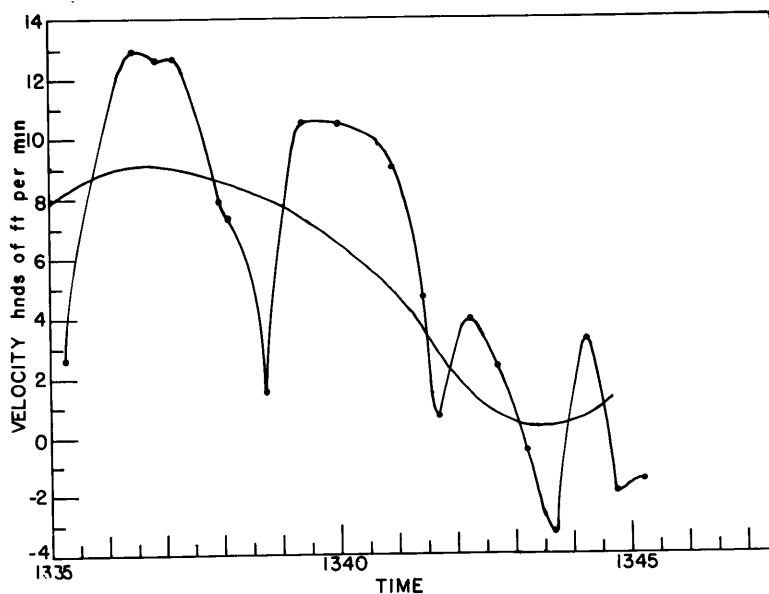


Fig. 2.34 Velocity-Time for Turret No. 1, Cloud No. 2, 24 July 1956.

It appears possible that Turret No. 1 may have been a neighboring cloud which was ingested into the main cloud as the latter underwent a large surge at 1332 hours. The basic measurements for this turret are given in Table 2.7. Although the volume continued to increase right up to the time the cloud turret ceased to grow (Fig. 2.35), the flux-time curve has a different shape than the parent cloud. The flux (Fig. 2.36) presents a sharp maximum midway through the time it was observed. No outstanding reason is apparent for this behavior.

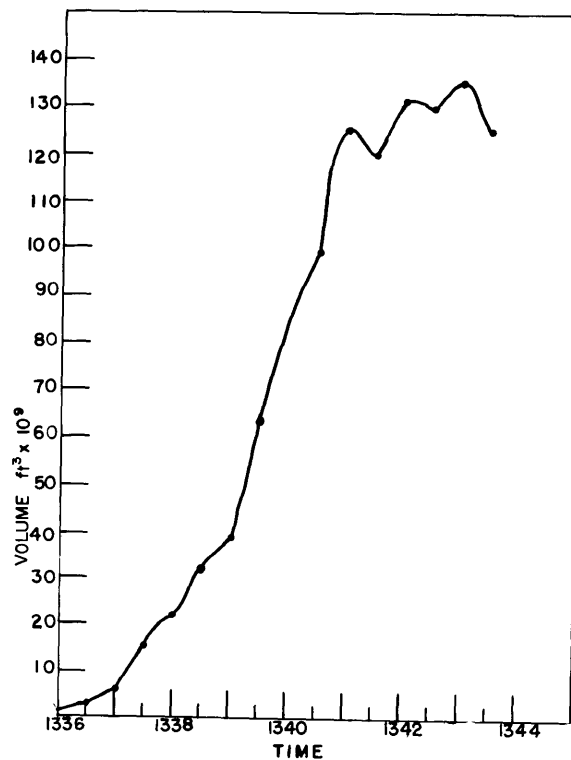


Fig. 2.35 Volume-Time for Turret No. 1, Cloud No. 2, 24 July 1956.

TABLE 2.7

Basic Measurements, Cloud No. 2, Turret No. 1, 24 July 1956

<u>Time</u>	<u>Height</u> (msl)	<u>Velocity</u>	<u>Volume</u> (Ft <sup>3</sup> x 10 <sup>9</sup> )	<u>Flux</u> (Ft <sup>3</sup> x 10 <sup>9</sup> ) min.
1335:00	21,204			
:15	21,268*	256		
:30	21,332			
:45	21,570*	950		
1336:00	21,807		.73	
:15	22,126*	1276		4.26
:30	22,445		2.86	
:45	22,760*	1258		6.10
1337:00	23,074		5.91	
:15	23,389*	1260		18.96
:30	23,704		15.39	
:45	23,912*	832		12.18
1338:00	24,120		22.0	
:15	24,402*	773		20.02
:30	24,684		32.1	
:45	24,734*	200		14.30
1339:00	24,784		39.25	
:15	25,059*	1040		49.70
:30	25,334		64.1	
:45				
1340:00	25,849*	1030		70.00
:15				
:30	26,364		99.3	
:45	26,572*	950		51.20
1341:00	26,779		124.9	
:15	26,893*	454		-9.8
:30	27,006		120.0	
:45	27,021*	60		22.92
1342:00	27,036		131.46	
:15	27,136*	398		-2.0
:30	27,235		130.64	
:45	27,296*	242		10.00
1343:00	27,356		135.05	
:15	27,344*	-48		-20.00
:30	27,532		125.18	
:45	27,249*	332		
1344:00	27,166			
:15	27,247*	326		
:30	27,329			
:45	27,280*	-198		
1345:00	27,230			
:15	27,293*	-146		
:30	27,157			

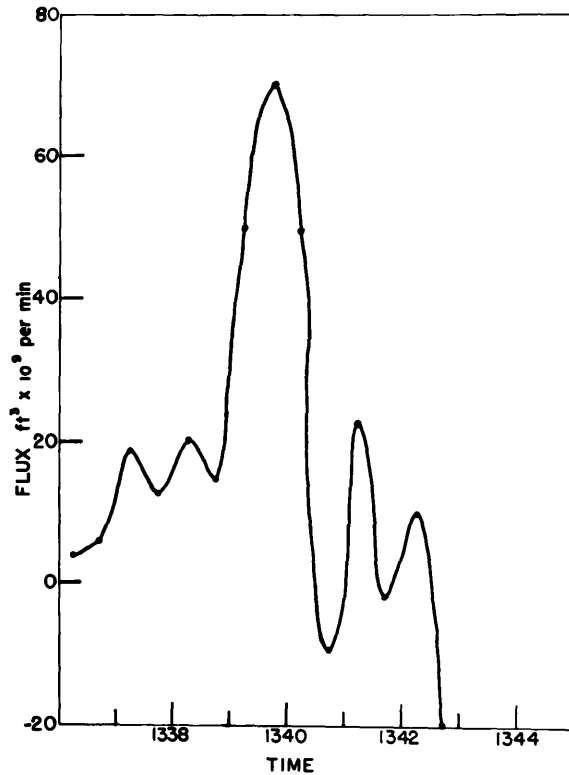


Fig. 2.36 Flux-Time for Turret No. 1, Cloud No. 2,  
24 July 1956.

Cloud No. 2, Turret No. 2, 24 July 1956

When Turret No. 2 appeared, the main cloud had definite signs of evolving into the anvil stage of development. Starting at 1342 hours (Plate 3, Fig. 2.6), it may be seen that the cloud top began to grow horizontally so that the anvil is definite by 1348 hours (Plate 6, Fig. 2.6). The basic measurements on Turret No. 2 are contained in Table 2.8. The vertical velocity curve (Fig. 2.37) is distinctly different than that for previous cloud towers. The mean velocity is drawn to illustrate the lack of any marked low frequency component as has been the characteristic of other towers. The volume (Fig. 2.38) and the flux (Fig. 2.39) increase monotonically with time, suggesting

TABLE 2.8

Basic Measurements, Cloud No. 2, Turret No. 2, 24 July 1956

<u>Time</u>	<u>Height</u> (msl)	<u>Velocity</u>	<u>Volume</u> (Ft <sup>3</sup> x 10 <sup>10</sup> )	<u>Flux</u> (Ft <sup>3</sup> x 10 <sup>10</sup> ) min.
1342:00	25,918			
:15	26,000*	330		
:30	26,083			
:45	26,004*	-318		
1343:00	25,924			
:15	25,940*	64		
:30	25,956			
:45	25,971*	60		
1344:00	25,986			
:15	26,061*	60		
:30	26,016			
:45	26,160*	576		
1345:00	26,304			
:15	26,432*	510		
:30	26,559			
:45	26,776*	868		
1346:00	26,993			
:15	27,147*	614		
:30	27,300		.883	
:45	27,558*	1034		1.64
1347:00	27,817		1.7	
:15	28,086*	1078		3.56
:30	28,356		3.48	
:45	28,491*	454		3.66
1348:00	28,627		5.31	
:15	28,717*	360		4.68
:30	28,807		7.65	
:45	29,068*	1044		6.26
1349:00	29,329		10.78	
:15	29,370*	164		5.50
:30	29,416		13.53	
:45	29,662*	502		5.94
1350:00	29,662		16.50	
:15	29,716*	214		7.00
:30	29,769		20.00	
:45	29,889*	480		6.40
1351:00	30,009		22.91	
:15	30,106*	388		6.74
:30	30,203		26.28	
:45	30,257*	214		10.24

TABLE 2.8 (Contd.)

<u>Time</u>	<u>Height</u> (msl)	<u>Velocity</u>	<u>Volume</u> (Ft <sup>3</sup> x 10 <sup>10</sup> )	<u>Flux</u> (Ft <sup>3</sup> x 10 <sup>10</sup> ) min.
1352:00	30,310		31.39	
:15	30,527*	868		8.46
:30	30,744		35.62	
:45	30,863*	478		12.94
1353:00	30,983		42.09	
:15	31,087*	418		12.32
:30	31,194		48.25	
:45	31,343*	498		12.84
1354:00	31,443		54.67	
:15	31,527*	328		12.78
:30	31,612		61.06	
:45	31,768*	624		33.22
1355:00	31,924		77.67	
:15	31,914*	-38		
:30	31,905			
:45	32,043*	554		
1356:00	32,182			
:15	32,368*	742		
:30	32,553			
:45	32,698*	578		
1357:00	32,842			
:15	32,897*	220		
:30	32,952			
:45	33,145*	770		
1358:00	33,337			



that when the development of the cumulus reaches the anvil stage the low frequency oscillations which accompany the vigorous upward growth are replaced by a steadily increasing flux of air up the cloud column. In keeping with this observation, it is suggested that the vertical velocity measured after 1345 hours is more of a measure of the radial expansion of the cloud top than that of a turret. The expansion of the entire cloud mass continued after 1400 hours but became indistinct because of the development of Cloud No. 3 which occurred immediately behind Cloud No. 2. The combined mass of cloud seemed to spread and drift in the wind field as a gigantic mass of ice crystals.

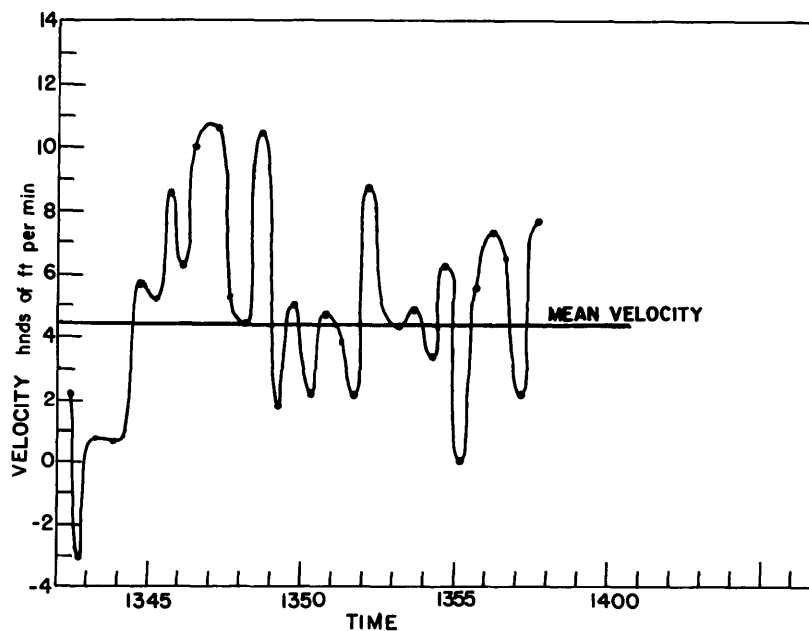


Fig. 2.37 Velocity-Time for Turret No. 2,  
Cloud No. 2, 24 July 1956.

Cloud No. 3, 24 July 1956

The last of the series of clouds studied on 24 July was a large cumulus congestus which grew over the plateau (7,200 ft) some two miles south of Lemmon Mountain. During the final stages of its growth, it became obscured by Cloud No. 2 so that its terminal changes were not observable. From the photographs (Figs. 2.6 and 2.7) Cloud No. 3 seemed to undergo the same terminal behavior as evidenced by Cloud No. 2.

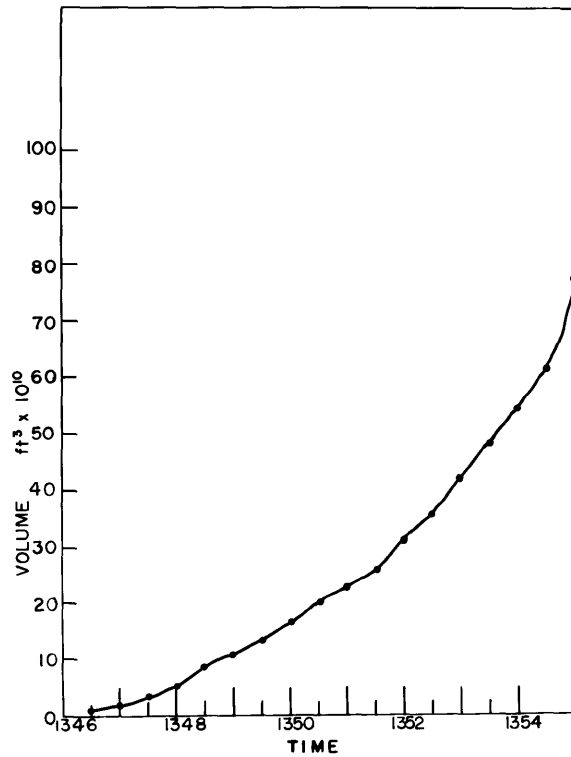


Fig. 2.38 Volume-Time for Turret No. 2, Cloud No. 2, 24 July 1956.

During the time it was observed, it had growth features quite similar to previous large cumulus congestus; i.e., Cloud No. 3, 23 July 1956. Owing to its partial obscuration, no trajectories were made for this cloud. The basic measurements on height, volume, vertical velocity, and flux are provided in Table 2.9.

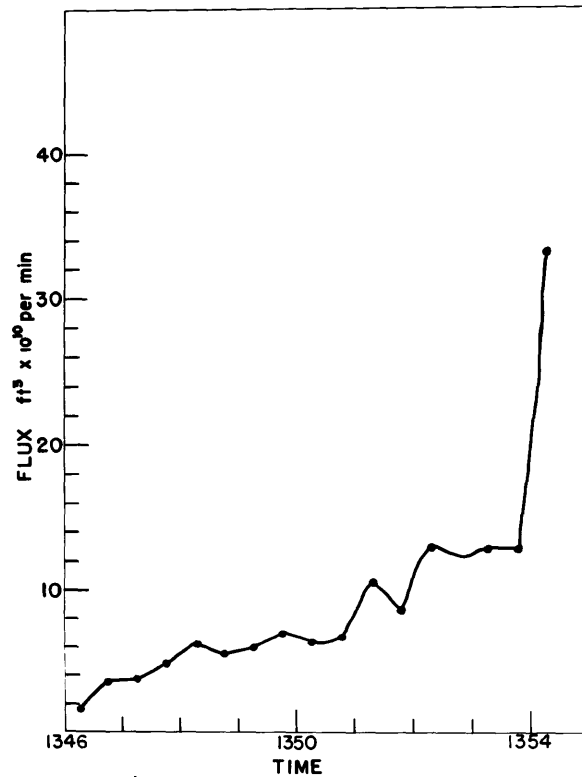


Fig. 2.39 Flux-Time for Turret No. 2, Cloud No. 2, 24 July 1956.

TABLE 2.9

Basic Measurements, Cloud No. 3, 24 July 1956, Tucson

<u>Time</u>	<u>Height (Above Cloud Base)</u> 10,135 ft	<u>Velocity</u> ft/min.	<u>Volume</u> ft <sup>3</sup> x 10 <sup>11</sup>	<u>Flux</u> ft <sup>3</sup> x 10 <sup>10</sup> min.
1340:00	8,738		.83	
:15	8,906*	670		6.6
:30	9,073		1.16	
:45	9,311*	954		5.0
1341:00	9,550		1.41	
:15	9,765*	860		4.8
:30	9,980		1.65	
:45	10,052*	286		3.0
1342:00	10,123		1.80	
:15	10,409*	1146		7.4
:30	10,696		2.17	
:45	10,815*	478		2.5
1343:00	10,935		2.30	
:15	11,126*	764		4.8
:30	11,317		2.53	
:45	11,580*	1050		4.6
1344:00	11,842		2.76	
:15	12,152*	1242		3.4
:30	12,463		2.93	
:45	12,654*	764		3.6
1345:00	12,485		3.15	
:15	12,988*	572		6.2
:30	13,131		3.46	
:45	13,465*	1338		7.6
1346:00	13,800		3.84	
:15	13,943*	572		.8
:30	14,086		3.88	
:45	14,277*	764		7.2
1347:00	14,468		4.24	
:15	14,587*	478		4.0
:30	14,707		4.44	
:45	14,850*	574		1.2
1348:00	14,994		4.50	
:15	15,090*	382		5.8
:30	15,185		4.79	
:45	15,281*	382		19.8
1349:00	15,376		5.78	
:15	15,472*	382		11.4
:30	15,567		6.35	
:45	15,758*	764		21.4

TABLE 2.9 (Contd.)

<u>Time</u>	<u>Height (Above Cloud Base)</u> 10, 135 ft	<u>Velocity</u> ft/min.	<u>Volume</u> ft <sup>3</sup> x 10 <sup>11</sup>	<u>Flux</u> ft <sup>3</sup> x 10 <sup>10</sup> min.
1350:00	15,949		7.42	
:15	16,116*	668		13.2
:30	16,283		8.08	
:45	16,545*	1050		20.2
1351:00	16,808		9.09	
:15	17,047*	956		17.0
:30	17,286		9.94	
:45	17,405*	476		12.8
1352:00	17,524		10.58	
:15	17,715*	764		
:30	17,906			
:45	18,050	574		
1353:00	18,193			
:15	18,646	1814		
:30	19,100			
:45	19,578	1910		
1354:00	20,055			
:15	20,246	764		
:30	20,437			
:45	20,809	1488		
1355:00	21,201			
:15	21,392	764		
:30	21,583			
:45	21,917	1338		
1356:00	22,252			
:15	22,419	668		
:30	22,586			
:45	22,848	1050		
1357:00	23,111			
:15	23,182	286		
:30	23,254			
:45	23,688	1338		
1358:00	23,923			
:15	24,138	860		
:30	24,353			
:45	24,520	668		
1359:00	24,687			

The height-time curve (Fig. 2.40) suggests two cycles of growth and this is borne out by the vertical velocity-time curve (Fig. 2.41).

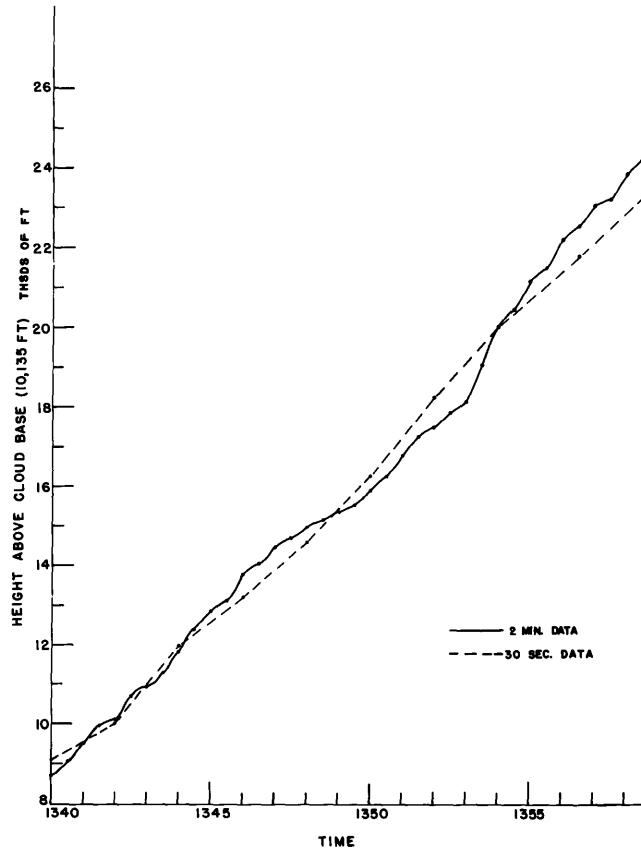


Fig. 2.40 Height-Time for Cloud No. 3,  
24 July 1956.

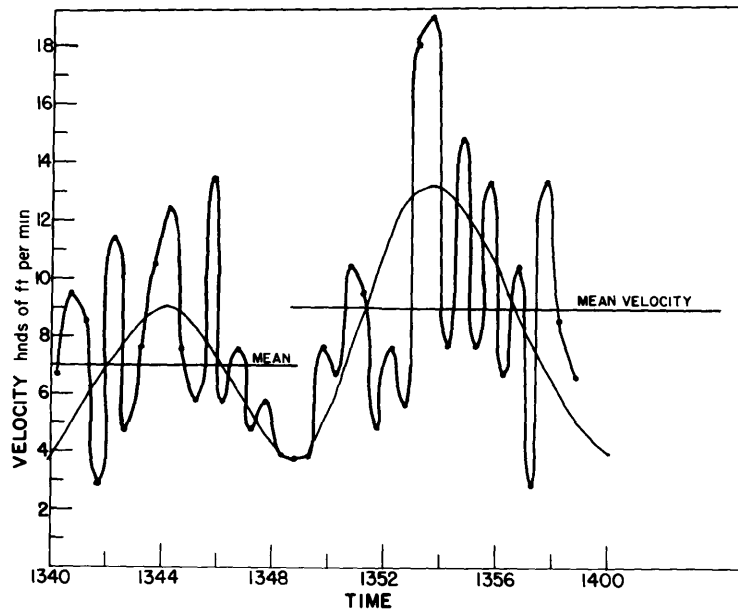


Fig. 2.41 Vertical Velocity-Time for Cloud No. 3,  
24 July 1956.

As in the case with Cloud No. 2, the final stages of upward growth were marked by a tremendous upsurge which had the effect of spreading the upper part of the cloud column and encouraging a necking-in about midway up the column. As previously observed for these large congestus clouds, the second growth cycle had a larger amplitude than the first. An astounding 1900 ft/min vertical velocity was reached at one point (1354 hours).

The cloud volume and flux were measured until 1352 when it became impossible to see the entire cloud because of the shielding due to Cloud No. 2. Both the volume-time curve (Fig. 2.42) and the flux-time curve (Fig. 2.43) reflect the substantial increase in activity during the second cycle of growth.

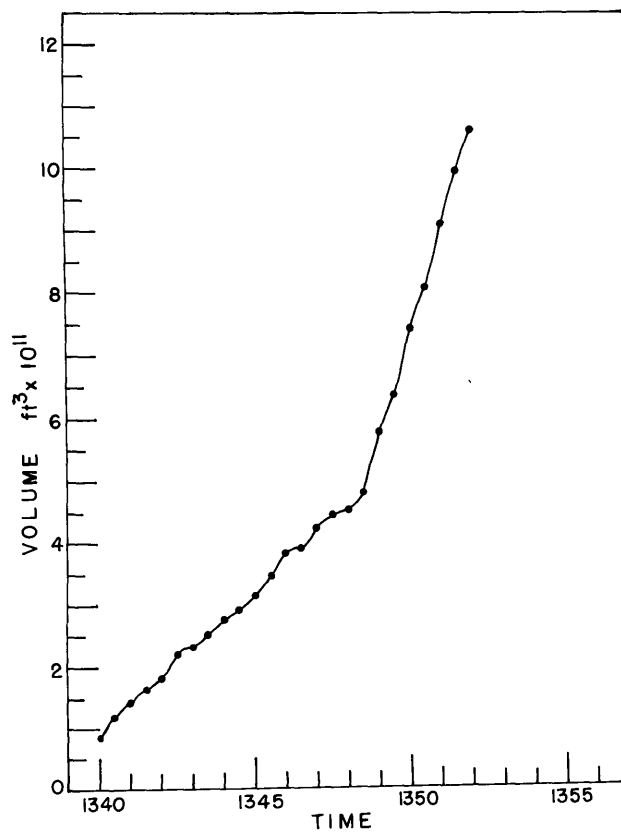


Fig. 2.42 Volume-Time for Cloud No. 3,  
24 July 1956.



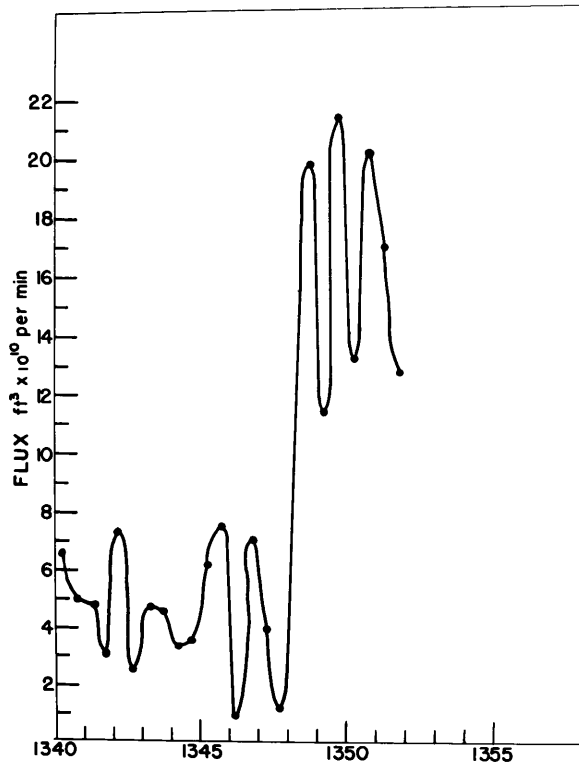


Fig. 2.43 Flux-Time for Cloud No. 3,  
24 July 1956.

### III. ANALYSIS OF DATA

In Chapter II the basic measurements on five different growing cumulus clouds are given without any serious attempt to explain these findings in terms of physical theory. As an additional prelude before a mechanistic interpretation is ventured, a more critical examination of these data will be undertaken. By such action it is hoped that the data will suggest particular lines for approaching the theoretical problem.

For each type of measurement, we have been concerned with its time-wise response. The vertical velocity, although measured at the cloud top, is believed, by reason of the arguments made in Chapter II, to be representative of the local acceleration. The cloud volume and flux are for the whole cloud. We have a series of values in time at a given place for a limited time, or a discrete time series for each type of measurement. A number of statistical techniques may be employed to reveal the outstanding features of a time series and several are used in this study. Among these are averaging, harmonic analysis, spectral analysis, and curve fitting. Even without these higher analyses, the curves presented in Chapter II are sufficiently revealing to yield definite suggestions. When the vertical velocity is smoothed as shown in Chapter II, rising cumulus towers always show a low frequency oscillation. Judging by eye alone, the period of the low frequency component is generally estimated to lie somewhere near ten minutes. Superimposed on the low frequency are numerous higher frequency oscillations. The low frequency component always oscillates about a mean value greater

than zero which indicates some steady component underlying the flow. The underlying flow may be constant with time or increasing with time, as suggested by clouds which undergo more than one cycle during growth. Finally, the increase may be linear, exponential, or some other characteristic function of time.

### 3.1 Harmonic Analysis

Although the velocity curves by themselves suggest the presence of certain frequencies, one would like to know what frequencies are actually dominant, and how well these account for the observed velocity-time curve. The danger in accepting immediately the presence of frequency components corresponding to noticeable cycles in the time curves is that one may be observing the result of the addition or subtraction of two or more frequencies which by themselves are not prominent. Harmonic analysis is most commonly used to investigate regular oscillations in a time series of limited duration. In this method, an infinite series of sine and cosine terms, called a Fourier series, is fitted to the data. Any continuous function,  $X(t)$ , defined over the interval  $0 - P$ , may be given by a corresponding Fourier series:

$$\begin{aligned}
 X(t) = & \bar{X} + A_1 \sin\left(\frac{360^\circ}{P} t\right) + B_1 \cos\left(\frac{360^\circ}{P} t\right) \\
 & + A_2 \sin\left(\frac{360^\circ}{P} 2 t\right) + B_2 \cos\left(\frac{360^\circ}{P} 2 t\right) + \dots
 \end{aligned}
 \tag{3.1}$$

where  $\bar{X}$  is the average value of the function over the interval and  $t$  is the time interval. Since the subject data are at discrete time intervals and are not continuous, only a finite number of points exist in the interval to be analyzed. Likewise, only a finite number of terms in the

series will be needed to fit the observed function. The determination of the finite series is the substance of harmonic analysis. The first harmonic is called the fundamental and has a period equal to the period studied. The second harmonic has a period one-half the fundamental, and so on. If the number of observations is  $N$ , the number of possible harmonics is  $N/2$ . Hence, harmonic analysis will not give any information on periodic components whose periods are larger than the period of observation,  $P$ , nor on components whose periods are shorter than  $N/2$ .

To find the coefficients of the sine and cosine terms and the resulting amplitudes and phase angles of the various harmonics, a numerical computation was carried out using the 24 ordinate scheme (Manley, 1945) for Cloud No. 1, 24 July 1956. The results are given in Table 3.1. In the table, it is seen that a large fraction of the energy is contained in the first two terms, the mean and the fundamental. On comparing the amplitudes contributed by the various harmonics, it is found that the fundamental frequency is larger than any other. The remaining harmonics show no particular trend, each contributing so that there are no holes in the spectrum. The per cent of the total variance accounted by each harmonic is given on the bottom line of Table 3.1. The sum of the eleven harmonics equals 90 per cent.

TABLE 3.1

Harmonic Analysis of Vertical Velocity for Cloud No. 1, 24 July 1956.

Mean	1	2	3	4	5	6	7	8	9	10	11	Harmonic
671.3	286.5	112.0	99.0	57.6	89.7	127.3	43.6	87.4	37.2	112.3	64.0	Amplitude (Ft/min)
	304	334	302	287	6	277	254	196	330	98	28	Phase Angle (Degrees)
	47.2	7.2	5.6	1.9	4.6	9.3	1.1	4.4	0.8	5.6	2.4	Per cent of Total Variance

In order to test how well the first eleven terms of the Fourier series reproduced the original curve, the laborious computation was made of the vertical velocities at each interval. Figure 3.1 shows the comparison between the observed and computed curves. From this comparison, it may be concluded that the first eleven harmonics reproduce the original curve fairly well in detail and account for ninety per cent of the variance in the original data. The harmonic analysis reaffirms the indication of an outstanding cycle near ten minutes for Cloud No. 1, 24 July 1956, but equally significant, all eleven harmonics

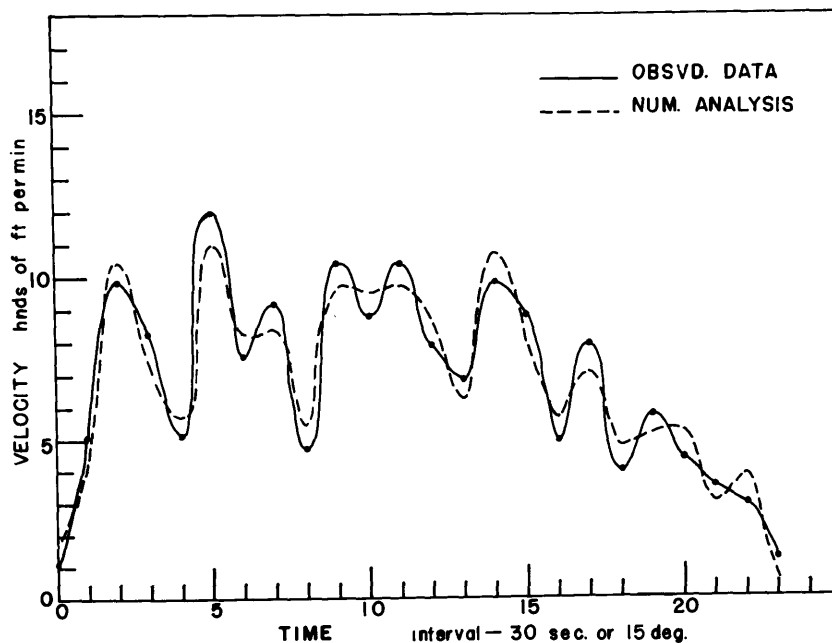


Fig. 3.1 Harmonic Analysis for Cloud No. 1, 24 July 1956.  
The curve computed using the first eleven harmonics is shown by the broken line compared to the actual observations on the solid line.

contribute to the total variance. Several of the subject clouds were analyzed in a like manner with similar results. On the basis of these results, one is not justified in neglecting any frequency over the frequency range of the observations. In this regard, the frequency response of the clouds is typical of meteorological data, wherein all periods ranging from the smallest to the largest are found in a given time series.

This last result suggests that the analysis of the vertical velocity time series may be approached from the standpoint of turbulence. By turbulence, we mean a flow which is characterized by random irregularities of many scales, but somehow these are related to the mean or bulk flow. The velocity curves in Chapter II are notable in the way the amplitudes of the high frequency fluctuations vary directly with the amplitude of the low frequency component. Following the standard terminology, the total flow may be conceived as being composed of a bulk component, either steady or slowly varying, and a turbulent component. Atmospheric turbulence is usually defined by the deviations of the instantaneous flow from the mean flow. As pointed out by Van der Hoven and Panofsky (1954), the definition of mean flow depends on the length of period used to compute the mean, and turbulence can thereby have different definitions. A commonly used mean is on the synoptic scale where the smoothed flow would characterize the weather map. Here the scale of turbulence would be eddies of the order of minutes. The mean flow would obey simplified forms of the hydrodynamic equations and the turbulent contributions would be included in certain terms described as friction, diffusion, or heat conduction. In the case

of the general circulation, the mean would be based on many years of data and the weather map cyclones and anticyclones would be considered as turbulent eddies. Similarly, the microscale motions use ten minute means and their scale of turbulence is of the order of seconds.

For cumulus clouds where the lifetime is of the order of one hour or less, the mean would correspond to the time average of this scale. We might consider the remaining fluctuating component as turbulence of the order of minutes. Applying this criterion to the time series of Chapter II, we are able to state that the turbulent component of the vertical velocity ranges from oscillations of periods as short as one minute to periods as long as ten minutes. Stated otherwise, the vertical flow measured at the top of a growing cumulus seems to have, in addition to a mean upward velocity, eddies of lengths varying from a few feet to several thousands of feet. These latter eddies would resemble the scale length considered by the "bubble" theory of convection.

### 3.2 The Trend

Those clouds whose life span permitted the observation of two or more ten-minute oscillations (Cloud No. 3, 23 July 1956; Cloud No. 2 and Cloud No. 3, 24 July 1956) seemed to have a steady upward trend in the vertical velocity component underlying the "turbulence" instead of a constant mean. The trend may be connected to the over-all life cycle of the cloud or it may be part of an even larger oscillation connected with the diurnal dependence of the convection. The trend was evaluated in two ways: by computing the slope of the regression line fitted to the vertical velocity-time curve, and by dividing the slope of the flux-time regression curve by the average cross sectional area of the cloud

column.

$$\frac{\partial w}{\partial t} = k_1, \text{ ft/min}^2 \quad (3.2)$$

$k_1$  = slope of the regression line for the velocity-time curve.

$$\frac{4}{\pi d^2} \frac{\partial \text{Flux}}{\partial t} = k_2, \text{ ft/min}^2 \quad (3.3)$$

$k_2$  = slope of regression line for the flux-time curve.

The computations are in Table 3.2.

TABLE 3.2

Computations of Vertical Acceleration

Cloud	$k_1$ ft/min <sup>2</sup>	$k_2$ ft/min <sup>2</sup>
Cloud No. 2, 24 July 1956	-18.2	47.0
Cloud No. 3, 24 July 1956	14.2	17.0
Cloud No. 3, 23 July 1956	35.3	145.0

The comparison between the two methods is favorable only in the case of Cloud No. 3, 24 July 1956. The other two cases show wide discrepancies between the two methods. It may be recalled that Cloud No. 3, 24 July 1956 had the best defined outline of all three, as well as a clearly delineated velocity curve. Much reliability may be placed on the data for this cloud. In view of the good agreement between the two methods for Cloud No. 3, it is felt that the estimate of vertical acceleration in this case (about 15 ft/min<sup>2</sup>) is reliable. Furthermore, one might expect the acceleration for the two other cases to be of the same order. Using this as a guide, one might tend to accept as good estimates



47 ft/min<sup>2</sup> for Cloud No. 2, 24 July 1956 and 35.3 ft/min<sup>2</sup> for Cloud No. 3, 23 July 1956. The order of magnitude seems to be entirely reasonable for a net vertical acceleration if the observed acceleration is the difference between the mean buoyancy force and the sum of the frictional retarding forces. A temperature difference of 1.0 degree between cloud and ambient air will produce an acceleration of about 300 ft/min<sup>2</sup>. The values found would represent an effective temperature difference (net accelerating force) of about 0.1 degree, a not unreasonable value.

### 3.3 Spectral Analysis

In recent years it has been customary to analyze turbulent motions by means of power spectra. The power spectrum for vertical velocity is a graph of the harmonic analysis of the contribution of the various harmonics to the variance as given in Table 3.1. In practice, the contribution of each harmonic is given by  $C_{i/2}^2$  and  $C_{i/2} = \frac{1}{2} \sqrt{A_i^2 + B_i^2}$ , where  $\sqrt{A_i^2 + B_i^2}$  is the amplitude of the  $i$ th harmonic. Since  $C_{i/2}^2$  has the units of  $\left(\frac{\text{length}}{\text{time}}\right)^2$ , the graph is called a power spectrum. Generally, the graph of the variance is normalized so that the area under the curve is unity. If a spectrum is prepared in the manner described, a stationary time series will exhibit different spectral properties, depending on the portions sampled. However, the smoothed spectra should be the same. The aim of spectrum analysis is to produce a smooth spectrum which is generally representative of the infinite stationary time series.

The latter aim may be accomplished by performing a harmonic analysis of the autocorrelogram. The method is based on the theorem that the cosine transform of the autocorrelation function of the time series

is essentially equivalent to the original series. The property of the cosine transform is that it is actually a Fourier analysis of the autocorrelation coefficients which are even functions, and hence, the sine terms vanish. The Fourier coefficients smoothed by a weighted moving average yield a smooth curve. The advantage of this method over ordinary Fourier harmonic analysis previously described, in addition to rendering a smoothed, reproducible spectrum, is that it is able to treat fluctuations with randomized phase shifts. In actual practice, machine computation is used to compute the autocorrelation functions and the power spectra.

The power spectra have been determined for the vertical component of air flows near the surface and as high as 2,000 ft. Panofsky and co-workers (1953, 1954) have made several studies of the flux of momentum, heat, and kinetic energy as high as 100 meters, using a tower at Brookhaven Laboratories; and Jones (1957), in Great Britain, examined spectra at 2,000 ft. The results of Panofsky are the most complete and are summarized by Van der Hoven and Panofsky (1954). The chief findings of this work are:

(1) The power spectra for vertical velocity are different for stable and unstable lapse conditions.

(2) Under unstable conditions, the spectra tend to have two maxima, one near a one-minute period, and one between six minutes and fifteen minutes. A sharply defined convective case placed the low frequency maximum at ten minutes exactly.

(3) From an examination of the quadrature spectra, the low frequency eddies appear to be taller relative to their breadth during

convection than at other times.

(4) On comparing spectra taken simultaneously at several heights under unstable conditions, the maximum appears to shift toward lower frequencies as the measurements rise through the friction layer.

The vertical velocity data of Chapter II were analyzed for the autocorrelation functions and the power spectra, using the Tukey method (Blackman and Tukey, 1958) programmed by the Weather Radar Group at M.I.T. and run on the M.I.T. IBM 704 electronic computer. The power spectra are shown in Figs. 3.2 through 3.8. Figures 3.2 through 3.5 represent spectra for rising towers which underwent only one cycle of growth, and Figs. 3.6 through 3.8 are for the larger cumulus congestus which had two or more growth cycles. In some of the examples, the spectra for two different total number of correlation coefficients were computed. This was done for two reasons. When  $m$ , the number of lags, is small; the scatter and uncertainty of the spectral estimate is better than when  $m$  is large. However, the period of the largest eddy obtainable is  $2m \Delta t$ , so small  $m$  gives little information about the low frequencies. If more detail is desired about low frequency contributions,  $m$  has to be large with resulting large sampling fluctuations. In practice,  $m$  was chosen to be 12 and either 20 or 24, depending on the length of data.

In Figs. 3.2, 3.3, and 3.4, the maximum amount of kinetic energy is in the low frequencies. The peak harmonic band is not clearly delineated by 12 lags, but when 20 lags are used (Fig. 3.3b), the peak is better defined and appears near a ten-minute period at the low frequency. There is no pronounced secondary maximum as found by Panofsky

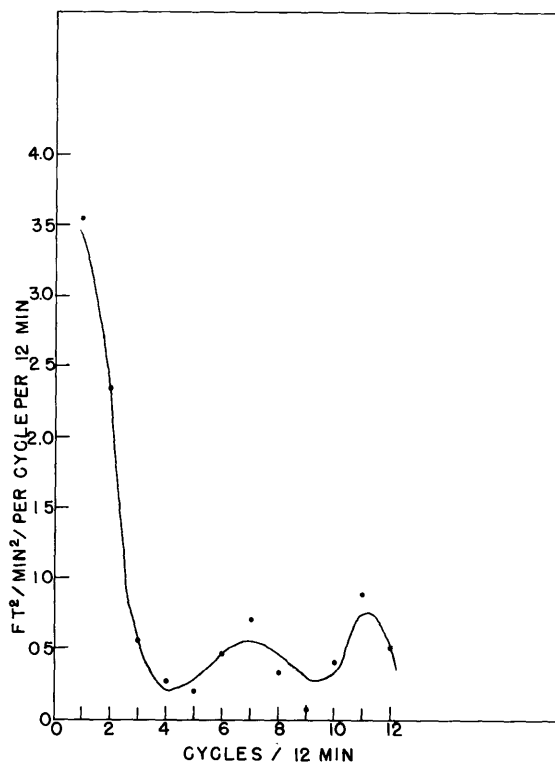
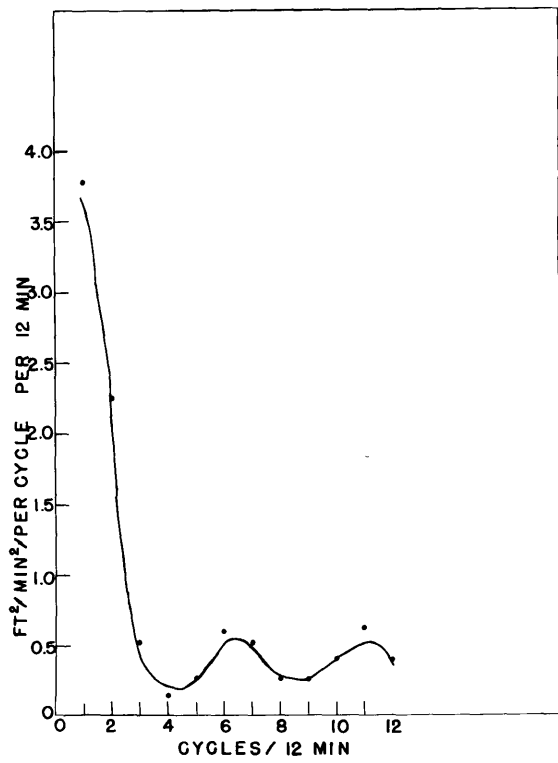
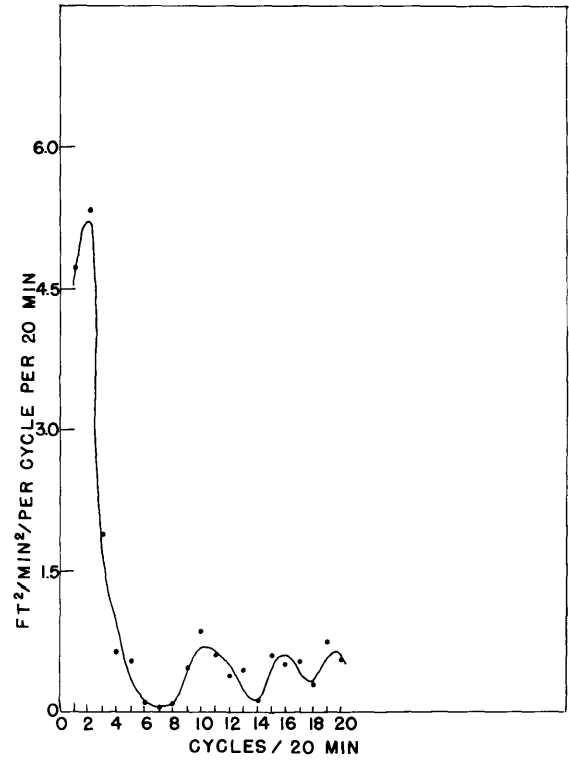


Fig. 3.2 Power Spectrum for Cloud No. 1,  
23 July 1956.  $m = 12$ .

at the high frequency end of the spectrum, but a not inconsiderable amount of energy appears near the two-minute period in all three clouds. This may be significant since the data are averaged at thirty second intervals to prevent "aliasing." The meaning of the term "aliasing" refers to the way high frequency oscillations contribute their energy to the spectrum at frequencies lower than their actual values. Averaging removes this effect. Figure 3.5a,b, the spectrum for Turret No. 2,



a.



b.

Fig. 3.3 Power Spectra for Cloud No. 1, 24 July 1956.  
In a,  $m = 12$  and in b,  $m = 20$ .

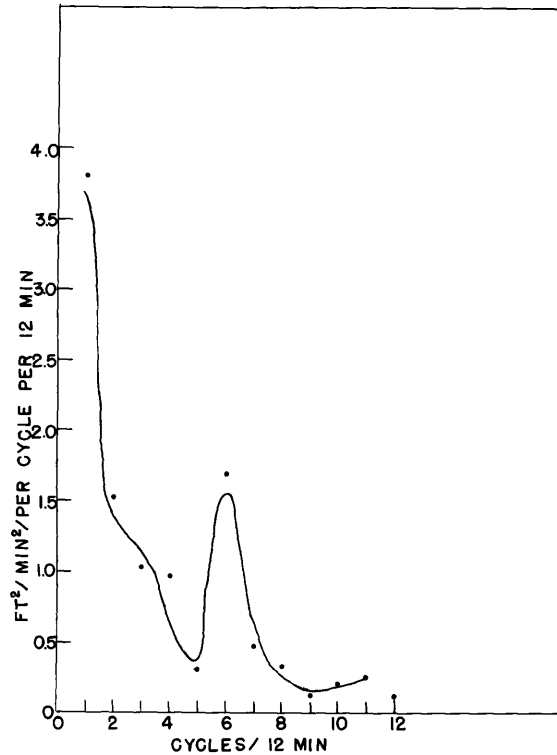
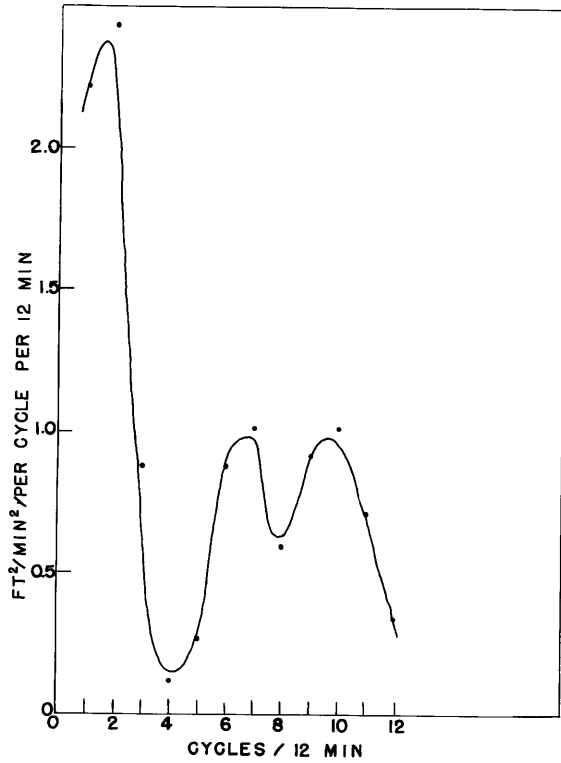
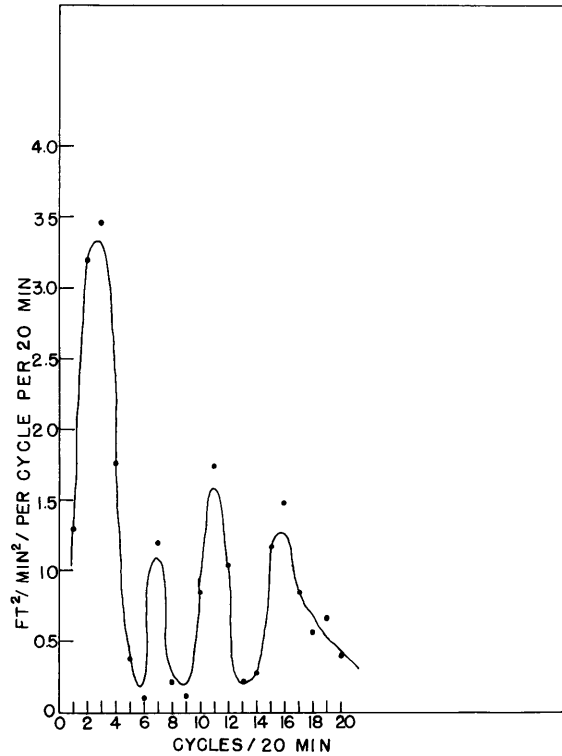


Fig. 3.4 Power Spectrum for Cloud No. 2, Turret No. 1,  
24 July 1956.  $m = 12$ .

Cloud No. 2, 24 July 1956 shows much more energy spread throughout the higher frequencies than the previous towers, although it repeats the pronounced maximum near ten minutes. During the late stages of this tower, the whole cloud commenced to spread horizontally in its upper portion. In view of this, it seems reasonable to connect this turret



a.



b.

Fig. 3.5 Power Spectra for Turret No. 2, Cloud No. 2, 24 July 1956.  
In a,  $m = 12$  and in b,  $m = 20$ .

with the main Cloud No. 2 and consider it as a third cycle in the growth of the whole cloud. A possible explanation for the presence of energy spread over the whole spectrum in this turret may be due to the shift in growth behavior of the parent cloud from essentially a rising tower to a larger fixed cellular circulation.

The clouds with two or more growth cycles (Figs. 3.6, 3.7, and 3.8) confirm the previous finding of large energy at the low frequency end of the spectrum. Moreover, in all of these clouds a secondary maximum appears in the high frequencies. As before, a slight rise exists in all three clouds near two minutes and a strong maximum is found near one minute in the case of Cloud No. 2 and Cloud No. 3, 24 July 1956.

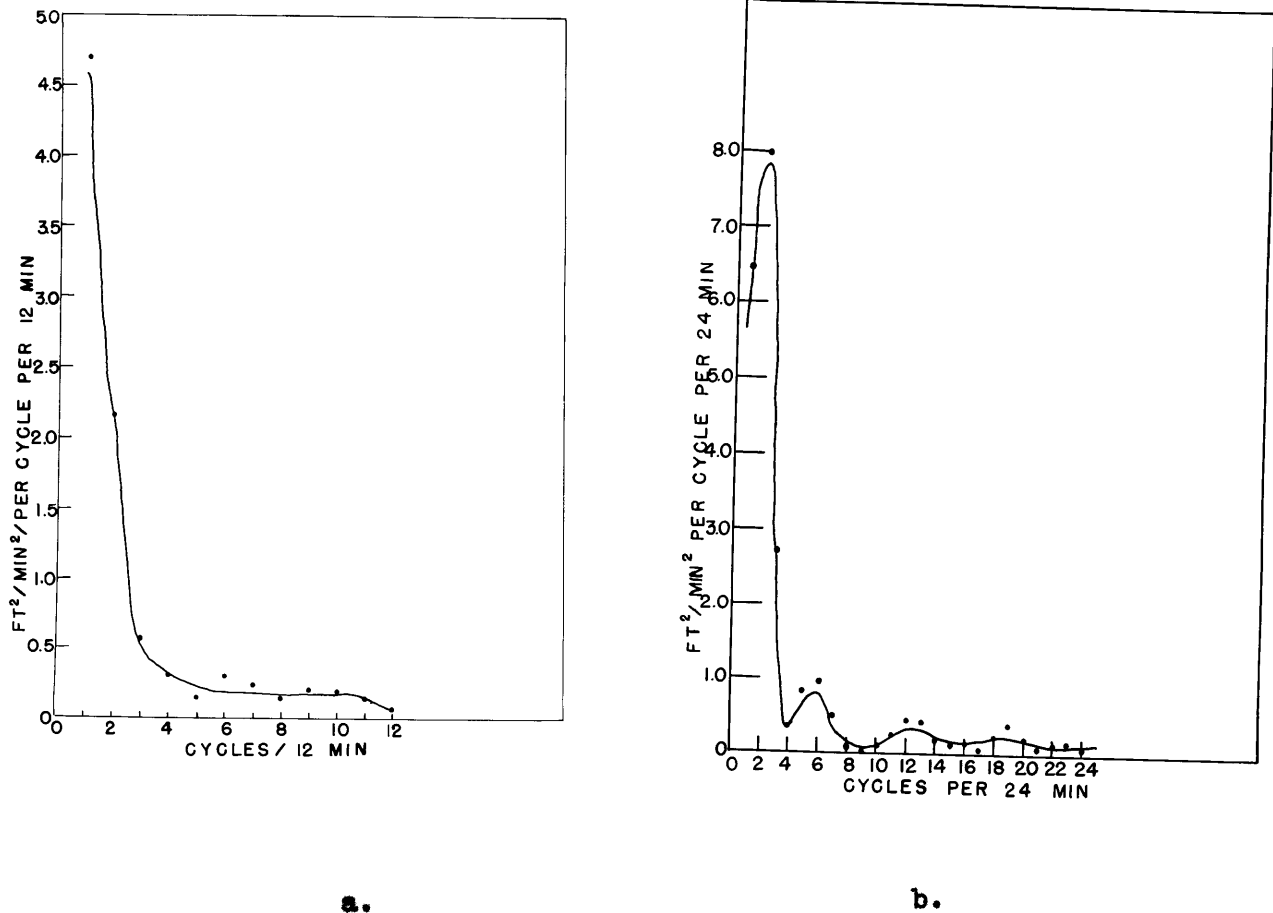


Fig. 3.6 Power Spectra for Cloud No. 3, 23 July 1956.  
In a,  $m = 12$  and in b,  $m = 24$ .



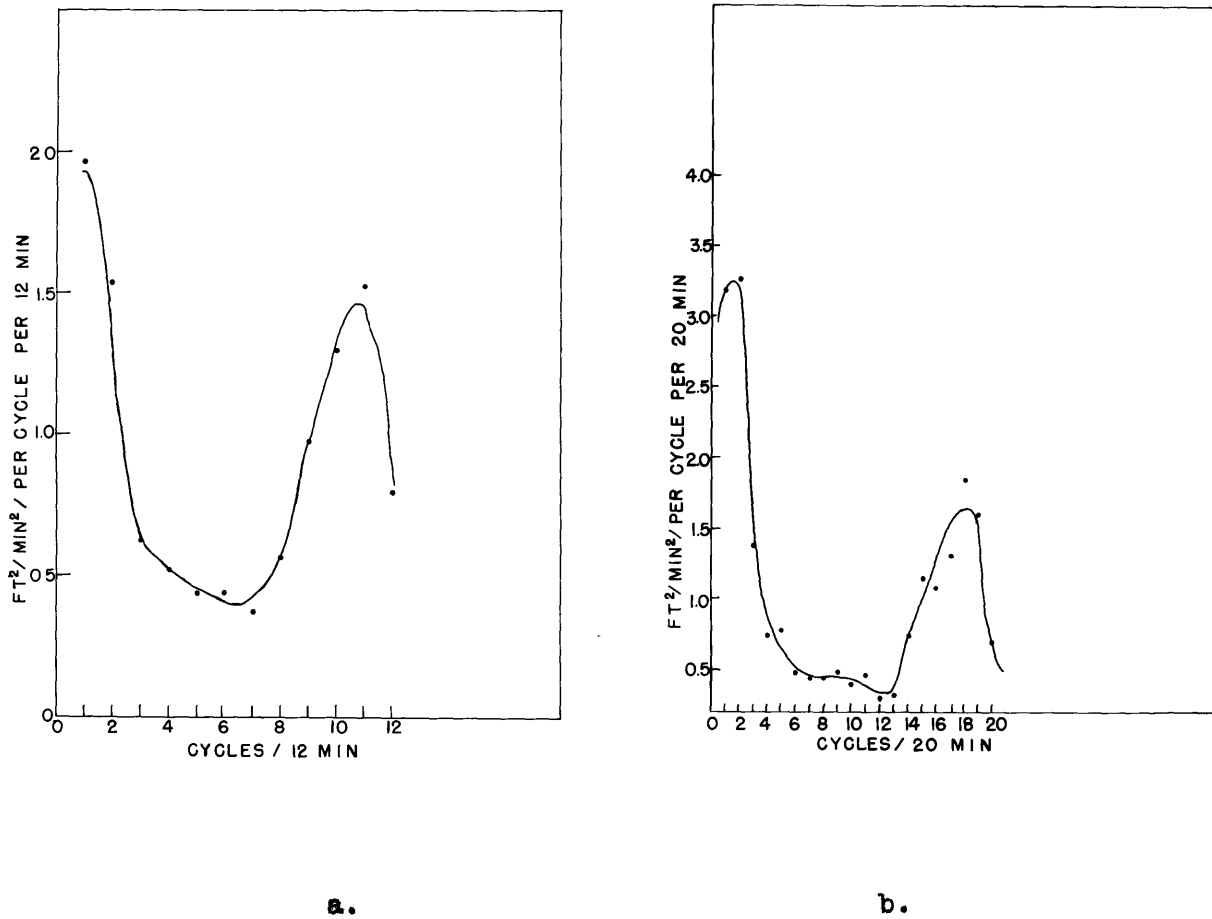


Fig. 3.7 Power Spectra for Cloud No. 2, 24 July 1956.  
 In a,  $m = 12$  and in b,  $m = 20$ .

Interestingly, these two clouds grew close to each other and would be expected to be influenced by the same mesoscale meteorological variables. Cloud No. 3, 23 July 1956 (Fig. 3.6) did not show the secondary maximum near one minute, but has a small rise near four minutes.

Perhaps these finer features in the spectra bear little significance to the meteorological situation, but there is uniformity of agreement for every cloud studied in placing a maximum in the spectrum near ten minutes.

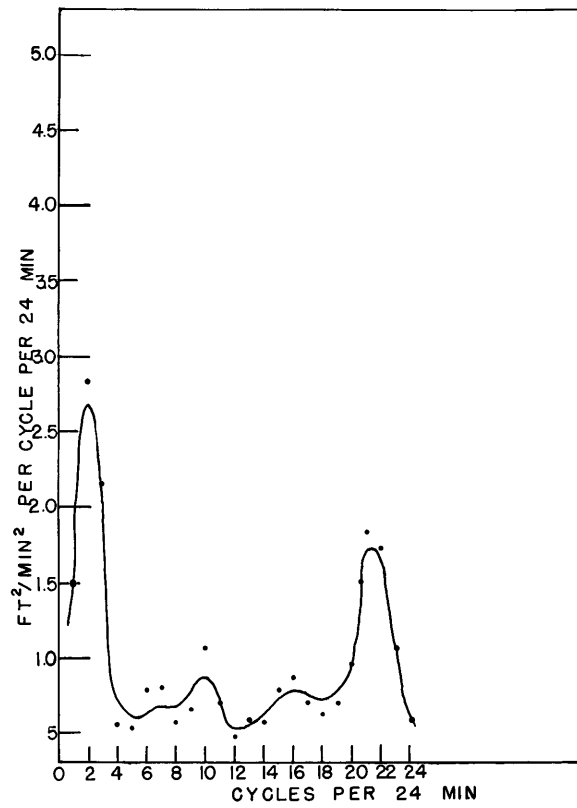


Fig. 3.8 Power Spectrum for Cloud No. 3, 24 July 1956.

The influence of  $m$  on the spectral estimate may be seen in the equation which defines the estimate. According to Blackman and Tukey (loc. cit.), the spectral estimates in a stationary time series have a distribution about the spectral estimate equal to  $\chi^2/f$ .  $\chi^2$  (chi-square) is tabulated in standard statistical works and  $f$ , the number of degrees of freedom, is given as

$$f = \frac{2N - m/2}{m} \quad (3.4)$$

where  $N$  is the number of observations and  $m$  is the number of lags. The larger  $m$ , the smaller the degrees of freedom and the larger the uncertainty. The uncertainty is illustrated for the low frequency peak for Cloud No. 2, 24 July 1956 (Fig. 3.7) in Table 3.3.

TABLE 3.3

Confidence Limits of Spectral Estimates

No. of Lags, $m$	Given Estimate	90% Limits	80% Limits
20	3.26	1.25 to 27.86	1.57 to 16.72
12	1.97	0.94 to 7.30	1.11 to 5.32

The wide confidence limits associated with the indicated peak makes the power spectrum not suitable to pinpoint the location or existence of outstanding single harmonics or narrow bands.

3.4 Autocorrelograms

To aid in isolating the important harmonics, the autocorrelation function was plotted against the lag. If we are dealing with a truly periodic phenomenon like a sine curve, strong valleys and peaks should

mark the autocorrelogram. In general, the autocorrelogram shows fluctuations with the same kinds of periods as the time series; however, all fluctuations have been put in phase. As in the case of the power spectra, the autocorrelograms are divided into two groups. The first group, Figs. 3.9 through 3.12, are clouds which show a single cycle. The autocorrelograms for these have a minimum around five to seven minutes (ten to fourteen lags) which should be the expected position if the total period is about ten to twelve minutes and is a one cycle sine curve.

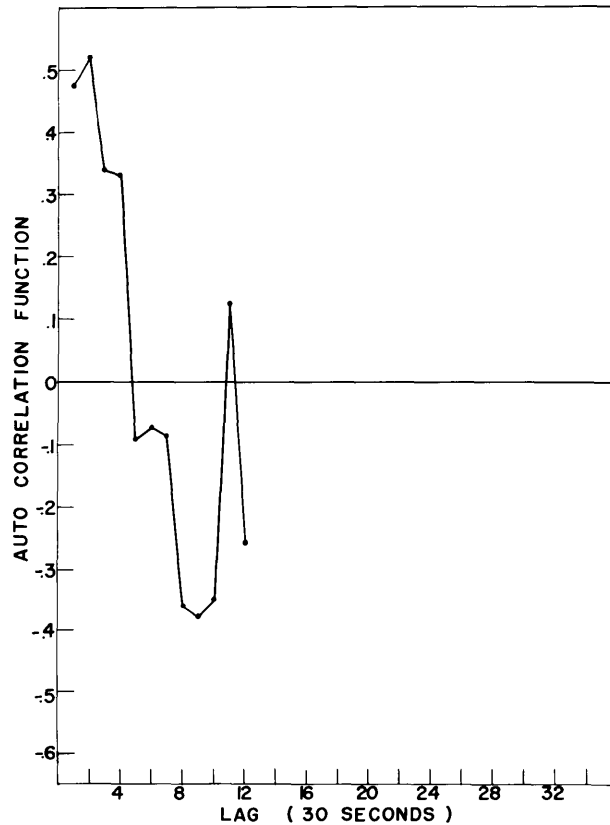


Fig. 3.9 Autocorrelogram for Cloud No. 1, 23 July 1956.

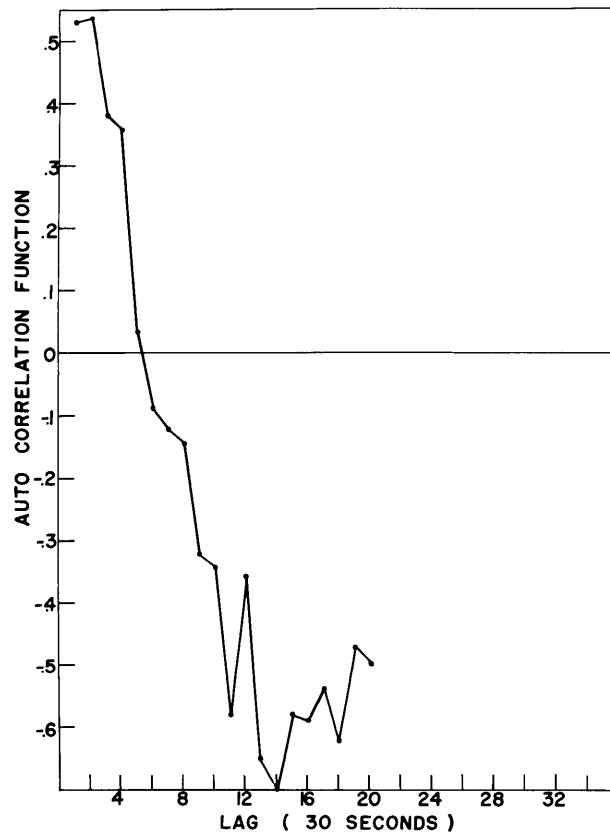


Fig. 3.10 Autocorrelogram for Cloud No. 1, 24 July 1956.

The curves do not complete the cosine shape because the vertical velocity decreases continuously as the clouds die. The exception is Cloud No. 2, Turret No. 2 (Fig. 3.12) which recovers to a maximum near nine (eighteen lags) minutes. In view of the highly fluctuating nature of this curve after nine lags, it appears more likely that the nature of the time series beyond five minutes is random. This is the same conclusion the power spectrum (Fig. 3.5) suggested.

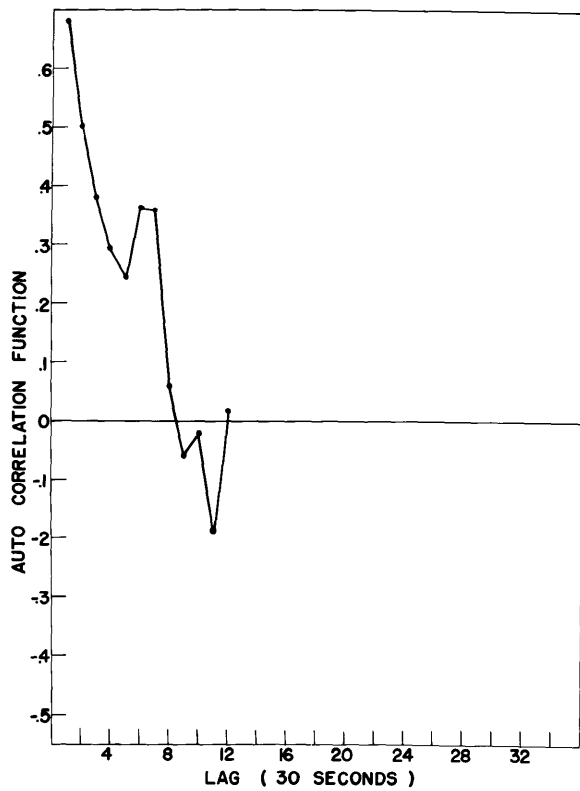


Fig. 3.11 Autocorrelogram for Cloud No. 2,  
Turret No. 1, 24 July 1956.

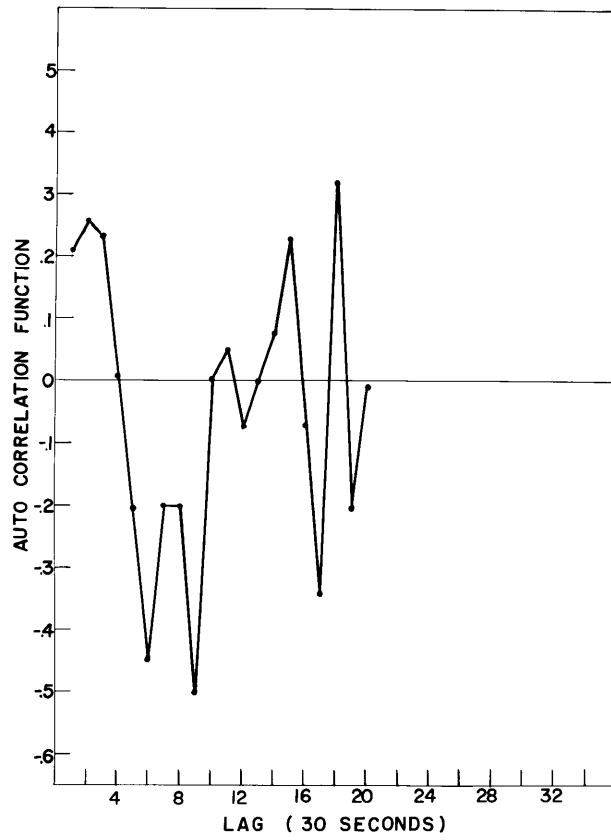


Fig. 3.12 Autocorrelogram for Cloud No. 2,  
Turret No. 2, 24 July 1956.

The remaining autocorrelograms, Figs. 3.13 through 3.15, are for the cumulus congestus clouds having two or more growth cycles.

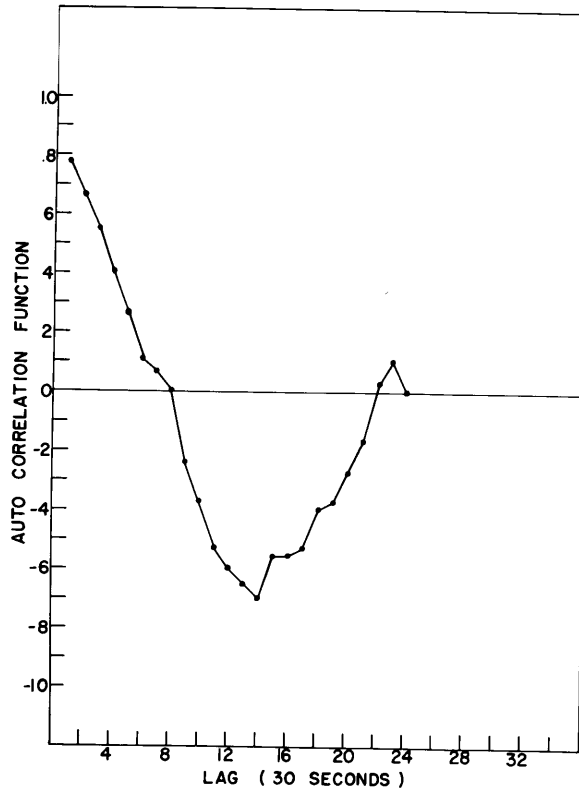


Fig. 3.13 Autocorrelogram for Cloud No. 3,  
23 July 1956.

If the growth is exactly periodic, the curves should be cosines with the maximum following the minimum at twice the lag,  $m$ , of the minimum.



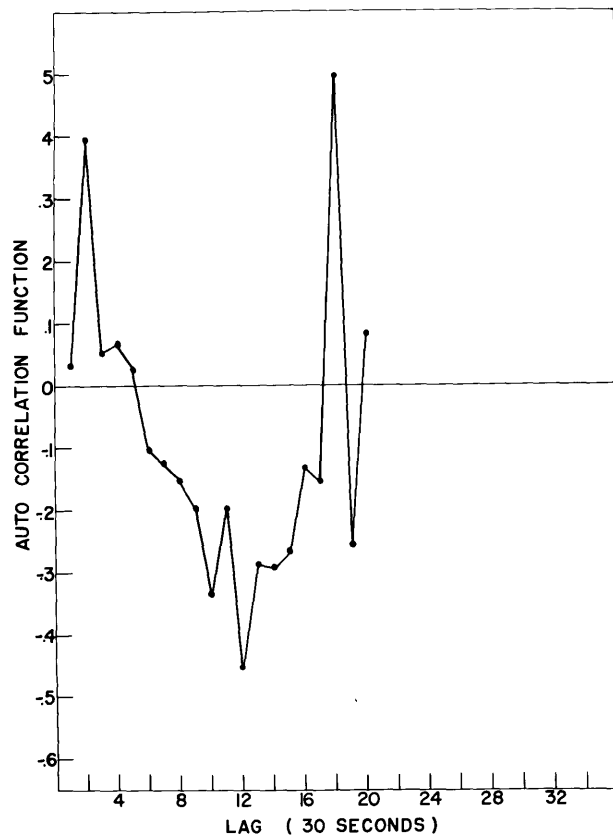


Fig. 3.14 Autocorrelogram for Cloud No. 2,  
24 July 1956.

The autocorrelograms fulfill the first requirement very well. All three have a maximum following the minimum in cosine fashion. However, the position of the maxima is not always exactly at twice the lag number of the minima. At best, we can conclude the phenomenon appears to be periodic but the original time series is not a perfect sine curve.

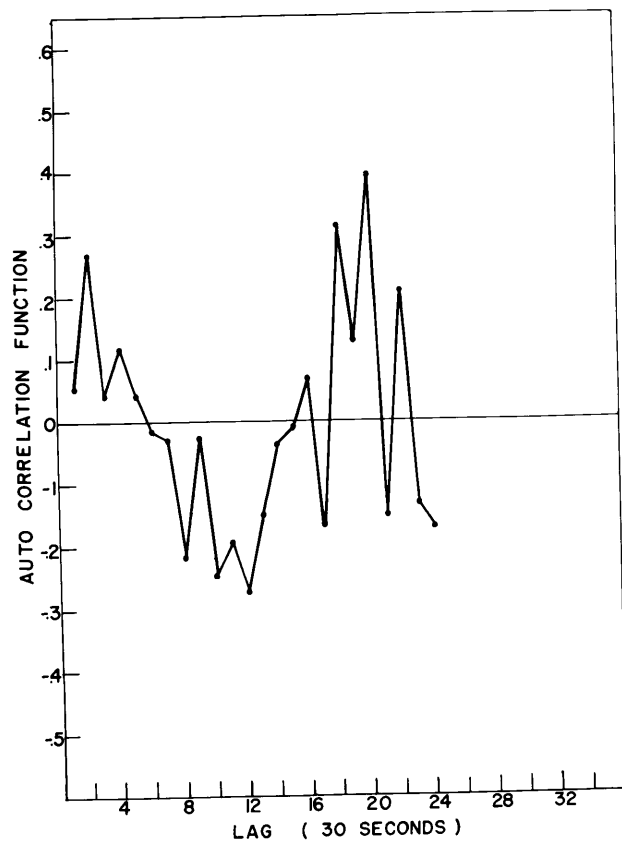


Fig. 3.15 Autocorrelogram for Cloud No. 3,  
24 July 1956.

In summary, the analyses of the original time series by the various techniques covered in the preceding sections reveal what we consider significant features to be encompassed by a theoretical explanation:

(1) Growth is achieved by pulsations superimposed on a positive trend.

(2) The trend implies a slowly increasing upward current, accelerating at an effective temperature difference of 0.1 degree between the cloud column and ambient air.

(3) The fluctuations about the trend contain many and varied frequencies but there is a maximum of the kinetic energy in the low frequency part of the power spectrum. A secondary maximum is sometimes found near one to two minutes.

(4) The autocorrelograms support the conclusion that the low frequency fluctuations tend to be periodic with a period near ten minutes.

#### IV. THEORETICAL BASIS FOR CUMULUS CIRCULATION

##### 4.1 Kinematical Contribution

The acceleration and flux analyses based on position data measured always at the top of the cloud are to be interpreted in terms of local changes only. Since the relative point of measurement remained constant, the data so obtained cannot provide any information on the instantaneous vertical profile of velocity and flux. Vertical gradients of temperature, moisture, and velocity are expected to be important in the development of the convection. For example, the dynamic entrainment hypothesis proposed by Houghton and Cramer (1951) depends on vertical velocity gradients along the vertical to induce horizontal mixing of environmental air into the cloud column. In a larger sense, the importance of local changes against advective contribution is bound up with the existence of appreciable vertical gradients. We shall see that a clear distinction may be drawn between the cellular mode and the parcel mode, using this approach.

In the parcel mode, the emphasis is on the vertical advection of a sharp velocity gradient comprising the disturbed volume or bubble by the buoyancy force acting on the bubble. In the cellular mode, a broad gradient in vertical velocity exists between the ground and the cell top which is basically parabolic, although it may be skewed to be more pronounced in the upper regions, as in Haltiner's (loc. cit.) and Hague's (loc. cit.) models. As the cellular circulation changes with time, the over-all shape of the vertical velocity vertical profile is expected to remain the same, in general. The minima and maxima should

be found at the same heights, for instance. Thus, the changes in circulation in the cellular mode are mainly local changes; whereas, the changes in the vertical profile for the parcel mode's vertical velocity are principally advective. This view recognizes that mixing and erosion as proposed by proponents of the bubble hypothesis are local changes and are responsible for the over-all decay of the bubble.

Specifically, if this argument is extended to a cloud, its over-all shape and appearance should depend on the particular mode of convection it is following. A cloud formed by vertically moving parcels would have a base which moves upward with the parcel. This is the case for a spherical vortex; and the mushroom atomic clouds are excellent examples. We may revert to the source-sink analogy of Chapter II to fix ideas. A bubble or spherical vortex is a doublet; i.e., a combination in which the distance of separation between the source and sink is infinitesimal. A moving doublet has a closed stream line which is identical to that of an equivalent sphere; e.g., Milne-Thomson (1950). On the other hand, a source-sink combination in which the sink remains fixed while the source moves away will generate the closed stream line of a rounded end cylinder. This example was illustrated in Fig. 2.11 where the sink is located at minus infinity. If the sink were placed at the cloud base and the source allowed to move upwards, the shape of the ensuing cloud would resemble very closely a cumulus tower. In view of the qualitative agreement between observed trajectories (Fig. 2.12) and those for a moving source (Fig. 2.11) and the fact that the cumulus towers are cylindrically shaped with fixed bases, it seems reasonable to take the moving source-fixed sink analogue as a kinematical model for rising

cumulus towers. This model defines a cellular circulation whose cell height is increasing with time. When the cell attains its maximum height, a larger circulation is revealed by the spreading anvils. The mature cell would have the stream lines for its circulation, as given by a stationary doublet.

Any tendency for a cumulus cloud to shift into the moving cell or parcel mode would be seen as a change in the shape of the cloud. Some hint of this possibility is seen in the manner of decay of some of the clouds wherein the column disappears by evaporation commencing at its lower part and progressing upward. This effect could be considered dynamic entrainment.

#### 4.2 Proposed Model of Cumulus Circulation

When the dynamic evidence of Chapters II and III is taken together with the kinematical considerations, the following cumulus model emerges to incorporate these features:

1. A large cell extending from the sub-cloud layer to near the tropopause with a horizontal diameter at least as great as its height.
2. A smaller cell whose vertical axis is common with that of the larger cell but whose horizontal diameter is quite smaller than the larger cell.
3. The larger cell has a circulation which has a fairly constant acceleration over much of its life. It begins as an exponential growth of the velocity but the mean cell and ambient air temperature difference becomes steady, which results in a linear increase of velocity with time.

4. The large cellular circulation decays because of the accumulated effect of non-symmetrical responses in the velocity along the closed cell stream line brought on by frictional effects and hastened by dynamic entrainment of dry air above the cloud base.

5. The small cell is a transient phenomenon existing only during the time the large cell is building vertically to its maximum height. Its circulation alternates in direction with a period near ten minutes.

6. The small cell derives its energy from the latent heat of condensation while the large cell utilizes this source as well as external (to the cloud) sources such as surface heating, orographic effects, and synoptic scale effects.

7. The large cell obeys hydrodynamical forces acting on the mean state of the cloud column and ambient air. The small cell behaves as if it reacts to the pseudo-adiabatic processes.

8. A chaotic confusion of even smaller motions exists because of the fine structure in the temperature distribution and these are reflected as higher frequency turbulence near one to two minute periods. An even finer scale of isotropic turbulence is presumed to exist which finally degrades the kinetic energy to heat.

The observational measurements have suggested the circulation of cumuli, particularly the larger forms, as being cellular. The task of theory is to derive in a logical way the governing mathematics.

#### 4.3 Mathematical Analysis

The clue to the proper mathematical formulation of the problem lies in the assumption that one is dealing with cellular circulations. The two cells may be treated as being independent of each other, or varying

degrees of mutual coupling may exist. The analysis should lead to a predicted behavior for each of these cases which can be compared to observation.

The Circulation Theorems of V. Bjerknes have been known since 1901, but it was not until Høiland's paper in 1939 (see Godske et. al. (1957) for an account since Høiland's paper is difficultly accessible) that oscillating circulations were shown to be possible under certain stability configurations, although the original theorems predicted exponential solutions.

In what follows, a quasi-rigorous treatment is used to obtain results quite similar to those yielded by the more rigorous development; e.g., Eliassen and Kleinschmidt (1957). This procedure was adopted in order to keep the physical connection as clear as possible yet avoid the awkward terminology employed in the treatment by Godske et al. (1957). If one proceeds from the classical perturbation equations for convective motions in two dimensions in an incompressible, inviscid fluid; e.g., Sutton (1953):

$$\frac{\partial u}{\partial t} = - \frac{1}{\rho} \frac{\partial p}{\partial x} \quad (4.1)$$

$$\frac{\partial w}{\partial t} = - \frac{1}{\rho} \frac{\partial p}{\partial z} + g \frac{(T' - T_0)}{T_0} \quad (4.2)$$

where  $u$  and  $w$  are the perturbed velocities,  $\rho$  a constant density throughout the fluid except where it is directly related to buoyancy,  $T'$  the perturbed temperature,  $T_0$  the steady state temperature, and  $p$  is the perturbed pressure caused by convection. The heating of the



fluid is supposed to have no dynamic consequences except that of producing buoyancy.

As a measure of the static stability of the atmosphere we may, after Eliassen and Kleinschmidt (1957), define the parameter  $\gamma'^2$ :

$$\gamma'^2 = \frac{g^2}{T} \rho \left( \frac{DT}{Dp} - \frac{\partial T / \partial z}{\partial p / \partial z} \right) \quad (4.3)$$

$\gamma'^2$  is the restoring buoyancy force per unit length of vertical displacement and has the dimension of frequency squared. The numerical value of  $\gamma'^2$  will depend on the particular physical process. For example, in the case considered by Brunt (1927), we have a particle displaced from its equilibrium position. For dry or non-saturated air

$$\gamma'^2 = \frac{g}{\theta} \frac{\partial \theta}{\partial z} = g/T (\gamma - \gamma_d) \quad (4.4)$$

$\theta$  = potential temperature

$\gamma_d$  = dry adiabatic lapse rate

$\gamma$  = environment lapse rate

While for saturated air,

$$\gamma'^2 = \frac{g}{T} (\gamma - \gamma_s) \quad (4.5)$$

$\gamma_s$  = saturated adiabatic lapse rate.

In general, we can replace the buoyancy term in Equation (4.2) by an expression involving the static stability parameter,

$$g \rho \frac{(T' - T_0)}{T_0} = -\gamma'^2 \rho z \quad (4.6)$$

where  $z$  is the vertical displacement

$\gamma^2$  is the static stability for the process.

When this substitution is made in (4.2) and the perturbation pressure terms eliminated by multiplying (1) by  $dx$  and (2) by  $dz$ , adding and integrating along a closed curve, we find V. Bjerknes' second circulation theorem after H6iland in a form shown by Eliassen and Kleinschmidt (1957):

$$\oint \rho \left( \frac{\partial u}{\partial t} dx + \frac{\partial w}{\partial t} dz \right) = - \oint \gamma^2 \rho z dz \quad (4.7)$$

This equation states that the circulation of the acceleration is equal to the circulation of the vertical restoring force. For a closed streamline, the motion will be either a stable standing oscillation, or an unstable cellular circulation, depending on the sign of  $-\gamma^2$ , which in turn depends on the particular process. The horizontal displacements do not produce any buoyancy forces, thus the restoring forces must drive the horizontal as well as the vertical oscillations. Cells which have tall vertical legs connected by short horizontal legs will produce the most intense acceleration, while predominantly horizontal cells will produce small accelerations. As will be pointed out later, the frequency,  $\gamma$ , is independent of the cell height but is dependent on the ratio of the widths of the two vertical legs.

The restoring force per unit length may be interpreted in terms familiar to the meteorologist if we make use of the concept of a thin horizontal section through the convection cell as a "slice" much in the same manner as introduced by J. Bjerknes (1938) and elaborated by

Petterssen (1956). Although this concept examines only a portion of the cell, since the frequency applies to all parts simultaneously, the frequencies so derived will be valid so long as the "slice" is through the vertical legs and a uniform lapse rate with height exists in the environment. In the more likely event that the environment lapse rate is not constant with height, this analysis applies to a mean lapse of temperature.

Consider the cellular circulation in air, Fig. 4.1, where ascending motion takes place in the left branch and descending motion in the right branch with temperatures

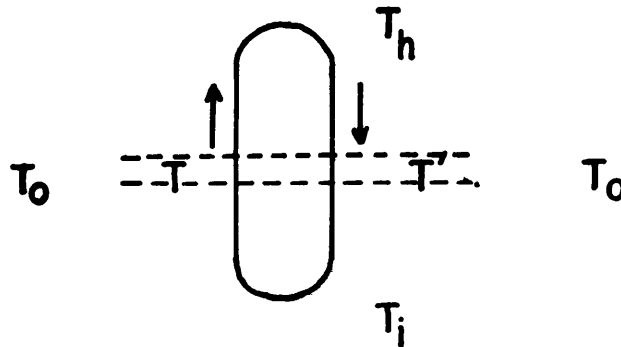


Fig. 4.1 Half Cell Illustrating the Slice Method.

$T$  and  $T'$  characterizing the slice through the left and right legs, respectively. These are perturbed temperatures; that is, temperatures due to the motion. The temperature of the air at rest at that level is  $T_0$  and the over-all environment is marked by a uniform lapse rate.

For the ascending branch, the restoring force,  $f_a$ , acting at the

slice, is given by:

$$f_a = \frac{g(T - T_0)}{T_0} \quad (4.8)$$

and for the descending branch at the slice, the restoring force,  $f_d$ :

$$f_d = -g \frac{(T' - T_0)}{T_0} \quad (4.9)$$

The total restoring force acting at the slice shown is the sum:

$$F = f_a + f_d = \frac{g}{T_0} (T - T_0) - \frac{g}{T_0} (T' - T_0) \quad (4.10)$$

which is similar to an expression derived by Godske et al. (1957). For a cloud, consider the ascending branch to lie on the inside of the cloud and the descending branch to be in the clear air away from the cloud. This type of circulation is pictured after Godske et al. (1957).

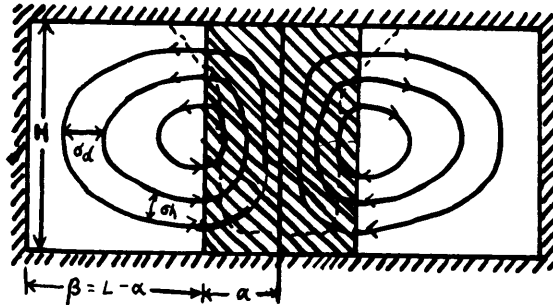


Fig. 4.2, Idealized Circulation, with saturated ascending and unsaturated descending air; the probable cloud limit in an analogous system in nature (cumulus circulation) is suggested by dashed line (after Godske et al, 1957).

In terms of the appropriate lapse rate

$$\begin{aligned} T - T_0 &= (T_1 + \gamma_s \Delta z_+) - (T_1 + \gamma \Delta z_+) \\ &= (\gamma_s - \gamma) \Delta z_+ \end{aligned} \quad (4.11)$$

$$\begin{aligned} T' - T_0 &= (T_h + \gamma_d \Delta z_-) - (T_h + \gamma \Delta z_-) \\ &= (\gamma_d - \gamma) \Delta z_- \end{aligned} \quad (4.12)$$

where  $T_1$  is the temperature of the environment at a lower level, a distance  $\Delta z$  from which the ascending air in the slice under consideration has come, and  $T_h$  is the temperature at a level  $\Delta z$  above the slice from which the descending air in the right hand slice has come. The process lapse rate,  $\left(\frac{\partial T}{\partial z}\right)_p = \gamma_p$ , is a negative quantity. Inserting

Eqs. 4.11 and 4.12 into Eq. 4.10 yields

$$F = \frac{g}{T_0} [(\gamma_s - \gamma) \Delta z_+ - (\gamma_d - \gamma) \Delta z_-] \quad (4.13)$$

Utilizing the equation of continuity as employed in the "slice" method; e.g. J. Bjerknes (1938), assuming constant density as before:

$$A_+ W_+ = - A_- W_- \quad (4.14)$$

where  $A_+$  and  $A_-$  are the cross sectional areas of the slice occupied by the ascending and descending air, respectively; and  $W_+$  and  $W_-$  are the corresponding vertical velocities. If  $W = \frac{\Delta z}{\Delta t}$ , for equal times,

$$\begin{aligned} A_+ \Delta z_+ &= - A_- \Delta z_- \\ \Delta z_- &= - \frac{A_+}{A_-} \Delta z_+ \end{aligned} \quad (4.15)$$

Inserting this result into Eq. 4.13, we get:

$$-\nu^2 \Delta z = F = \frac{g}{T_0} \left[ (\gamma_s - \gamma) + (\gamma_d - \gamma) \frac{A_+}{A_-} \right] \Delta z \quad (4.16)$$

$$-\nu^2 = \frac{g}{T_0} \left[ (\gamma_s - \gamma) + (\gamma_d - \gamma) \frac{A_+}{A_-} \right] \quad (4.17)$$

This result is identical with that achieved by Petterssen (1956). Beers (1945) arrives at a similar result starting from V. Bjerknes' first circulation theorem. Beers has extended the slice method to measure the total circulation acceleration over a finite cell height by performing the slice integration over a number of atmospheric layers, guided by the vertical sounding.

We are interested in the motions likely to develop when the atmosphere is conditionally labile, or more commonly called conditionally unstable. Conditional instability is easily demonstrated by the use of a thermodynamic diagram. In Fig. 4.3, taken from Petterssen (1956), following Petterssen's description, a parcel of air at R is stable if lifted dry adiabatically from R to A, the lifting condensation level, LCL, and thence along a wet adiabatic to B, the level of free convection, LFC. All along its path R to B, the parcel is colder than the surrounding environment and will tend to sink unless some external lifting force is employed. However, when the parcel reaches B, it will be in equilibrium with its environment and if it were moved a small distance above B, it would acquire positive buoyancy and would accelerate upward until it exceeded level D. Thus, the parcel is conditionally unstable; i.e., provided it is lifted above the level of free convection.



saturated ascent through a nonsaturated environment,

$$\Delta T = \Delta Z [(\gamma_s - \gamma) + \frac{A_+}{A_-} (\gamma_d - \gamma)] \quad (4.18)$$

It should be noted that Petterssen defines  $\gamma_p = - \left( \frac{\partial T}{\partial z} \right)_p$ . According to the slice method, the limit between stability and instability (where  $\Delta T = 0$ ) depends on both the lapse rates and the ratio of cloudy to cloudless air, or more exactly, the ratio between the area of ascending air and area of descending air. It is assumed that cumulus circulations will develop only if  $\Delta T$  is positive. This corresponds to the instability required to initiate circulation acceleration believed necessary for cumulus development; e.g., Beers (1945) or Godske et al (1957).

Under ordinary circumstances,  $\gamma_d > \gamma > \gamma_s$ , which is the definition for conditional instability. Thus, in Eq. 4.18, if the factor  $\frac{A_+}{A_-}$  is omitted; that is, set equal to one, one will most always find  $\Delta T < 0$  because the term  $(\gamma_d - \gamma)$  is a larger negative quantity than  $(\gamma_s - \gamma)$  is a positive quantity:

$$|\gamma_d - \gamma| > |\gamma_s - \gamma|$$

To allow  $\Delta T > 0$ , the ratio  $\frac{A_+}{A_-}$  is adjusted to allow

$$\frac{A_+}{A_-} < (\gamma_s - \gamma) / \gamma_d - \gamma \quad (4.19)$$

Petterssen concludes that energy-producing clouds occur only when the ratio  $\frac{A_+}{A_-}$  is less than 0.5.

The following table is taken from Petterssen (1956).



TABLE 4.1\*

Critical Values of the Ratio  $A_+/A_-$  For Various Values of  $\gamma$  and  $\gamma_s$

$\gamma$ °C per 100 m	$\gamma_s$ , °C per 100 m					
	0.3	0.4	0.5	0.6	0.7	0.8
0.3	0.0					
0.4	0.17	0.0				
0.5	0.40	0.20	0.0			
0.6	0.75	0.50	0.25	0.0		
0.7	1.33	1.00	0.67	0.33	0.0	
0.8	2.50	2.00	1.50	1.00	0.50	0.0

\* Note: Petterssen defines  $\gamma_p = - \left( \frac{\partial T}{\partial z} \right)_p$ .

If the disturbance is such that the ratio  $A_+/A_-$  is less than the critical ratio as shown in the table, acceleration of the vertical currents would occur and a cloud would grow. On the other hand, if  $A_+/A_-$  were greater than the critical value, convection is suppressed. Godske et al. (1957) have used this criterion to state a number of "rules" for cumulus development.

At a point where the closed stream line of the cell is tangent to the vertical axis of the cloud, we may determine the nature of the vertical velocity variation with time because the frequency of the circulation acceleration applies to all portions of the fluid along the stream line.

From Eq. 4.7 we may write for this point

$$\frac{\partial w}{\partial t} = -\nu^2 z \quad (4.20)$$

or

$$\frac{\partial^2 w}{\partial t^2} = -\nu^2 w \quad (4.21)$$

When  $-\gamma^2 < 0$ ,  $w = A \sin \gamma t$ , and when  $-\gamma^2 > 0$ ,  $w = A \sinh \gamma t$  if  $w = 0$  at  $t = 0$ .

When  $-\gamma^2 > 0$ , we have an exponential increase in the circulation with time and when  $-\gamma^2 < 0$ , harmonic oscillations about an equilibrium value of period  $\frac{2\pi}{\gamma}$  are expected. We have seen how  $-\gamma^2$  depends greatly on the lapse rate in the environment and even more greatly on the choice of the ratio  $\frac{A_+}{A_-}$ . We cannot go further in deciding what  $\frac{A_+}{A_-}$  is representative to use without recourse to experimental data.

In III, the vertical velocity measured at the cloud top demonstrated a periodic variation. Under no circumstances did the measured vertical velocity suggest a runaway tendency such as the exponential solution will generate. Other authors have observed no exponential increase in the vertical velocity at the top of growing cumulus. Even under thunderstorm development, the vertical velocity remains limited. Malkus and Scorer (1955) found a fairly constant velocity for the cloud top over the active portion of its upward growth. Scorer and Ludlam (1953) reported for measurements of cumulus that a limiting velocity for the rate of rise of cumulus towers was reached within two minutes or so and thereafter for many minutes over nearly all of its life the vertical velocity of the cloud top seemed constant. If we rely on observational evidence, we are led to accept the novel idea that cumulus growth occurs as a stable oscillation imposed on a constant acceleration instead of an unstable runaway development. This hypothesis is supported overwhelmingly by the Tucson data and the suspicion lurks that curve smoothing by other investigators has prevented this possibility from being observed before now.

We see from Eq. (4.21) if the temperature difference between cloud and environment is governed by pseudo-adiabatic processes, depending on the size of the disturbance, either stable or unstable solutions result. In the mathematical development, the cloud temperature is directly proportional to the vertical motion and related to it only. However, in a real cloud other processes will be at work to limit the local temperature change. Such factors as eddy conduction of heat, eddy diffusion of mass, entrainment and mixing will tend to create an equilibrium temperature which is steady in time and less than the moist adiabatic temperature.

To examine this aspect, we have to return to Eq. (4.7) and insert the relationship given by Eq. (4.6). The simplified form along the vertical axis, as expressed in Eq. (4.20), now becomes:

$$\frac{\partial w}{\partial t} = \frac{g}{T_0} (T' - T_0) \quad (4.22)$$

where  $(T' - T_0)$  no longer is a function of  $z$  or  $w$ . In this sense,  $\frac{g}{T_0} (T' - T_0)$  may be regarded as a vertically averaged net buoyancy force which remains constant over most of the cell life. In Chapter III, it was shown that the effective magnitude of  $(T' - T_0)$  was about 0.1 degree.

Although it is beyond the scope of this investigation to inquire into the details of the decay of these motions, it is conceivable that a suitable representation of the opposing frictional forces may be a lumped term,  $\sum f(t)$  which is given as

$$\frac{\partial w}{\partial t} = \frac{g}{T_0} (T' - T_0) - \sum f(t) \quad (4.23)$$

where it can grow with time to ultimately bring the circulation to rest.

We can re-examine the role of the parameter  $A_+/A_-$  in cumulus development with this new concept in mind. In Eqs. 4.17 and 4.19, the term  $[(\gamma_s - \gamma) + (\gamma_d - \gamma) \frac{A_+}{A_-}]$  will fix the nature of the solution of Eq. 4.21. We may inquire into what values  $\frac{A_+}{A_-}$  must take on to generate stable solutions and compare these with observation.

Using measured values from the soundings on 23 and 24 July, the period may be computed for various assumed  $A_+/A_-$  values from Eq. 4.17:

$$\omega^2 = -\frac{g}{T} [(\gamma_s - \gamma) + (\gamma_d - \gamma) \frac{A_+}{A_-}]$$

and Period,  $P = \frac{2\pi}{\omega}$ .

TABLE 4.2

The Period of Oscillation as a Function of  $A_+/A_-$

23 July		24 July	
$A_+/A_-$	Period (min.)	$A_+/A_-$	Period (min.)
0.5	17	0.5	13.2
1.0	13	0.6	12.1
2.0	8	0.65	11.7
3.0	6.6	10	2.97
50	1.6	52.4	1.3

Although the frequency for the buoyancy oscillation could not be found exactly in Chapter III, we see that a period in the range 10 - 12 minutes leads to a ratio  $A_+/A_-$  near 1.0. The favorable comparison with the aircraft traverses described in Chapter I supports the conclusion that the oscillations at the low frequencies are buoyancy induced and come into play when the larger cell is building upward.

The oscillations near one to two minutes cannot be explained as cellular buoyancy oscillations for two reasons. Firstly, the  $A_+/A_-$

ratio required leads to an unrealistic cellular circulation, as seen in Table 4.2. Secondly, the limiting frequency to which the atmosphere will respond is given by the static stability and as such would have periods no shorter than five or six minutes. It seems reasonable to ascribe these motions to inhomogeneities in the temperature field inside the cloud and to mechanical turbulence from the updraft.

#### 4.4 Coupling Between the Cells

The two principal components of the vertical motion observed for a growing cumulus, according to the power spectra, are the underlying trend and the buoyancy oscillation. Several choices for combining these motions are possible, ranging from linear superposition to non-linear coupling.

Using the solutions of Eqs. 4.21 and 4.22 as linear combinations,

the total vertical velocity  $w = w_1 + w_2$

$$\text{or } w(t) = A \sin z) t + k_1 t \quad (4.24)$$

$$\text{where } k_1 = \frac{g}{T_0} (T' - T_0)$$

The observed behavior of  $w(t)$  corresponds very closely to the values of  $z)$  and  $k_1$  as computed for independent cellular circulations. It is considered that the linear model approximates the observed behavior well enough to eliminate consideration of more complex interactions. When the cell reaches its maximum height, the oscillatory term disappears from Eq. 4.24.

## V. SUMMARY AND CONCLUSIONS

The chief contribution of this work, in the opinion of the author, is that the cumulus problem has been identified as one belonging to the class of stable oscillating flows. With this definition, the vagueness surrounding the manner in which cumulus convection occurs has been replaced by a definite set of concepts which carry quantitative implications, capable of measurement.

A technique has been devised whereby simple yet reliable measurements from photographs of growing clouds are made which are capable of analysis to reveal pertinent dynamical and kinematical characteristics of the growth. We have been able to show that cumulus growth is essentially a cellular circulation problem with the important restraint of the static stability of the atmosphere. The observations support uniformly the growth as an oscillating, cumulative, vertical displacement under certain eigen frequencies.

Based on the observations, a physical model is proposed for the velocity field within and around the growing cumulus. Reasonable explanations are offered for the measured variables, consistent with this physical model. The release of potential instability contained in the water vapor accompanying cloud formation will cause the release of additional potential energy (heat) which is converted into kinetic energy and gravitational potential energy. Due to the dependence of the rate of energy release on the motion and vice versa, the situation contains the possibility for non-linear interaction between these variables and an unstable transition could occur. This instability might manifest

itself as a violent overturning of the fluid stratification. Instead of this behavior, the observations indicate a controlled overturning taking place with the displaced air forming the down current. The overturning occurs as a generally positive, stepwise upward growth of the cloud column, accompanied by a possible shallow countercurrent in the outer sheath of the cloud column in addition to the broader sinking motion in the environment.

These discoveries will find practical application in the areas of weather forecasting and weather modification. On the way to the final result, the "slice" method of cumulus forecasting was re-examined and found in need of new interpretation. The cumulus may be treated experimentally as a controlled experiment, if the dynamical and kinematical observations, shown to be possible, are made during the course of artificial stimulation. The release of energy within a cumulus may be revealed by the amplitudes or frequencies of the vertical displacements and compared to those computed for untreated cases. It was found possible to compute from the ordinary RAOB certain of these dynamical characteristics which will distinguish a natural behavior from an unnatural one.

## VI. SUGGESTIONS FOR FUTURE RESEARCH

This study is limited to five cases of cumulus development over the Santa Catalina Mountains near Tucson. The generality of its conclusions cannot be established until many other cases of cumulus growth in different orographic conditions have been examined. One of the first extensions to this present research should enlarge the sample.

A consistent feature of the growth was the high frequency components. This aspect did not receive a satisfactory explanation and it may lie in the direction of a modified turbulence theory. Aside from its academic attraction, the high frequencies appear to be important as a possible means of entraining dry air into the cloud top.

The observations were on cumulus congestus types. The cumulus humilis and the cumulonimbus should be studied for evidence of pulsating growth, and the theory expanded to take into account, more specifically, the horizontal dimensions of the clouds.

A complete dynamical solution will require much more complexity than the physical model proposed in this work. The knotty questions of perturbation pressure, finite amplitude cellular convection, non-linearity of temperature and velocity interactions will have to be taken into account. A possible sidestepping of these difficulties may be through the numerical approach. Using a working model of the velocity, temperature, and moisture fields, suitable prognostic equations can be formulated for machine solution. This approach will have the restriction of limited applicability unless sufficient calculations are made to span the variation in values of the initial parameters.



## ACKNOWLEDGEMENTS

The author wishes to express his appreciation to all of those who assisted in the shaping of the ideas which finally took expression in the form found here. Among these are: Prof. Houghton, Prof. Starr, Prof. Charney, Prof. Phillips, and Dr. Kuo, of the Department of Meteorology, Massachusetts Institute of Technology. Dr. Louis Berkofsky, of GRD, proved to be a willing and helpful listener when requested and the author is grateful for his patience.

Without the cooperation of many individuals this work would not have been possible. The raw data were provided generously by the Institute of Atmospheric Physics, University of Arizona. Mr. Daniel Schurz, Photogrammetry Laboratory, M.I.T., and Mr. Allen Gunn, ACIC, were of great value in rendering technical assistance in the reduction of the photographic data to contours. The laborious task of compiling, reducing, and assembling the many observations was performed in an admirable manner by Mrs. Elaine Sanders, who showed painstaking care and unlimited patience in performing the endless number of detailed computations.

Above all, the devoted concern of my wife, Marjorie, made it possible for me to concentrate my energies on this work which took three years to complete. My sincere appreciation and heartfelt thanks are extended to her.

## BIBLIOGRAPHY

1. Abe, M., 1928: Cinematographic studies of rotary motions of a cloud mass near Mt. Fuji. Geophysical Mag. (Tokyo), Vol. 1, pp. 211-228.
2. Ackerman, B., 1959: Variability of water contents in tropical cumuli. Jour. of Met., Vol. 16, pp. 191-198.
3. American Society of Photogrammetry, 1952: Manual of Photogrammetry, 2nd Ed., Washington, D.C.
4. Aubert, J., 1957: On the release of latent heat as a factor in large scale atmospheric motions. Jour. of Met., Vol. 14, pp. 527-542.
5. Austin, J.M., 1948: A note on cumulus growth in a non-saturated environment. Jour. of Met., Vol. 5, pp. 103-107.
6. Battan, L.J., 1959: Radar Meteorology. The University of Chicago Press, 161 pp.
7. Beers, N., 1945: Atmospheric Stability and Instability. In: Handbook of Meteorology, F.A. Berry et al., ed., pp. 693-725, McGraw-Hill, New York.
8. Berkofsky, L., 1957: A Numerical Model for the Prediction of Hurricane Formation. Ph.D. thesis, Mass. Institute of Technology, Cambridge, Mass.
9. Bjerknes, J., 1938: Saturated ascent of air through dry-adiabatically descending environment. Quar. Jour. Roy. Met. Soc., Vol. 64, pp. 325-330.
10. Blackman, R.B. and J.W. Tukey, 1958: The Measurement of Power Spectra. Dover Publications, New York, N.Y.

11. Brunt, D., 1927: The period of simple vertical oscillations in the atmosphere. Quar. Jour. Roy. Met. Soc., Vol. 53, pp. 30-32.
12. Bunker, A., 1952: Recognition of the presence of convective currents within a nonsaturated turbulent layer of the atmosphere. In: International Symposium on Atmospheric Turbulence in the Boundary Layer, E.W. Hewson, ed., Air Force Cambridge Research Center, Technical Report 53-9, Bedford, Mass.
13. Byers, H. and R. Braham, 1949: The Thunderstorm. U.S. Government Printing Office, Washington, D.C., 287 pp.
14. Christians, H., 1935: The dynamics of cumulus clouds. Beitr. z. Phys. d. Freien Atmosph., Vol. 22, pp. 149-160.
15. Cunningham, R.M., V.G. Plank, and C.F. Campen, 1956: Cloud Refractive Index Studies. Air Force Cambridge Research Center, Report TR-56-210, Bedford, Mass.
16. Cunningham, R.M., 1959: Cumulus Circulation. In: Recent Advances in Atmospheric Electricity, pp. 361-367, L. Smith, ed., Pergamon Press, London.
17. Draginis, M., 1958: Liquid water within convective clouds. Jour. of Met., Vol. 15, pp. 481-485.
18. Eliassen, A. and E. Kleinschmidt, 1957: Dynamic Meteorology. In: Encyclopedia of Physics, S. Flugge, ed., Vol. XLVIII, Geophysics II, pp. 1-154. Springer-Verlag, Berlin.
19. Godske, C., T. Bergeron, J. Bjerknes, and R. Bundgaard, 1957: Dynamic Meteorology and Weather Forecasting.
20. Gutman, L., 1957: Theoretical model of the cumulus cloud. Doklady Akademii Nauk SSSR, Vol. 112, pp. 1033-1036, Moscow.

21. Haltiner, G.J., 1959: On the theory of convective currents.  
Tellus, Vol. 11, pp. 4-15.
22. Haque, S.M.A., 1952: The initiation of cyclonic circulation in a vertically unstable stagnant air mass. Quar. Jour. Roy. Met. Soc., Vol. 78, pp. 394-406.
23. Høiland, E., 1939: On the interpretation and application of the circulation theorems of V. Bjerknes. Arch. Math. Og Naturv., Vol. 42, 68 pp.
24. Houghton, H. and H. Cramer, 1951: A theory of entrainment in convection patterns. Jour. of Met., Vol. 8, pp. 95-102.
25. Jones, R.A., 1957: Studies of Eddy Structure in the First Few Thousand Feet of the Atmosphere. Porton Tech. Paper No. 588, Ministry of Supply, Gt. Britain.
26. Kassander, A.R. and L. Sims, 1957: Cloud photography with ground located K-17 aerial cameras. Jour. of Met., Vol. 14, pp. 43-49.
27. Letzmann, J., 1930: Cumulus pulsations. Met. Zeits., Vol. 47, pp. 236-238.
28. Levine, J., 1959: Spherical vortex theory of bubble-like motion in cumulus clouds. Jour. of Met., Vol. 16, pp. 653-662.
29. Ludlam, F.H. and R.S. Scorer, 1953: Convection in the atmosphere. Quar. Jour. Roy. Met. Soc., Vol. 79, pp. 317-341.
30. Malkus, J., 1953: Some results of a trade cumulus cloud investigation. Jour. of Met., Vol. 11, pp. 220-237.
31. Malkus, J.S., 1954: Some results of a trade cumulus cloud investigation. Jour. of Met., Vol. 11, pp. 220-237.

32. Malkus, J.S., 1955: On the formation and structure of downdrafts in cumulus clouds. Jour. of Met., Vol. 12, pp. 350-354.
33. Malkus, J.S. and R.S. Scorer, 1955: The erosion of cumulus towers. Jour. of Met., Vol. 12, pp. 43-57.
34. Malkus, J.S. and G. Witt, 1959: The Evolution of a Convective Element: A Numerical Calculation. In: The Rossby Memorial Volume. The Rockefeller Institute Press, New York.
35. Malkus, W.V.R. and G. Veronis, 1958: Finite amplitude cellular convection. Jour. of Fluid Mechanics, Vol. 4, pp. 225-260.
36. Manley, R., 1945: Waveform Analysis. John Wiley, New York, 275 pp.
37. Milne-Thomson, L., 1950: Theoretical Hydrodynamics, 2nd Ed., MacMillan Co., New York, 600 pp.
38. Morton, B.R., 1957: Buoyant plumes in a moist atmosphere. Jour. of Fluid Mechanics, Vol. 2, pp. 127-144.
39. Panofsky, H.A., 1953: Statistical Properties of the Vertical Flux and Kinetic Energy at 100 Meters. Sci. Rep. No. 2. The Penn. State College, Contract AF 19(604)-166, Air Force Cambridge Research Center, Bedford, Mass.
40. Petterssen, S., 1956: Weather Analysis and Forecasting, 2nd Ed., Vol. 2, McGraw-Hill, New York, 266 pp.
41. Prandtl, L. and O. Tietjens, 1934: Fundamentals of Hydro- and Aeromechanics. McGraw-Hill, New York, 270 pp.
42. Priestley, C.H.B., 1953: Buoyant motion in a turbulent environment. Austral. Jour. of Physics, Vol. 6, pp. 279-290.
43. Priestley, C.H.B., 1959: Turbulent Transfer in the Lower Atmosphere. The University of Chicago Press, 130 pp.

44. Rayleigh, Lord, 1916: On convection currents in a horizontal layer of fluid when the higher temperature is on the under side. Phil. Mag., Vol. 32, pp. 529-546.
45. Schmidt, F.H., 1957a: On the diffusion of stack gases in the atmosphere. Konig. Nederlands Met. Inst. Med. in Verhandelingen. No. 68.
46. Schmidt, F.H., 1957b: On the diffusion of heated jets. Tellus, Vol. 9, pp. 378-383.
47. Scorer, R.S. and F.H. Ludlam, 1953: Bubble theory of penetrative convection. Quar. Jour. Roy. Met. Soc., Vol. 79, pp. 94-103.
48. Squires, P., 1958a: Penetrative downdraughts in cumuli. Tellus, Vol. 10, pp. 381-389.
49. Squires, P., 1958b: The spatial variation of liquid water and droplet concentration in cumuli. Tellus, Vol. 10, pp. 372-380.
50. Stommel, H., 1947: Entrainment of air into a cumulus cloud. Jour. of Met., Vol. 4, pp. 91-94.
51. Stommel, H., 1951: Entrainment of air into a cumulus cloud, II. Jour. of Met., Vol. 8, pp. 127-129.
52. Sutton, O.G., 1953: Micrometeorology. McGraw-Hill, New York, 333 pp.
53. Väisälä, V., 1925: Über die Wirkung Windschwankung auf die Pilotbeobachtungen. Soc. Sci. fenn. comm. phys-math., Vol. 2, 46 pp.
54. Van der Hoven, I. and H.A. Panofsky, 1954: Final Report on Statistical Properties of the Vertical Flux and Kinetic Energy at 100 Meters. The Penn. State University Contract AF19(604)-166, Air Force Cambridge Research Center, Bedford, Mass.

55. Vonnegut, B., C.B. Moore, and A.T. Botka, 1959: Preliminary results of an experiment to determine initial precedence of organized electrification and precipitation in thunderstorms. Jour. of Geophy. Res., Vol. 64, pp. 347-357.
56. Vul'fson, N.I., 1957: Compensating descending currents caused by developing cumulus clouds. Iz. Aka. Nauk. SSSR Ser. Geo., Vol. 1, pp. 94-103, Moscow.
57. Warner, J., 1955: The water content of cumuliform clouds. Tellus, Vol. 7, pp. 449-457.
58. Workman, E.J. and S.E. Reynolds, 1949: Time of rise and fall of cumulus cloud tops. Bull. Amer. Met. Soc., Vol. 30, pp. 359-361.
59. Yates, A.H., 1953: Atmospheric convection; the structure of thermals below cloud base. Quar. Jour. Roy. Met. Soc., Vol. 79, pp. 420-424.
60. Zeller, M., 1952: Textbook of Photogrammetry. Lewis and Co., London, 281 pp.

### BIOGRAPHICAL NOTE

The author was born in St. Louis, Missouri, on August 13, 1919. He attended public schools there and graduated from Sumner High School in January, 1937. From September, 1937 to June, 1941, the author attended Lincoln University, Jefferson City, Missouri, where he majored in chemistry and minored in mathematics. Upon graduation in 1941, he was awarded the B.S. degree.

He entered the Army Air Corps in 1942 as an aviation cadet and was trained as a weather officer at the University of Chicago "A" course, finishing in May 1943. After serving in various parts of the continental U.S. during the War, the author entered the Polytechnic Institute of Brooklyn in 1946. The M.S. degree in chemistry was awarded him in 1948 and shortly thereafter he accepted a position as a research scientist with the Geophysics Research Directorate. Since 1948, he has been in charge of the cloud physics program at GRD, occupying the position of Chief of the Cloud Physics Branch. The author is a member of:

American Meteorological Society

American Geophysical Union

RESA

He is serving currently on the following national committees:

Cloud Physics Committee, American Geophysical Union

Committee on Cloud Physics and Weather Modification, American Meteorological Society

Committee on the Meteorological Aspects of the Effects of Atomic Radiation, National Academy of Sciences, National Research Council.



His publications include:

Evaluation of Results of Joint Air Force-Weather Bureau Cloud Seeding Trials Conducted During Winter and Spring 1949. Geophysical Research Papers No. 4, 1950.

The Application of Weather Modification Techniques to Problems of Special Interest to the Strategic Air Command. Air Force Surveys in Geophysics No. 12, 1952.

The Efficiency of Precipitation as a Scavenger. Air Force Surveys in Geophysics No. 13, 1952.

The Suppression of Aircraft Exhaust Trails. Air Force Surveys in Geophysics No. 58, 1954.

Volume 4.1, Cloud Physics, Report of Scientific Director Project Greenhouse, AEC, Los Alamos, N. M.

The mechanism of atmospheric ice formation I: The chemical composition of nucleating agents. Jour of Met. Vol. 12, pp. 68-73, 1955.

Studies on Re-evaporation Ice Nuclei. IN: Artificial Stimulation of Rain. H. Weickmann ed., pp. 404-408, Pergamon Press, New York, 1957.

Diffusional Growth Problems in Cloud Physics. IN: Artificial Stimulation of Rain. H. Weickmann ed., pp. 153-160, Pergamon Press, New York, 1957.

The author is married to the former Marjorie L. Robinson, of Jefferson City, Missouri. They have three children: Cheryl Elaine, born February 4, 1944; Charles Edward II, born March 4, 1946; and Linda Louise, born September 4, 1952. The family is at home in Bedford, Mass.